POLYPUBLIE
Polytechnique Montréal

POLYTECHNIQUE MONTRÉAL
UNIVERSITÉ D'INGÉNIERIE

Titre: Title:	Performance, Stability and Erosivity of Nitrogen-Rich Gun Propellants
Auteur: Author:	Jonathan Lavoie
Date:	2017
Type:	Mémoire ou thèse / Dissertation or Thesis
Référence: Citation:	Lavoie, J. (2017). Performance, Stability and Erosivity of Nitrogen-Rich Gun Propellants [Ph.D. thesis, École Polytechnique de Montréal]. PolyPublie. https://publications.polymtl.ca/2925/

URL de PolyPublie: PolyPublie URL:	https://publications.polymtl.ca/2925/
Directeurs de recherche: Advisors:	Charles Dubois, & Catalin-Florin Petre
Programme: Program:	Génie chimique

UNIVERSITÉ DE MONTRÉAL

PERFORMANCE, STABILITY AND EROSIVITY OF NITROGEN-RICH GUN
PROPELLANTS

JONATHAN LAVOIE

DÉPARTEMENT DE GÉNIE CHIMIQUE

ÉCOLE POLYTECHNIQUE DE MONTRÉAL

THÈSE PRÉSENTÉE EN VUE DE L'OBTENTION

DU DIPLÔME DE PHILOSOPHIAE DOCTOR

(GÉNIE CHIMIQUE)

DÉCEMBRE 2017

UNIVERSITÉ DE MONTRÉAL

ÉCOLE POLYTECHNIQUE DE MONTRÉAL

Cette thèse intitulée:

PERFORMANCE, STABILITY AND EROSIVITY OF NITROGEN-RICH GUN
PROPELLANTS

présentée par : LAVOIE Jonathan

en vue de l'obtention du diplôme de : Philosophiae Doctor

a été dûment acceptée par le jury d'examen constitué de :

M. TAVARES Jason-Robert, Ph. D., président

M. DUBOIS Charles, Ph. D., membre et directeur de recherche

M. PETRE Catalin-Florin, Ph. D., membre et codirecteur de recherche

M. AJJI Abdellah, Ph. D., membre

M. BATES Philip John, Ph. D., membre externe

ACKNOWLEDGEMENTS

RÉSUMÉ

Plusieurs chercheurs considèrent que les approches actuelles au contenu énergétique de propulsifs ont atteint leur maturité et leurs limites. L'oxydation de molécules à base de carbone est l'approche utilisée depuis plusieurs décennies et a atteint son plein potentiel. Des structures sous forme de cage ont un contenu énergétique très élevé, mais restent dispendieuses. De plus, des défis supplémentaires en termes de vulnérabilité réduite, d'impact environnementaux et de réduction d'usure de systèmes d'armes. Il attendu des composés riches en azote qu'ils remédient à ces défis. Cependant, les efforts des scientifiques se sont principalement concentrés sur la synthèse de nouveaux composés riches en azote avec peu d'attention sur les effets de ces composés lorsqu'incorporés dans des poudres propulsives. Cette thèse vise à caractériser les effets de composés riches en azote dans des poudres propulsives en termes de performance, de stabilité et d'érosivité.

Quatre composés riches en azote, soit le 5,5'-hydrazinebistétrazole (HBT), le 5,5'-bis-(1H-tetrazolyl)-amine (BTA), le nitrate de 5-aminotétrazolium (HAT-NO$_3$) et le 3,6-dihydrazino-s-tétrazine (DHT) ont été incorporés en concentrations massiques de 5%, 15% et 25% dans un propulsif pour canon de type base triple. La triple base était composée de nitrocellulose, trimethylol éthane trinitrate et triéthylène glycol dinitrate. L'ajout de composés riches en azote a résulté en une augmentation de la vitesse de combustion dans tous les cas, cette augmentation atteignant jusqu'à 93% pour le BTA comparativement au propulsif de référence. Les exposants de pression et coefficients linéaires étaient hautement variés, certains exposants atteignant des valeurs indésirables de 1.4. La stabilité thermique à court terme et à long terme des propulsifs a aussi été évaluée. Le HBT et le BTA se sont avéré thermiquement stables à court terme et compatibles à long terme avec les esters nitrés. Le DHT et le HAT-NO$_3$ se sont avérés peu compatibles avec les esters nitrés à long terme. Le DHT en particulier s'est avéré incompatible avec une décomposition autocatalytique. La baisse de stabilité due au HAT-NO$_3$ est attribué à la dissociation partielle de ce dernier en l'acide et la base qui en sont les précurseurs, ce qui favorise la décomposition des esters nitrés dû à la présence d'acide nitrique. La décomposition autocatalytique des propulsifs incorporant du DHT est attribués aux effets oxydants des autres constituants et des produits de décomposition des autres constituants du propulsif.

Les effets du HBT et BTA sur l'érosivité de poudres propulsives aussi été quantifié, une première dans la littérature scientifique des composés riches en azote. L'ajout de matériaux riches en azote a résulté en une diminution significative de l'érosivité des propulsifs comparativement à la formulation de référence. Cette diminution a aussi démontré que la modélisation semi-empirique de l'érosion de canons actuelle est potentiellement inadaptée aux propulsifs riches en azote étant donné que les modèles sont basés sur des propulsifs conventionnels et à faible vulnérabilité. Les effets des réactions entre l'acier de canon et l'azote sont un autre aspect qui est absent des modèles. De plus, les vitesses de combustion des propulsifs incorporant 35% de HBT et BTA ont été mesurés. Ces mesures ont mené à la découverte d'un changement significatif dans la cinétique de combustion des propulsifs qui est reflété par une augmentation des coefficients linéaires et une baisse des exposants.

Finalement, une série d'heuristiques a été proposé pour guider les formulateurs dans la sélection de composés riches en azote. Ces heuristiques sont proposés au lieu de modèles puisqu'il a été déterminé que la création de modèles adéquats sera une entreprise importante et complexe.

ABSTRACT

It is believed that the current approaches to energetic content in gun propellants have reached their limits. Oxidation of molecules with a carbon backbone is the approach that has been in use for decades and has reached its full potential. Strain cage structures like CL-20 provide good energetic content but remain very expensive. Additional challenges in gun propellant design include reduced sensitivity, improved thermal stability, lowered environmental impact and reducing wear of gun systems due to propellants. Nitrogen-rich materials are anticipated to be a solution to these challenges without having to sacrifice performance. However, efforts have mostly been centered on the synthesis of new molecules with little attention paid to their effects in gun propellants. This thesis aims to fill this gap in energetic materials research by measuring the effects of nitrogen-rich materials in gun propellants. More specifically, the properties investigated were the performance, stability and erosivity of nitrogen-rich propellants.

A total of four nitrogen-rich materials, 5,5'-hydrazinebistetrazole (HBT), 5,5'-bis-(1H-tetrazolyl)-amine (BTA), 5-aminotetrazolium nitrate (HAT-NO$_3$) and 3,6-dihydrazino-s-tetrazine (DHT) were incorporated at concentrations of 5%, 15%, 25% and 35% (HBT and BTA only) in a modified triple base gun propellant. The triple base was composed of nitrocellulose, trimethylolethane trinitrate and diethylene glycol dinitrate. All nitrogen-rich materials resulted in a burning rate increase regardless of concentration with the burning increase reaching as high as 93% for 5,5'-bis-(1H-tetrazolyl)-amine. Significant changes in burning rate laws also indicated changes in the combustion kinetics of the propellants which were due to the nitrogen-rich materials.

The thermal stability, both short-term and long-term, was evaluated for all propellants. BTA and HBT proved to have no significant effect on the long-term stability of the propellants and the short-term thermal stability of the propellants incorporating these materials remained within acceptable levels. Both DHT and HAT-NO$_3$ proved to have poor long-term stability. The decrease of the stability of the propellant incorporating HAT-NO$_3$ is attributed to the salt dissociating into its acid-base precursors which leads to accelerated decomposition of nitrocellulose due to nitric acid. Propellants incorporating DHT exhibited a catastrophic autocatalytic decomposition behavior. This behavior is attributed to the decomposition products of the other materials in the propellant oxidizing DHT which leads to its decomposition and further decomposition of the propellant.

The effects of HBT and BTA on the erosivity of gun propellants were characterized, a first for nitrogen-rich materials in propellants. The addition of nitrogen-rich materials significantly lowered the erosivity of the propellants. It also demonstrated that current modeling of erosion may not be adequate for nitrogen-rich materials given their semi-empirical nature and the effects of nitrogen gas diffusing and reacting with the gun steel

Finally, a set of heuristics based on the results obtained is proposed to help formulators with the initial screening of nitrogen-rich materials in gun propellant applications. These heuristics are proposed in lieu of models as it was discovered that such models could only be the result of a complex and important series of experimental works outside of the scope of a single PhD thesis.

TABLE OF CONTENTS

LIST OF TABLES

LIST OF FIGURES

LIST OF SYMBOLS AND ABBREVIATIONS

2,4-DNT   2,4-Dinitrotoluene

5-AT   5-Amino-1H-tetrazole

AAT   Ammonium Azotetrazolate

AATA-NQ   1-Nitroguanyl-3-azido-5-amino-1,2,4-triazole

ADN   Ammonium Dinitramide

AFZT   Bis(azidoformamidinium) 5,5'-Azotetrazolate

AGZT   Bis(aminoguanidinium) 5,5'-Azotetrazolate

AN   Ammonium Nitrate

ANTA-NQ   1-Nitroguanyl-3-nitro-5-amino-1,2,4-triazole

AP   Ammonium Perchlorate

ARDEC   US Army Armament Research Development and Engineering Center

ARL   Army Research Laboratory

ATEC   Acetyl Triethyl Citrate

ATT   5-(5-Amino-1H-1,2,4-triazole-3-yl)-1H-tetrazole

BDDT   3,6-Bis(3,5-dimethylpyrazol-1-yl)-1,2-dihydro-s-tetrazine

BDNPA/F   Bis(2,2-dinitropropyl)-acetal/formal mixture

BHaTz   Bis(hydrazinium) 5,5'-Azotetrazolate

BKW   Becker-Kistiakowsky-Wilson

BR   Burning Rate

BT   5,5'-Bistetrazole

BTA   5,5'-Bis-(1H-tetrazolyl)-amine

BTA·H_2O BTAw, 5,5'-Bis-(1H-tetrazolyl)-amine monohydrate

BTATz   3,6-Bis(1H-1,2,3,4-tetrazol-5-ylamino)-s-tetrazine

CAB	Cellulose Acetate Butyrate
CAZ	Chemically Affected Zone
CL-20	HNIW; 2,4,6,8,10,12-Hexanitro-2,4,6,8,10,12-hexaazaisowurtzitane
CMDB	Composite Modified Double Base
DAAF	4,4'-Diamino-3,3'-azoxyfurazan
DAAT	3,3'-Azobis(6-amino-1,2,3,5-tetrazine)
DAATO$_{3,5}$	N-oxides of 3,3'-Azobis(6-amino-1,2,3,5-tetrazine)
DAG2MNAT	Diaminoguanidinium 2-Methyl-5-nitraminotetrazolate
DAGN4BIM	Diaminoguanidinium 4,4',5,5'-Tetranitro-2,2'-biimidazolate
DAGZT	Bis(diaminoguanidinium) 5,5'-Azotetrazolate
DANT	4,6-Diazido-N-nitro-1,3,5-triazine-2-amine
DBP	Dibutyl Phthalate
DHT	3,6-Dihydrazino-s-tetrazine
(DMAT)$_2$ZT	1,4-Dimethyl-5-aminotetrazolium 5,5'-Azotetrazolate
DNAT	3,3-Dinitro-5,5'azo-1,2,4-triazole
DNBT	3,3'-Dinitro-5,5'-bis(1H-1,2,4-triazole)
DNMBT	3,3'-Dinitromethyl-5,5'-bis(1,2H-1,2,4-triazole)
DOP	Dioctyl Phthalate
DPA	Diphenyl Amine
DRDC	Defense Research and Development Canada
DSC	Differential Scanning Calorimetry
EC	Ethyl Centralite; 1,3-Diethyl-1,3-diphenylurea
EDS	Energy Dispersive X-ray Spectroscopy
EM	Energetic Material

EOS	Equation of State
ESD	Electrostatic Discharge
EtOH	Ethanol
FOX-7	2,2-Dinitroethene-1,1-diamine
FOX-12	1,1-Dinitro-2,2-diaminoethylene
G2MNAT	Guanidinium 2-Methyl-5-nitraminotetrazolate
G_2ZT	Bis(3,4,5-triamino-1,2,4-triazolium) 5,5'-Azotetrazolate
GA	Guanidinium 5-Aminotetrazolate
GD-OTS	General Dynamics - Ordnance and Tactical Systems
GN	Guanidinium Nitrate
GZT	Bis(guanidinium) 5,5'-Azotetrazolate
HAT^+	5-Aminotetrazolium
$HAT-NO_3$	5-Aminotetrazolium Nitrate
HBT	5,5'-Hydrazinebistetrazole
$HDAT-NO_3$	Diaminotetrazolium Nitrate
HEDM	High Energy Density Materials
HMX	Octahydro-1,3,5,7-tetranitro-1,3,5,7-tetrazocine
HTPB	Hydroxyl Terminated Polybutadiene
Hy-At	Hydrazinium 5-Aminotetrazolate
HZT	4,4',6,6'-Tetra(azido)hydrazo-1,3,5-triazine
FS	Friction Sensitivity
IM	Insensitive Munitions
IS	Impact Sensitivity
LAX-112	3,6-Diamino-1,2,4,5-tetrazine 1,4-dioxide

LOVA   Low Vulnerability Ammunition

MAGN4BIM   Monoaminoguanidinium 4,4',5,5'-Tetranitro-2,2'-biimidazolate

(MeDAT)$_2$ZT   1,5-Diamino-4-methyltetrazolium 5,5'-Azotetrazolate

MSB   Modified Single Base

MTB   Modified Triple Base

NaZT   Na$_2$ZT Sodium 5,5'-Azotetrazolate

NC   Nitrocellulose

NG   Nitroglycerin

NQ   Nitroguanidine

NQ2Tz3,6-Bis-nitroguanyl-s-tetrazine

NTT   5-(3-Nitro-1,2,4-1H-triazol-yl)-2H-tetrazole

OB   Oxygen Balance

ONC   Octonitrocubane

PVA   Polyvinyl Alcohol

RDX   1,3,5-Trinitro-1,3,5-triazacyclohexane

RF   Relative Force

RQ   Relative Quickness

SEM   Scanning Electron Microscopy; Scanning Electron Microscope

TAGAZ   Triaminoguanidinium Azide

TAGBT   Triaminoguanidinium 5,5'-Bistetrazolate

TAGDNAT   Triaminoguanidinium Salts of 3,3-Dinitro-5,5'azo-1,2,4-triazole

TAGDNATO Triaminoguanidinium Salts of 3,3-Dinitro-5,5'azoxy-1,2,4-triazole

TAGN   Triaminoguanidinium Nitrate

TAGN4BIM   Triaminoguanidinium 4,4',5,5'-Tetranitro-2,2'-biimidazolate

TAGNQ$_2$Tz   Triaminoguanidinium 3,6-Bis-nitroguanyl-s-tetrazine Salt

TAGZT   Triaminoguanidinium Azotetrazolate

TATB   1,3,5-Triamino-2,4,6-trinitrobenzene

TAZ   Thermally Affected Zone

TEG   Triethyleneglycol

TEGDN   Triethyleneglycol Dinitrate

TMETN   Trimethylolethane Trinitrate

TNT   Trinitrotoluene

Uro2MNAT   Uronium 2-Methyl-5-nitraminotetrazolate

UXO   Unexploded Ordnance

LIST OF APPENDICES

CHAPTER 1   INTRODUCTION

There are multiple challenges in the field of energetic materials and more specifically chemical propulsion that need to be addressed. There are growing environmental concerns related to the toxicity of currently used energetic materials. Other challenges include lower sensitivity of energetic materials, wear associated with using propellants and of course the performance of new energetic materials must remain equivalent to the ones that are currently in use.

Most of the research to tackle these issues has focused on the synthesis of new materials and their chemistry. The performance evaluation of these new energetic materials has mostly been limited to their use as explosives and is often simulated using thermochemical codes rather than determined experimentally. Furthermore, the effects of these new energetic materials when used in solid propellant applications has been largely ignored.

One family of energetic materials that suffers from this is nitrogen-rich molecules. The propellant performance of nitrogen-rich materials is largely unknown. The small amount of research performed was for rocket applications whereas the gun propellant applications have been largely ignored. This results in a common problem associated with new materials: for new materials to be synthesized in significant quantities, there must be a demand and for there to be a demand, the properties of these materials need to be known. Characterization of gun propulsion applications require a non-negligible amount of material and the absence of research on nitrogen-rich gun propellants is a direct result of the problem defined above.

This illustrated a need to characterize the effects of novel nitrogen-rich materials in gun propellants. This was the main aim of the research project under the hypothesis that significant improvements to propellants would be afforded by the inclusion of nitrogen-rich materials in their formulation. The main research goal was therefore to quantify the effects of nitrogen-rich materials in nitrocellulose based propellants. The research goal can further be divided in specific objectives:

- Quantify the impact of nitrogen-rich materials on propellant performance

- Quantify the effects of nitrogen-rich materials on the stability of propellants

- Quantify the erosivity of nitrogen-rich propellants

- Develop a set of heuristics or if possible models to guide the selection of nitrogen-rich materials for formulators.

CHAPTER 2   LITERATURE REVIEW

The intent of this literature review is to cover the fundamentals of energetic materials and propellants. This is to provide the necessary basis to understand the extent of the work performed in the field of nitrogen-rich materials and gun propulsion. While certain aspects of this literature review may appear trivial to researchers in the fields of energetic materials, propulsion and internal ballistics, it is intended to impart the necessary notions for a good understanding to someone new to those fields. The scope and limits of the work available in the literature will also be covered.

2.1   Energetic Materials

Energetic materials (EMs) can be defined as one or more chemical species taking part in rapid exothermic reactions generating liquid or gaseous products sufficient to obtain usable work [1]. This definition applies well to propellants. Propellants generate a significant amount of gases during their decomposition or combustion. Those gases can be used to propel a projectile or rocket. While this definition also applies to explosives, propellants differ from the former in that their rate of combustion is subsonic rather than supersonic. The United Nations recommendations for the transport of dangerous good also has a comprehensive definition of materials that should undergo testing for acceptance into class 1 which is the class for explosives, propellants and fireworks. This definition includes the presence of chemical groups common to energetic materials (NO_3, contiguous nitrogen atoms, ClO_3, etc.), an oxygen balance of -200% or higher, an exothermic decomposition energy of 500 $J \cdot g^{-1}$ or higher and a decomposition onset below 500°C [2].

The work derived from energetic materials can come from one or more of three sources. The first one, considered to be the "classical" approach is the oxidation of a molecule composed mainly of carbon and hydrogen which generates CO_2, CO, H_2O and H_2. It is the most common source of energy used in currently fielded propellants. The oxygen required for combustion is generally contained in the molecule itself. Nitrocellulose (NC), 1,3,5-trinitro-1,3,5-triazacyclohexane (RDX), Octahydro-1,3,5,7-tetranitro-1,3,5,7-tetrazocine (HMX), nitroglycerin (NG), nitroguanidine (NQ) are good examples of this type of materials. Many researchers estimate that this approach has reached its full potential and that higher amounts of energy will come from different sources [3]. The second approach is the use of so-called strain cage structures. The energy released upon decomposition of these molecules comes from the strain to which the bonds of the

molecule are subjected combined with the oxidation of its carbon backbone. 2,4,6,8,10,12-hexanitro-2,4,6,8,10,12-hexaazaisowurtzitane (CL-20) and octonitrocubane (ONC) are two good examples of strain cage structures. The main advantage of this type of molecule is the high energy content, however strain cage structures can be difficult to synthesize, requiring multiple reaction steps with an overall low yield [4, 5]. CL-20 is a prime example of this, while its synthesis has been reported decades ago, it is only produced on a small scale and remains quite expensive [5, 6]. EMs that use oxidation of a carbon backbone and strain cage structures are shown in Figure 2.1.
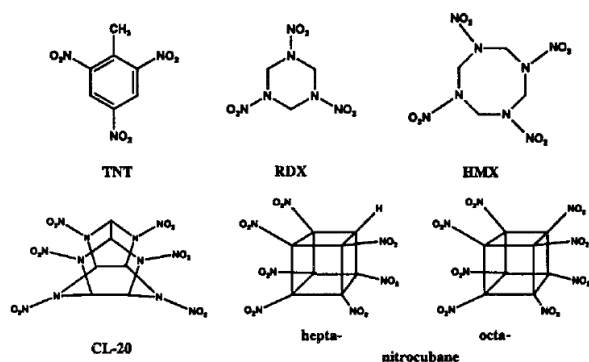
Figure 2.1: Examples of classic molecule design approaches to energetic content in EMs [7]

The last approach and the one that is the focus of this work is the use of molecules mainly composed of nitrogen. Nitrogen is unique in that the bond energy per two electrons bond increases from single to double to triple bonds [8]. Figure 2.2 shows the average bond energy per two electrons for a few select elements. This is the reason why cyclic nitrogen compounds or polynitrogen compounds decompose in a highly exothermic fashion by forming nitrogen gas.
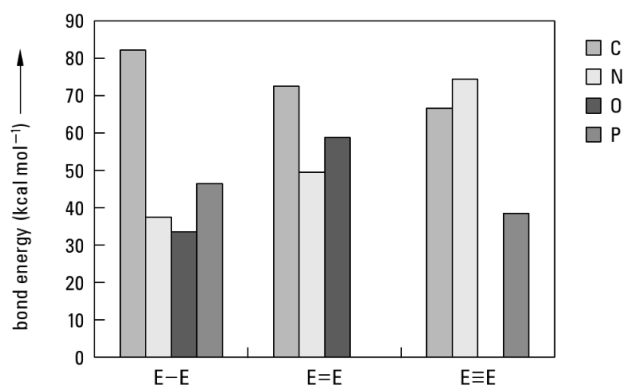
Figure 2.2: Average bond energy per two electron bond for elements present in energetic materials [8]

Figure 2.3 shows one path through which energetic materials evolved and one possible future evolution. It can be seen from this figure that nitrogen-rich materials are expected to serve as replacements for most energetics currently in use. The potential advantages of using nitrogen-rich materials will be discussed in this review.
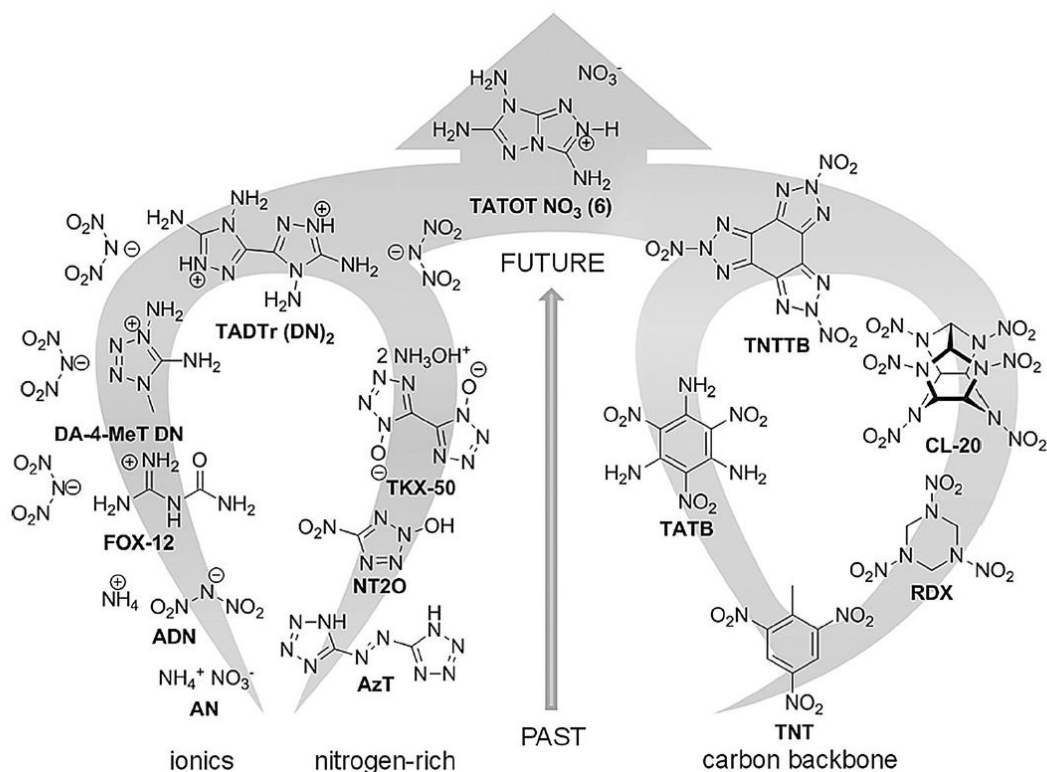
Figure 2.3: Past, present and predicted evolution of energetic materials [9]

While research on nitrogen-rich materials has been ongoing for more than two decades, it only truly took off in the last decade or so. Before nitrogen-rich materials can be discussed in detail and the limits of the current research on these materials defined, important properties of energetic materials must first be discussed.

2.1.1 Important Properties of Energetic Materials

In propulsion applications, be it for rockets or guns, the role of EMs remains the same: to propel an object: the rocket itself or a projectile that is accelerated inside a metal barrel in the case of a gun system. The principal difference between the two is the conditions under which the energetic materials react. In rocket propulsion applications, the combustion is isobaric (constant pressure). In the case of a gun system, the combustion can be considered as isochoric (constant volume). This

is only an approximation; the energetic materials continue reacting after the projectile in the gun system starts moving. A second important distinction is the pressure reached in the different systems: up to 70 bars for rockets and upwards of 4000 bars for gun systems [8]. Regardless of those differences, the important of properties of energetic materials remain the same regardless of their application.

The properties related to the characterization of energetic materials are numerous. These properties aren't only related to the performance of energetic materials, some are associated with safety, stability and environmental impact. The main properties related to performance are the oxygen balance, the enthalpy of formation and the density of the material [10].

2.1.1.1 Properties Related to Performance

One key property of energetic materials is the **oxygen balance** (OB). The OB is especially important for energetic materials where the main source of energy comes from the oxidation of carbon and hydrogen. The oxygen balance can be expressed in terms of complete combustion as the percentage of oxygen required for full conversion of a given molecule with the general composition $C_aH_bN_cO_d$ to CO_2 and H_2O. It can be calculated according to equation 2.1 [8, 11].

$$\Omega = \frac{\left(d - 2a - \frac{b}{2}\right) \times 1600}{M} \tag{2.1}$$

Where Ω is the oxygen balance and M is the molecular weight of the molecule in g·mol^{-1}. A negative oxygen balance indicates that the energetic molecule is oxygen deficient, a value of 0 indicates that the exact amount of oxygen required for full combustion is present and a positive value indicates an excess of oxygen. The amount of energy released from oxidation of energetic materials is directly related to the oxygen balance up to the point where the OB reaches a value of 0. Any additional oxygen will not contribute to the oxidation reaction and will absorb part of the heat generated by the combustion reactions. The final combustion products are also influenced by the oxygen balance. These two factors influence the overall amount of work that can be extracted from the oxidation of energetics. The OB also has potential effects on the environment in that incomplete combustion will yield CO and other harmful gases [12]. It is undesirable to increase the oxygen content past a balance of 0% either as production of O_2 will not yield improvements in performance. Any surplus O_2 will absorb part of the energy generated by the combustion of the

material. Practical concerns may push towards a slight excess to ensure full combustion at a minimal energy loss.

The effects of the **enthalpy of formation** of the material are rather straightforward. Energetic materials decompose according to equation 2.2.

$$energetic\ material \xrightarrow{\Delta H_R^o} gas\ products \tag{2.2}$$
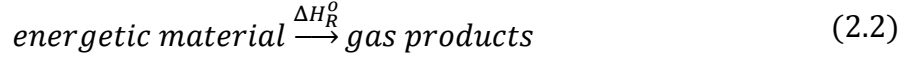
The heat released from the decomposition of an energetic materials can be calculated from equation 2.3.

$$\Delta H_R^o = \Delta H_{f,products}^o - \Delta H_{f,EM}^o \tag{2.3}$$

Ideally, an energetic material would have a highly positive enthalpy of formation (endothermic material) with decomposition products having highly negative enthalpies of formation [13]. This would yield hotter combustion gases and thus higher pressure and more usable energy.

The **density** of energetic materials also has an impact on performance, especially on explosive performance. For an explosive, the detonation velocity (velocity of the shockwave front), an important performance parameter will increase with density of a given material until the maximum density, that of the crystalline material is achieved [11]. For propellants, the mass of gas generated (*m*) and hence the resulting pressure applied on the object to propel can be defined by equation 2.4 [11].

$$m = rA\rho \tag{2.4}$$

Where r is the linear burning rate, A is the surface area and ρ is the density of the propellant. However, the effects of lower density could be offset with a different propellant geometry. The surface area of a propellant can be controlled during the manufacturing step. This means that the burning rate of a propellant is a crucial property related to its performance as at equal density, the rate of gas generation is solely dependent on the burning rate of the propellant.

2.1.1.2 Sensitivity and Thermal Stability

The sensitivity is a measure of how likely an energetic material is to decompose under external stimuli. Sensitivities usually measured are those to friction (FS), impact (IS) and electrostatic discharge (ESD) [6, 8]. IS and ESD sensitivity are expressed in Joules and FS is expressed in Newtons. Thermal stability, or how likely an energetic material is to decompose with heat, is also important as materials decomposing at low temperatures can pose significant hazards. Tables 2.1

and 2.2 and show the classification of energetic materials according to their sensitivity and the sensitivity of some common energetic materials.

Table 2.1 : Sensitivity classification of EMs, adapted from [8]

	Impact [J]	Friction [N]	ESD [J]
Insensitive	> 40	> 360	> 0.1 J
Less sensitive	35-40	360	-
Sensitive	4-35	80-360	< 0.1 J
Very sensitive	< 4	10-80	-
Extremely sensitive	-	< 10	-

Table 2.2: Sensitivity of some common EMs, adapted from [8]

EM	Impact [J]	Friction [N]	ESD [J]
Lead Azide	2.5-4	0.1-1	0.005
TNT	15	>353	0.46-0.57
RDX	7.5	120	0.15-0.20
β-HMX	7.4	120	0.21-0.23
PETN	3	60	0.19
NQ	>49	>353	0.60
TATB	20	>353	2.5-4.24

When researching new potential energetic materials, some sensitivity and stability criteria are often encountered with the aim to improve safety during handling and processing of these materials. These criteria include IS $\geq$ 7.5J; FS $\geq$ 120N, in other words equal or better than RDX and HMX and $T_{decomposition} \geq 200^{\circ}C$ for next generation EMs [4, 8, 9]. Some applications such as primers may also require the use of more sensitive materials.

2.1.1.3   Environmental Impacts

The environmental concerns associated with the use of EMs are now an integral part of the design of new propellants formulations. Domestic use of propellants used for training account for around 95% of all rounds fired by Canadian Armed Forces (CAF) before Afghanistan [14]. Given that the deployment of the CAF abroad since then has decreased, it is expected that the problems associated with the environment and energetic materials remain principally domestic. Materials currently in use for insensitive munitions (IM) such as RDX and HMX have proven harmful to the environment [15]. Energetic materials that are soluble in water eventually seep into the ground and aquifers due to rainfall and will be absorbed by flora and fauna. This implies that energetic materials that are

toxic will eventually poison living organisms once absorbed causing loss of biological functions such as chlorophyll degradation in certain plants and loss of biomass in plants and worms [15]. Soil contamination of training grounds from the residue of energetic materials that result either from direct use or on site burning of the excess munitions is a pressing concern for most military forces due to the costs associated with decontamination not to mention the harmful effects on the environment and potentially human life [16]. Costs associated with the decommission of unexploded ordnance (UXO) in the United States is estimated to be in the tens of billions of US dollars [17]. While these costs include the removal and disposal UXOs on top of the cost of environmental remediation, this figure gives an idea of how expensive the environmental impacts of UXOs can be. These issues require more environmentally friendly EMs to replace the ones currently fielded. Efforts have been made to develop new binders and energetic fillers that have either reduced environmental impact [9] or are biodegradable [18, 19].

2.1.2 Nitrogen-rich Materials

Nitrogen-rich materials, also designated as high-nitrogen materials, are characterized by their high nitrogen content. This in turn results in a large amount of nitrogen gas being released by the decomposition of these materials.

Reducing the muzzle flash caused by the combustion of fuel rich gases (CO and H_2) generated from propellant has been one of the goals of propellant research for a long while [20]. Muzzle flash has a distinct signature which hinders stealth as it gives away the position of gun systems and the intensity of the flash can also be indicative of the type of propellant and ammunition being fired. Nitrogen-rich materials are expected to reduce muzzle flash by shifting the composition of the combustion products towards nitrogen to reduce the amount of fuel rich gases generated.

Nitrogen-rich materials can be categorized by their structure or by their neutral or ionic nature. Three families of neutral compounds will be discussed: polynitrogen, azoles and azines. Ionic compounds based on azole and azine materials will then be briefly discussed. This review of nitrogen-rich energetic materials does not have the pretense of being exhaustive. The amount of nitrogen-rich materials that have been synthesized could be described as extravagant and multiple reviews of different "families" of nitrogen-rich materials are available [10, 21, 22]. The following sections will however provide a good overview of various nitrogen-rich structures as well as their wide range of properties.

A note on the acronyms encountered in this review: while an effort has been made to be consistent with the available literature, some acronyms have been used interchangeably or multiple acronyms have been used to designate the same compound. Examples of this are TAGAZ being used for triaminoguanidinium azotetrazolate rather than being used for triaminoguanidinium azide as is the case in this literature review and DHT and DHTz being used to designate the same compound interchangeably between publications. Acronyms are consistent within this review, but may differ from those used in the cited literature.

2.1.2.1 Polynitrogen Materials

Polynitrogen materials can be considered as the "holy grail" of nitrogen-rich energetic materials. They possess high enthalpies of formation and decompose solely into nitrogen gas [8, 23]. This would avoid the creation of muzzle flash and allow for cooler propellants without loss of performance due to lower molecular weight combustion gases. However, the only stable poly nitrogen compounds known to date are N_2 and N_3, the azide anion. Other polynitrogen materials are either still in the realm of theoretical compounds or are metastable compounds that are impractical to produce on any large scale [23]. Still, polynitrogen materials can be seen as the ultimate goal of nitrogen-rich material research.

2.1.2.2 Azole Compounds

Azole based materials are heterocyclic compounds that comprise at minimum a pyrazole, imidazole, triazole, tetrazole or pentazole heterocycle. These hetero cycles contain two, three, four or five nitrogen atoms in the cycle respectively. The general structures of azoles are shown in Figure 2.4. Pyrroles, pyrazoles and imidazoles have low nitrogen content while pentazoles have poor stability. This make triazoles and tetrazoles the most interesting of the azole based nitrogen-rich materials [8]. Triazoles provide better stability compared to tetrazoles which have the advantage of higher nitrogen content while retaining acceptable stability [24].
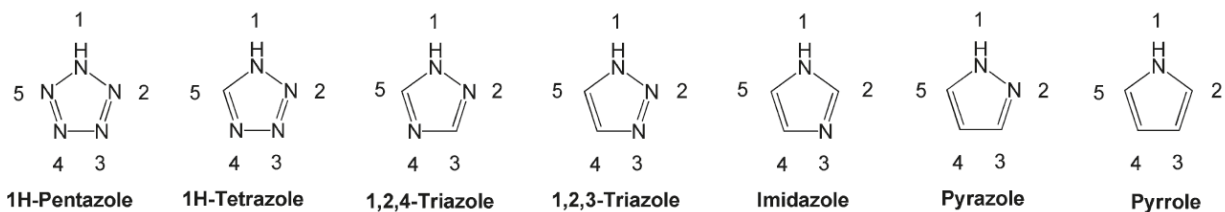
Figure 2.4: Azole bases heterocycles encountered in energetic materials [10]

Azole based compounds show a wide range of properties and often show low sensitivities to impact and friction. This makes such materials desirable for the design of propellants. Tetrazole and bistetrazole materials are often encountered in the literature as having good energetic properties while meeting the previously mentioned criteria of sensitivity and thermal stability for new energetic materials [3, 4, 8, 25-38]. The neutral compounds are often characterized by low oxygen content. Figure 2.5 shows typical tetrazoles, from left to right: 5-aminotetrazole (5-AT), 5-azidotetrazole, 5-nitriminotetrazole and tetrazolone.
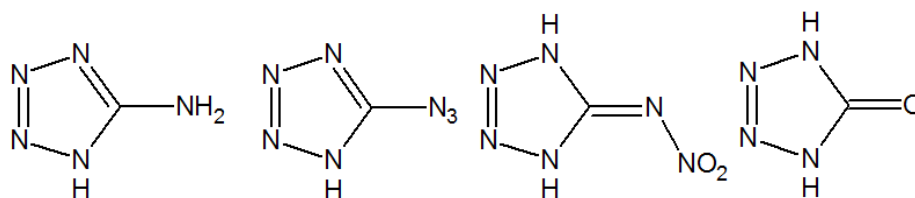
Figure 2.5: Structure of some tetrazole based energetic materials

Figure 2.6 shows a few neutral bistetrazole compounds, from top left to bottom right: 5,5'-bistetrazole, 1,5'-bistetrazole, 5,5'-bis-(1H-tetrazolyl)-amine (BTA) and 5,5'-hydrazinebistetrazole (HBT).
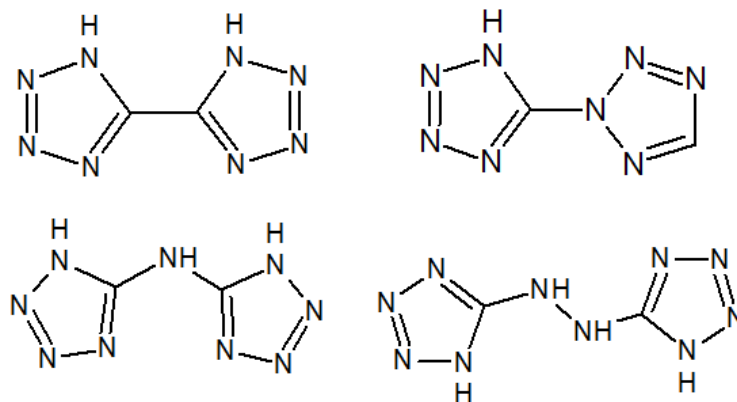
Figure 2.6: Structure of some bistetrazole energetic materials

Tetrazole based salts represent another family of compounds that are often encountered as high energy materials. It is possible to convert most neutral tetrazole materials into salts of one kind or another [3, 6, 7, 9, 10, 22, 29, 31, 32, 39-50]. Figure 2.7 shows some tetrazole based ions: 5-aminotetrazolium (HAT$^+$), 5-azideotetrazolate, 5-oxotetrazolate, 5,5'-azotetrazolate and 5,5'-aminotetrazolate. These ions can be divided in two categories; those that help maintain or increase the nitrogen content and those that increase the oxygen content of the compound.
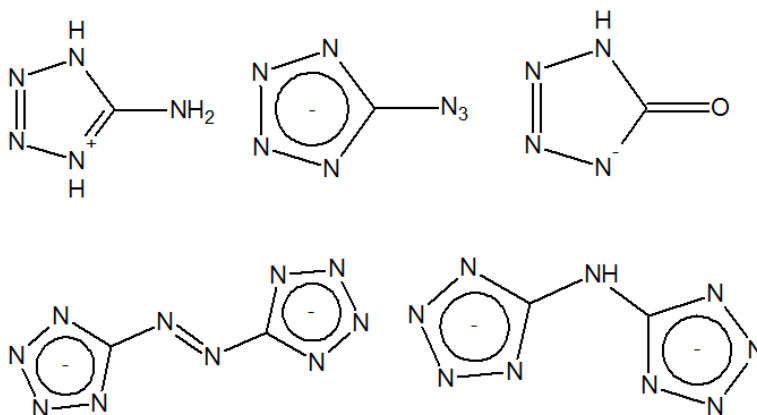
Figure 2.7: Structure of some energetic tetrazole ions

These various tetrazolium and tetrazolate ions can be combined with corresponding counter-ions in order to modify properties such as thermal stability, density, sensitivity, oxygen content and nitrogen content [10]. A series of common counter-ions are shown in Figure 2.8. Those include the nitrogen-rich ammonium, hydrazinium, guanidinium, diaminoguanidinium, triaminoguanidinium and azidoformamidinium cations, the oxygen rich nitrate, perchlorate and dinitramide anions as well as the nitrogen-rich azide anion.
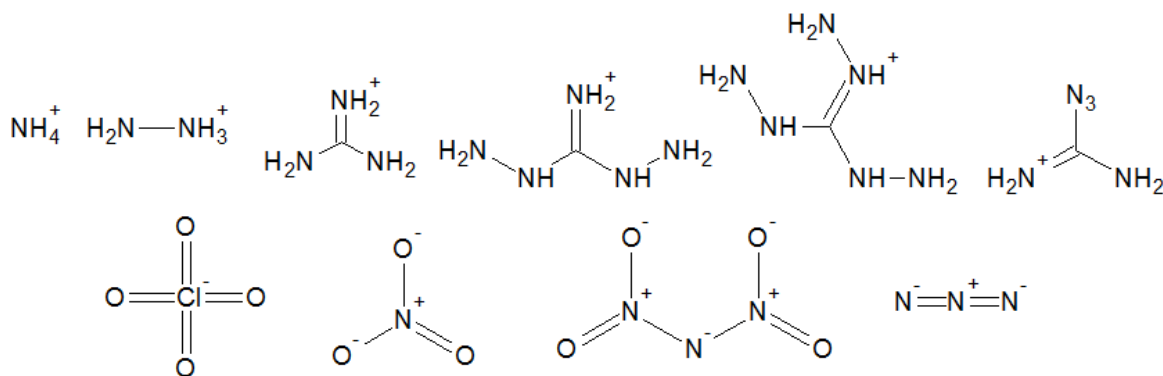
Figure 2.8: Counter ions often encountered in nitrogen-rich energetic salts

Triazoles contain less nitrogen than tetrazoles, on the other hand, they usually offer the advantage of better thermal stability and lower sensitivity than tetrazoles [9, 39]. Some structures are shown in Figure 2.9.
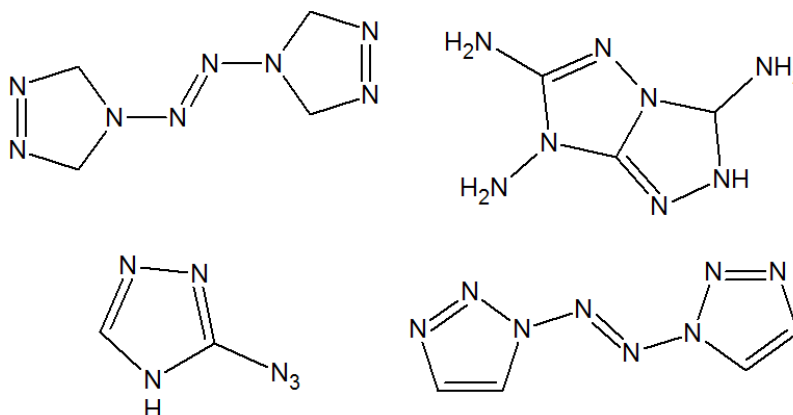
Figure 2.9: Structure of some triazole energetic materials

Triazoles can also be converted to salts in the same way that tetrazoles can be [10, 39, 51, 52]. The same counter ions used in tetrazole salts are also often encountered in triazole salts.

2.1.2.3 Cyclic Azine Based Compounds

Cyclic azines are nitrogen-rich heterocycles structures comprised of 6 atoms with varied functional groups attached. Tetrazines and triazines based compounds are often countered as nitrogen-rich energetic materials. Tetrazines, not unlike tetrazoles present good thermal stability and sensitivity. A few tetrazine based energetic materials, dihydrazino-*s*-tetrazine (DHT), 3,6-bis(1H-1,2,3,4-tetrazol-5-yl-amino)-s-tetrazine (BTATz), 3,6-diamino-1,2,4,5-tetrazine-1,4-dioxide (LAX-112) and 3,3'-Azobis(6-amino-1,2,3,5-tetrazine) (DAAT), are shown in Figure 2.10. 1,2,4,5-tetrazines or *s*-tetrazines are the ones usually encountered in the literature [53-58].
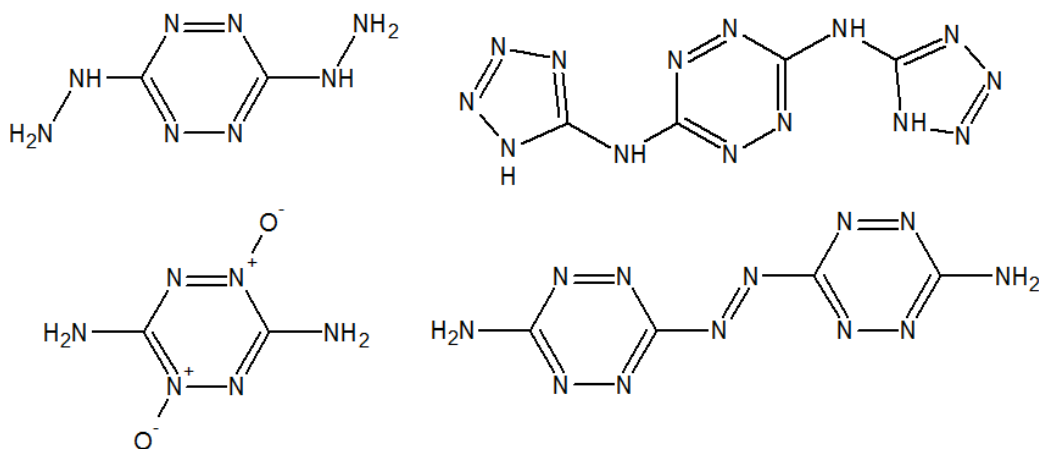
Figure 2.10 Structure of some s-tetrazine based nitrogen-rich energetic materials

Table 2.3 shows the properties of many energetic materials of the various types discussed in this review. The properties of TNT, RDX, HMX and CL-20 are provided as a reference and comparison. TNT, RDX and HMX are common energetic materials used in many applications while CL-20 is one of the most powerful explosives discovered to date. The detonation velocity is provided as a measure of energetic performance. Is should however be noted that this property doesn't necessarily reflect the performance of these materials when used as a propellant. However, as there is a real lack of data on the performance of nitrogen-rich materials as propellants, the detonation velocity is given as presented as a measure of energetic potential.

Table 2.3 : Properties of some EMs

EM	ρ [g·cm^{-3}]	N [%]	Ω [%]	IS [J]	FS [N]	$\Delta_f H^o$ [kJ·g^{-1}]	V_{det} [km·s^{-1}]
Common Ems							
TNT [59]	1.71	18.5	-73.96	15	353	0.24	6.9
RDX [3, 8, 60]	1.80	37.8	-21.6	7.5	120	0.32	8.9
HMX [3, 8, 61]	1.91	37.8	-21.6	7.4	120	0.40	9.2
CL-20 [62]	2.04	38.4	-1.0	3	96	0.83	9.7
Neutral nitrogen-rich EMs							
DHT [37, 63]	1.61	78.8	-78.8	16	-	3.77	-
BTA [64]	1.86	82.3	-57.5	20	>360	4.12	9.1
HBT [38]	1.84	83.3	-57.1	>30	>108	2.46	8.5
5-AT [38]	1.71	82.3	-65.8	>40	>100	2.44	-
BTATz [58, 63]	1.74	79.0	-64.5	7	>360	3.55	-
DAAT [58, 65]	1.76	76.0	72.7	5	324	4.70	7.4
Ionic nitrogen-rich EMs							
HAT-NO$_3$ [48]	1.85	25.7	-10.8	10	324	0.59	8.9
TAGZT [40, 44]	1.52	82.3	-72.7	4	84	2.87	9.1
GA [41]	1.54	77.8	-75.1	>50	>360	1.54	-
HDAT-NO$_3$ [47]	1.72	60.1	-14.7	6	-	1.56	8.8

In summary, the energetics material community has executed a shift from more previously used design guidelines of energetic materials to a different approach. This approach is mostly based on the use of nitrogen-rich structures with high enthalpies of formation. Nitrogen-rich materials that possess an enthalpy of formation an order of magnitude higher than that of traditional EMs can be seen in Table 2.3. However, hybrid approaches have also been advocated where oxygen balanced nitrogen-rich materials are proposed [66]. This is also represented in Table 2.3 where materials with nearly balanced oxygen content have lower enthalpies of formation, but still retain good explosive performance. Additionally, a part of the design concerns has shifted from performance and cost to safety and environment. That is not to say that the performance aspects have taken a

"backseat", but that a more inclusive approach is now preferred. The goals have moved from obtaining the highest performance possible to obtaining similar performance to existing energetics with added value in the form of better stability, lower sensitivity and lower environmental impact. To put it in the words of Chavez & Parrish "The "holy grail" of energetic material could be described as an explosive with the performance of HMX or CL-20, but with the insensitivity of TATB" [67]. This statement reflects the new design philosophy for new energetics well. The number of new energetic materials discovered is staggering and leads to a vast selection of properties for tailoring to a given application.

2.2 Solid Propellants

While liquid propellants do exist, they are outside of the scope of this thesis and will not be discussed. The reader should however be aware of their existence. The following chapter will cover solid propulsion mainly from the standpoint of gun propulsion, but some aspects of rocket propulsion will also be covered when they are relevant to discussing propellant performance in general. The performance aspects will be covered first; the processing aspects of gun propellants and the erosivity of gun propellants will then be discussed. Finally, nitrogen-rich materials both as monopropellants and components of more complex propellants will be discussed.

The first solid propellant discovered is black powder for which records date from at least the 14th century [20]. Modern gun propellants differ greatly from black powder. They are composed at the very least of a polymeric binder, one or more plasticizers and a stabilizer. Other EMs can be incorporated in the propellant formulation. Commonly used polymeric binders include nitrocellulose and cellulose acetate butyrate (CAB). Nitrocellulose is energetic while CAB is an inert binder. Nitroglycerin is the most commonly used plasticizer in commercially available smokeless powders, other energetic plasticizers include, but are not limited to trimethylolethane trinitrate (TMETN), triethyleneglycol dinitrate (TEGDN) and a mixture of bis-2,2-dinitropropyl acetate and bis-2,2-dinitropropyl formal (BDNPA/F). Inert plasticizers often encountered are dioctyl phthalate (DOP), dibutyl phthalate (DBP) and acetyltriethyl citrate (ATEC). Other energetic materials are too numerous to list, but often encountered materials are: nitroguanidine, RDX and HMX. Stabilizers are present to avoid premature aging of the propellant as well as combustion resulting from the heat generated by the ageing reactions in the propellant [68].

Typical propellant formulations include single base propellants made mainly from nitrocellulose, double base propellants (NC/NG), triple base propellants (NC/NG/NQ) and composite modified double propellants (CMDB) usually composed of CAB and multiple energetic materials. It should however be noted that the terms single base, double base and triple base denote the number of energetic components of the propellant rather than specific constituents [6, 68]. Still, these terms are quite often used to describe the compositions mentioned above. In this thesis, the term modified will be used to denote double and triple base propellants not based on NC/NG or NC/NG/NQ respectively.

2.2.1 Propellant Performance

There are many factors that influence propellant performance, the thermochemical aspects of propellant performance can be derived from first principles and calculated using thermochemical codes without the need to perform experiments. These codes are iterative and solve a set of equations to find thermodynamic and stoichiometric equilibrium between gaseous, liquid and solid chemical species. Cheetah and EXPLO5 are examples of such codes. The iterative procedure to calculate the thermochemical parameters of a propellant is fairly simple [20].

- The atomic composition of the propellant is determined.

- The heat of formation of the propellant is calculated from the properties of its constituents.

- An adiabatic flame temperature (T) is selected

- The composition of the combustion gases is calculated using a gas equation of state and the equilibrium between the main decomposition products (CO_2, CO, H_2O, H_2, N_2).

- The internal energy of the gas products and heat of reaction of the propellant decomposition are calculated.

- If the energy of the gases at the chosen temperature and the heat of reaction do not match, a different flame temperature is selected, and the procedure is repeated.

Cheetah uses either the BKW EOS or the virial EOS [69]. In the case of calculations on gun propellants, it is also assumed that the volume is known through the supplied loading density.

The thermochemical parameters that can be calculated for gun propellants include the **adiabatic flame temperature**, the **maximum pressure** at a given loading density, the **impetus**, the

molecular weight of the gas products, the composition of the gaseous decomposition products, the **covolume** and the **ratio of heat capacities**. In the case of rocket propellants, the **specific impulse** will be given rather than the impetus.

The **covolume** is a measure of the non-ideality of the combustion gases and is used in the Noble-Abel EOS (equation 2.5) [20, 68, 69]. This equation is a variation of the Van der Waals equation of state where the intermolecular forces are ignored due to the high kinetic energy of the gases (high pressure and temperature).

$$P(V - nb) = nRT \qquad (2.5)$$

Where P is the pressure, V is the volume, n is the number of moles, b is the covolume, R is the universal gas constant and T is the temperature. The covolume is usually expressed in $cm^3 \cdot mol^{-1}$ as in equation 2.5 or in $cm^3 \cdot g^{-1}$. The Noble-Abel EOS is often used in the calculation of propellant performance.

The **impetus** is used as a measure of the total usable energy stored in the propellant and it is defined by equation 2.6.

$$F = \frac{RT_{ad}}{M_g} \qquad (2.6)$$

Where R is the gas constant, M_g is the gas product molecular weight and T_{ad} is the adiabatic flame temperature [70]. From equation 2.6, higher flame temperatures and lower molecular weight gases will result in overall higher impetus. Typical combustion gases include CO, CO_2, N_2, H_2O and H_2. It would seem that H_2 and CO are desirable comparatively to H_2O and CO_2 since they would yield higher gun performance due to their lower molecular weight. However, during the discussion of gun propellant erosivity, certain drawbacks associated with combustion gas composition and flame temperature will be brought to light.

Another measure of propellant performance is the **specific impulse**. The specific impulse is a measure of the thrust generated. It is often expressed in time seconds which reflect how long the propellant can sustain its own weight under earth's gravitational force [69]. This measure of performance is usually associated with rocket propellants as it is calculated from isobaric conditions. Normally, gun propellant performance is calculated assuming isochoric conditions. However, the specific impulse as defined in equation 2.7 is still sometimes used to measure gun propellant performance in the literature [24, 38].

$$I_{sp} = 1000 * \frac{\sqrt{2(H_1 - H_0)}}{g} \tag{2.7}$$

Where H_1 is the enthalpy in the rocket chamber, H_0 is the enthalpy of the exhaust gases, g is the gravitational constant and I_{sp} is the specific impulse expressed in seconds.

The specific impulse (I_{sp}) and impetus (F) are related to each other from the ratio of specific heats as defined in equation 2.8 [11].

$$I_{sp} = \left\{ \frac{2F}{\gamma - 1} \left[1 - \left(\frac{P_e}{P_c} \right)^{\frac{\gamma - 1}{\gamma}} \right] \right\}^{\frac{1}{2}} \tag{2.8}$$

Where $\gamma = \frac{C_p}{C_v}$ is the ratio of specific heats, P_e is the pressure at the rocket nozzle and P_c is the pressure inside the combustion chamber. It is therefore possible to convert one performance measurement to the other should it be desired.

The properties of propellants discussed so far are all derived from theory and while they provide quantitative comparison of the energy stored inside a propellant, they do not entirely reflect the usable work provided by a propellant. Adiabatic conditions are assumed and in an actual gun, adiabatic conditions are not a given. The same can be said for a closed vessel apparatus. The energy imparted to a projectile will also be dependent on the pressure-distance profile resulting from the combustion of the propellant inside an actual gun. The amount of energy imparted is proportional to the integral of this curve and the combustion gas temperature and pressure will also influence heat losses. The burning rate of a propellant greatly influences the pressure-distance profile developed by the combustion of a gun propellant [70].

The combustion of a propellant is a surface phenomenon where the propellant burns in the direction normal to its surface. The **burning rate** of a propellant can usually be described by Vielle's law, equation 2.9 [71].

$$r = \beta P^\alpha \tag{2.9}$$

Where r is the burning rate, β is the **linear burn rate coefficient**, P is the pressure and α is the **pressure exponent**. The linear burn rate coefficient is also a function of the initial temperature of the propellant and increases with increasing temperature [6]. The values of α and β can vary greatly. High values of α (>1) are indicative that the combustion is mainly driven by gas phase reactions between fuel rich decomposition gases [55, 72]. Lower values of α indicate that condensed phase

reactions are prevalent and thus, the burning rate is much less sensitive to pressure variation. Measurement of burning rates can be performed using a strand burner or a closed vessel. The strand burner is an apparatus where a cylindrical strand of propellant is coated with an inhibitor on the outer surface except for the ends. The strand burner is filled with an inert gas to obtain the desired pressure. One end of the strand is then ignited, and the progress of the linear combustion is measured. The progress of the combustion can be measured through the use of a series of fuses or using a camera and image treatment software if the strand burner is equipped with a window [63, 68]. Strand burner results reported in the literature are often reported at pressures suitable for rocket motors (<10 MPa). Figure 2.11 shows the evolution of a strand burner test for TAGZT where image treatment was used to measure the linear burn rate.
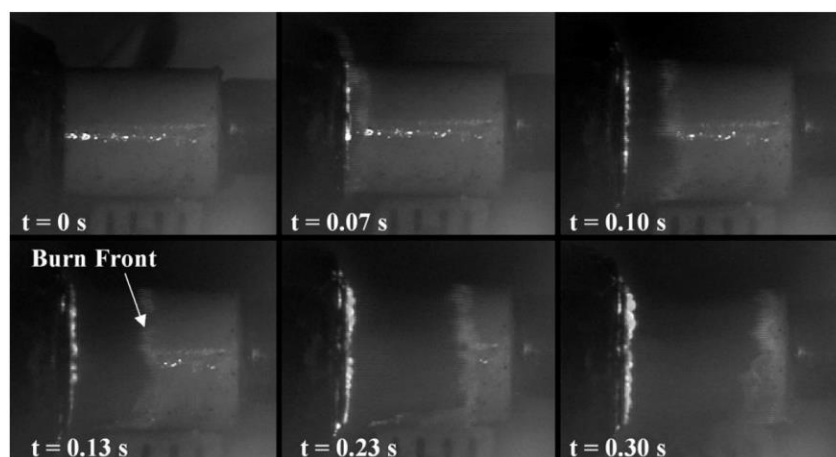
Figure 2.11: Linear burning of a TAGZT pellet in a strand burner [73]

A closed vessel is a cylindrical jacketed steel vessel equipped with a piezoelectric pressure transducer. Water is circulated inside the jacket to cool the vessel, it is loaded with the propellant to obtain the desired loading density, often 0.2 g·cm^3. The vessel is then sealed, and the propellant ignited. The pressure-time data is recorded by the transducer and the burning rate is calculated from this event [68, 74]. The closed vessel is useful to measure burning rate of propellants at pressures ranging in the hundreds of MPa, however, the calculation of the burning rate from the pressure event recorded in a closed vessel requires a few hypothesis and more complex calculations than the strand burned. A typical closed vessel setup is shown in Figure 2.12.
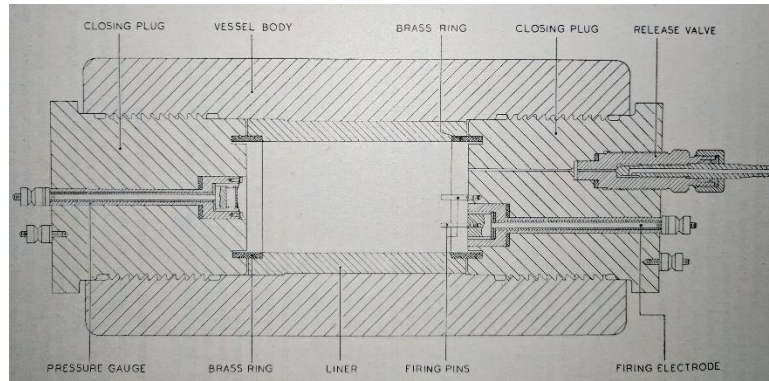
Figure 2.12: Diagram of a closed vessel used to measure propellant performance, from [20]

In order to calculate the burning rate of a propellant from closed vessel data, the thermochemical parameters and the geometry of the propellant are required [74]. The propellant grain geometries that can be fired in a closed vessel are numerous, common propellant geometries are shown in Figure 2.13.
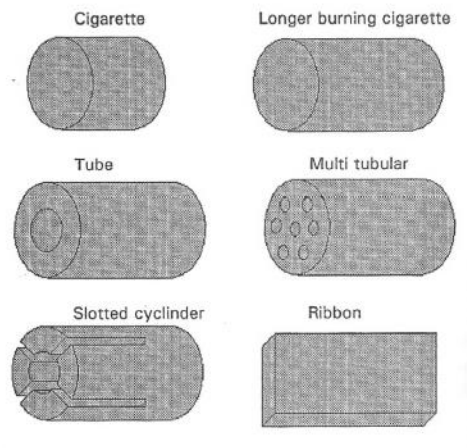
Figure 2.13: Common geometries of gun propellants [11]

Different geometries will produce different pressure-time curves. The cylinder geometry is considered regressive as the surface area diminishes as the combustion progresses. This will result in slower pressure increases compared to progressive or neutral geometries. Multi-tubular geometries are progressive as the perforations will induce an increase in surface area as the combustion progresses. This will generate a much faster increase in pressure over a shorter period than regressive geometries. This effect must be taken into account and the dimensions of the propellant grain geometry often designated "web" are crucial to the deduction of burning rates from

closed vessel experiments. Figure 2.14 shows how the surface area of different geometries varies as the propellant undergoes combustion.
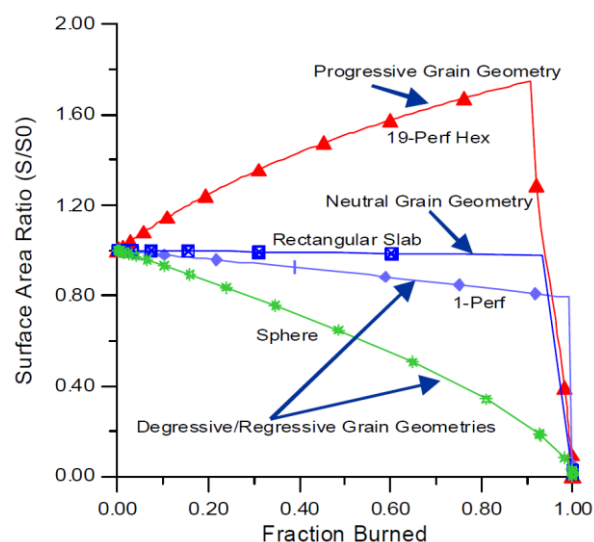
Figure 2.14: Surface progression during combustion of various propellant geometries [75]

Thermochemical parameters can easily be obtained using commercially available computer codes. The igniter's thermochemical parameters also need to be known as the pressure generated from the ignition needs to be removed prior to the calculation of the propellant's burning rate. These thermochemical parameters are however calculated assuming adiabatic conditions. In a closed vessel, adiabatic conditions are not achieved, and assumptions must be made for the treatment of heat losses. This treatment of heat loss can have an effect on the calculated burning rates and conditions have to be kept constant if multiple propellants are to be compared [74]. Finally, uniform ignition of all propellant grains is assumed. Gun propellant processing and manufacturing will be discussed briefly.

2.2.2 Gun Propellant Processing

The main method of formulating gun propellants is called the solvent incorporation method. This method consists of using a horizontal sigma type mixer and solvents to insure uniform mixing of the propellant's constituents [20, 68]. A typical sigma type mixer is shown in Figure 2.15. These mixers are used to mix high viscosity fluids with high shear rates. The solvents serve the role of splitting the fibers of the nitrocellulose (or other polymeric binder) to allow the dispersion of the

plasticizer, other energetics and stabilizer in the binder. The propellant mixture will eventually attain the consistency of a dough suitable for extrusion.

Figure 2.15: Interior of the sigma type mixer shown in Figure 2.16

The propellant dough is extruded through a hydraulic ram press into the desired geometry (cylindrical, 7 perforations, etc.). The resulting strands are then cut to the desired length and dried to remove the solvent used during processing which finally yields the propellant grains. Figure 2.16 shows the complete setup required for processing propellants using the solvent incorporation method.

Figure 2.16: Propellant manufacturing facility [76] a) sigma mixer, b) extrusion press, c) cutting machine, d) 7 perforation propellant grains.

The propellant dough extrusion process is similar to that of polymers in that similar types of defects can occur. The dough is a viscoelastic fluid and as such die swell may also occur [77]. The presence of solvent and viscous heating could also cause evaporation of the solvent in extreme cases.

This processing method is not the only one that can be used, but it is often encountered in the production of propellants at the industrial scale. Other methods such as dry roll milling exist and using screw extruders has also been attempted. [68]

2.2.3 Erosivity of Gun Propellants

The erosivity of gun propellants was previously mentioned during this review of the literature. However, the particulars of this phenomenon have not yet been discussed. Erosion refers to the progressive wear a gun steel barrel and its rifling if present. As the barrel gets eroded, the performance of the gun system decreases until it is no longer reliable [78, 79]. The worst case scenario would be additional wear eventually leading to the rupture of the gun barrel although such a scenario is unlikely [80]. An additional concern is the replacement of barrels. As wear increases, barrels need to be replaced, the cost of new barrels and of transportation of the barrels can be significant. As a result, gun propellant erosivity has impacts on the performance, safety and economic aspects of gun systems. The erosion of a gun barrel can be divided into three different categories: thermal erosion, chemical erosion and mechanical erosion [80]. Mechanical erosion refers to the erosion due to the friction caused by a projectile and the gases passing through the barrel. Mechanical erosion is not as directly related to the composition of the propellant than thermal or chemical erosion are and will only be discussed where it is relevant to the discussion of thermal and chemical erosion. Figure 2.17 shows a rifled gun barrel before wear, a rifled barrel subjected to erosion and another where melt of the barrel steel occurred. This figure demonstrates well what the effects of gun barrel wear.
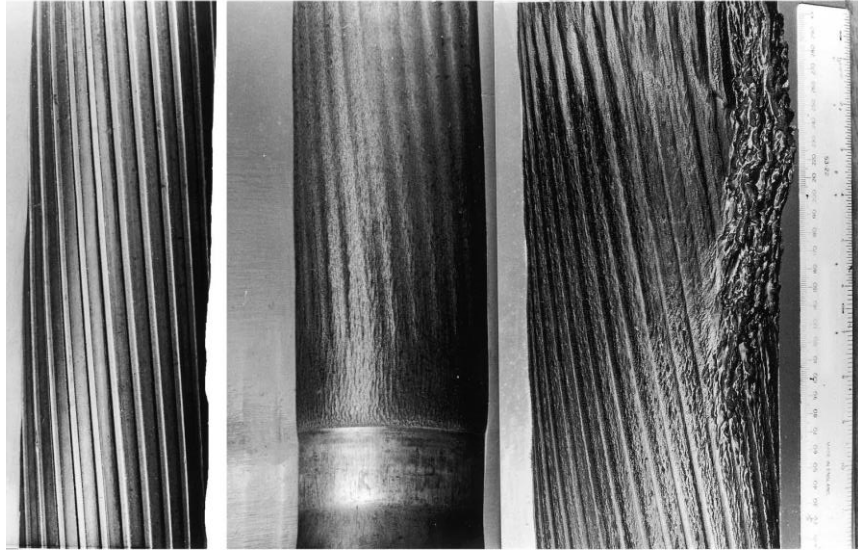
Figure 2.17: Erosion of gun barrels, from left to right: non-eroded barrel, typical erosion and melt erosion [79]

Chemical erosion refers to the wear incurred by the various gas species generated by the propellant charge reacting with gun steel [80]. When a propellant combusts, hot gases will be formed. These gases are mainly CO, CO_2, H_2O, N_2 and H_2. Another fraction of other gas species present in lower concentrations are oft referred to as the dissociated (or dissociation) products. The fact that reactions occur with the gun barrel materials implies that the temperature also plays a part as to which reactions occur and the rate of those reactions is also temperature dependent. The temperature in a gun system at the bore may reach temperatures in the range of 1800 K in a matter of milliseconds after the propellant has been ignited [81]. Additionally, the peak pressure in a gun system will reach hundreds of megapascals, the pressure varies significantly between different gun systems. Pressures of 400 MPa are typical or artillery systems while tank guns may reach pressures in the range of 700 MPa [81]. Reaction taking place in the gas phase are also highly influenced by the pressure. The pressure will also influence the rate at which a gas may diffuse in the gun material. This illustrates clearly that erosion types are linked to one another and that while it is practical to separate erosion between three types, there is no way to draw a clear line where each type of erosion starts and ends. Equations 2.10 to 2.15 show various reactions that can take place inside with gun steel due to the high temperatures and cause barrel erosion [80, 82, 83].

$$2CO \rightarrow C + CO_2 \qquad (2.10)$$
$$CO \rightarrow C + O \qquad (2.11)$$

$$3Fe + 2CO \rightarrow Fe_3C + CO_2 \tag{2.12}$$
$$Fe + CO_2 \rightarrow FeO + CO \tag{2.13}$$
$$4Fe + CO \rightarrow FeO + Fe_3C \tag{2.14}$$
$$5Fe + CO_2 \rightarrow 2FeO + Fe_3C \tag{2.15}$$

Each gas resulting from the combustion of propellants has an impact on the erosivity of gun propellants. The impact of each gas however is still open for debate as different works came up with different levels of erosivity for each decomposition gas. According to Kimura, the chemical erosivity of combustion gases can be summarized by equation 2.16 [83].

$$CO_2 > CO > H_2O > H_2 > 0 > N_2 \tag{2.16}$$

It was postulated that the presence of nitrogen in a propellant's combustion gases can lead to the formation of iron nitride which is used to mitigate gun barrel erosion [78]. This would either reduce erosion by the creation of an iron nitride layer or help regenerate an already present iron nitride treatment on the gun barrel. This has been referred to as dynamic nitriding and has been previously observed [84]. Efforts have also been made into the prediction of the erosivity of propellants where empirical models have been developed for common propellant (equations 2.17 to 2.22) [78, 79, 85].

$$w = A\exp(bT_{max}) \tag{2.17}$$

$$A = \exp(0.27f_{CO} + 0.23f_{CO_2} + 0.74f_{H_2} + 0.28f_{H_2O} + 0.16f_{N_2} + 1.55f_R = 31.36 \tag{2.18}$$

$$w = At_0\sqrt{\frac{T_i}{T_a}}\exp\left(-\frac{\Delta E}{RT_{max}}\right); T_a = 300 \, K \tag{2.19}$$

$$A = 114\exp\left[0.0207\left(f_{CO} - 3.3f_{CO_2} + 2.4f_{H_2} - 3.6f_{H_2O} - 0.5f_{N_2}\right)\right] \tag{2.20}$$

Where w is the wear per round, A is the erosivity of the propellant, T_{max} is the maximum temperature in the gun or vented vessel setup, b is a measure of the hardness of the gun barrel, f is the volume fraction of a given gas, T_i is the initial temperature of the gun battel, ΔE is an activation energy (estimated at ~69 kJ·mol^{-1} for gun steel), R is the universal gas constant and t_0 is a time constant related to the heat transfer from the combustion of the gun propellant to the gun barrel.

$$m_l = A \cdot \exp\left(\frac{1.5T_{max}}{B_0}\right) \tag{2.21}$$

$$\ln(10^3 A) = -0.273f_{CO_2} + 0.079 - 0.141f_{H_2} + 0.348f_{H_2O} - 0.019f_{N_2} + 1.002f_R \tag{2.22}$$

Where m_l is the mass loss fraction, A is an erosion coefficient based on the gas composition, T_{max} is the maximum surface temperature of the eroded material, B_0 is a hardness coefficient and f refer to the mole fraction percentage of the gas species in subscript.

This demonstrates the erosivity of gases differ and that these models are highly dependent on the propellants that used to generate these models. All models do have one thing in common however: CO is considered as an erosive gas. The erosivity of carbon monoxide is mostly due to the formation of iron carbide, see equations 2.29 and 2.31. Hydrogen has a somewhat more complex effect on gun barrel erosion. Hydrogen gas is a very small molecule compared to other gases, this gives it the ability to diffuse more easily into the gun steel and this results in reactions occurring deeper in the gun barrel [86]. Another suggested cause for the erosivity of hydrogen is that it increases heat transfer between the combustion gases and the gun barrel which results in increased chemical and thermal erosion due to increased reaction rates [83]. Even in the presence of a protective coating like hard chromium, this can lead to reaction occurring below the coating resulting in cracking and flaking of the protective layer. LOVA propellants containing nitramines often generate high amounts of hydrogen regardless of their flame temperature which can lead to cool propellants that are highly erosive [87].

The erosion models are not only dependent on the gas composition of the propellants, but also temperature dependent. The temperature plays two important roles on gun barrel erosion. Firstly, any chemical reaction is accelerated with increasing temperature. Erosion became a concern as early as the 1910s [88]. The other effect of temperature is to heat induced morphological changes in gun steel. These effects along with the effects of the combustion gases can be separated into two distinct layers: the chemically affected zone (CAZ) and thermally affected zone (TAZ), this is shown in Figure 2.18 [79] where changes in the morphology of the steel is easily observed. Figure 2.18 is a cut from a single barrel and gives an estimation of the relative depth of the different affected zones.
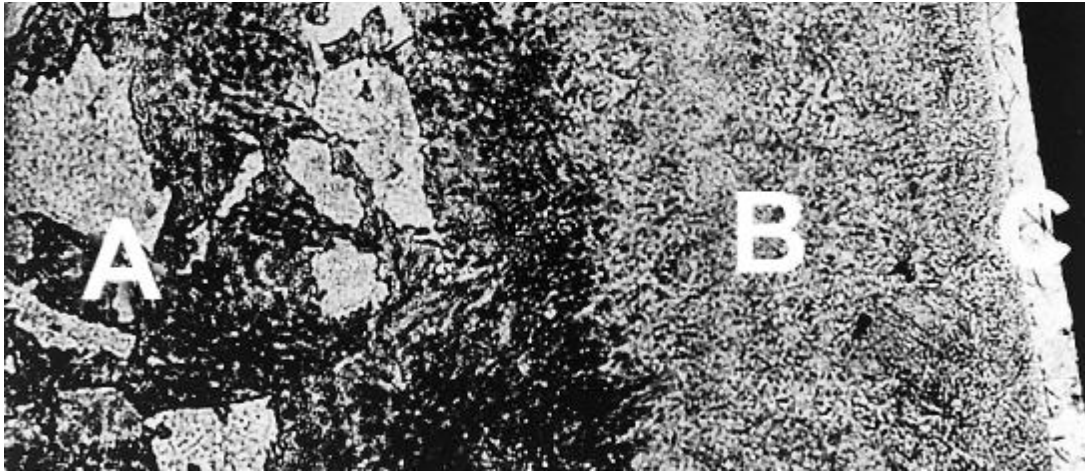
Figure 2.18: Microstructure of a gun barrel undergoing wear: A) steel at an unaffected depth from the bore surface, B) thermally affected zone, C) chemically affected zone, adapted from [79]

Table 2.4 shows the effects of temperature on gun steel. Gun steel is designed for mechanical properties that can withstand the pressure caused by the combustion of propellants. However, given the high flame temperature of propellants, repeated firings can cause temperatures high enough for the steel to incur morphological changes. It is also important to distinguish the flame temperature of the propellant from that of the gun barrel. Propellant flame temperatures can reach as high as 3500K, well above the temperatures shown in Table 2.4, the temperature of the gun barrel will be lower due to heat transfer from the gases to the steel via convection and radiation. The temperature of the gun barrel will be dependent on the flame temperature of the propellant, but also the firing rate and the composition of the combustion gases [79, 83, 89]. Lower firing rates will allow the steel to cool down between each firing compared to higher firing rates. This does not affect the erosivity of a propellant, but it will affect the wear rate of the gun barrel.

Table 2.4: Effects of temperature on gun steel [80]

Temperature [K]	Phenomenon
1000	Austenite phase transformation of steel
1050	Oxidation of iron
1270	Sulphidation of iron
1420	Melting point of iron carbide
1470	Melting point of iron sulphide
1640	Melting point of iron oxide
1720	Melting point of gun steel

In extreme cases, the increase in temperature will be enough to melt a thin layer of steel which will be removed by the passage of the projectile and the hot propellant gases in the barrel. This phenomena is referred to as melt wipe [84]. This is a good example of the combination of thermal and mechanical erosion. It can be considered a worse scenario and it is more likely that the gun steel will instead undergo morphological change to a different type of steel. These changes in the steel morphology can induce multiple effects that increase the erosion of the gun barrel [80]. The rapid heating and cooling due to propellant firings can lead to cracking, especially in austenite. The formation of iron carbide due to the presence of CO and CO_2 is also highly problematic. The melt temperature of iron carbide is significantly lower compared to gun steel. This leads to an increased likelihood of melt of a thin layer of the barrel due to propellant combustion. This type of phenomenon illustrates the interdependence of chemical and thermal erosion well. Another example of this is that austenite is more susceptible to chemical attacks resulting in higher erosivity [80]. These changes in the morphology of gun steel leading to softer and more brittle types of steel also impact mechanical erosion. These materials are more likely to be eroded due to the passing of a projectile or its driving band [79, 80]. In summary, the ideal propellant would be one with low flame temperature that generates a high amount of nitrogen, carbon dioxide and water rather than carbon monoxide and hydrogen. This also should be balanced with propellant performance where higher flame temperature and lower molecular weight gases generate higher performance for the same amount of propellant.

Often, to limit erosion, a hard chromium coating will be used to protect the inside of the gun barrel. However, the repeated thermal expansion and contraction of the steel and chromium will lead to cracks [81]. These cracks then lead to part of the gun steel being exposed to the combustion gases which will lead to thermal and chemical erosion. The coating will also eventually flake exposing entire areas of the barrel to erosion which leads to very uneven wear [90].

The measurement of erosion requires either a gun system or a vented vessel. The use of a gun system while more representative of actual erosion is expensive and access to those kind of systems is also limited. Vented vessels allow for laboratory scale testing, their design can be separated into two categories, choke type and with rupture discs. The choke type vessel allows for the propellant gases to escape as they burn and has been used for some erosion modeling [79, 83, 91] while vessels equipped with rupture discs were used in other modeling efforts [84, 85]. Both types of vented vessels are shown in Figures 2.19 and 2.20.
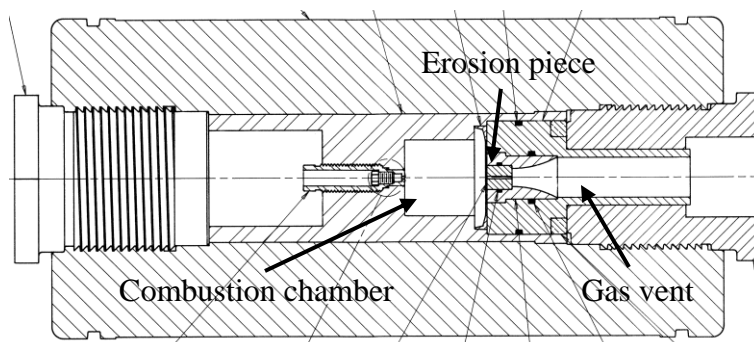
Figure 2.19: Choke type vented vessel used by DRDC-Valcartier used for erosion testing
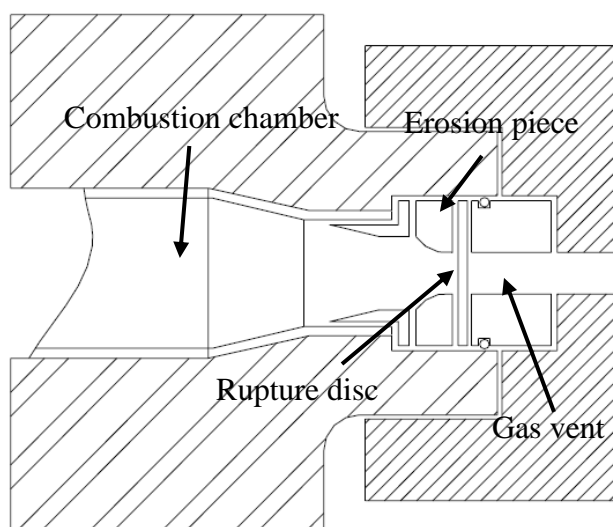
Figure 2.20: Vented vessel with rupture disc used for erosion testing by ARL, adapted from [91]

The problem associated with erosion of gun barrels is a complex one as demonstrated in this section. However, it is possible to draw a few conclusions from the literature surveyed. Firstly, propellants that generate low amounts of hydrogen and carbon monoxide will be less erosive. This favors the production of carbon dioxide and nitrogen over other combustion products. However, CO_2 is a heavier gas which will lead to a lower impetus at the same flame temperature (less moles of gas are produced). This favors nitrogen gas over CO_2 in terms of performance and erosivity of the combustion gases. The second important conclusion is that lower flame temperature of propellants will lead to lower erosivity. This puts the production of CO_2 at a further disadvantage as a more complete combustion of carbon will lead to higher flame temperatures. As a result, nitrogen-rich materials are of interest to develop less erosive novel propellants. Despite this, the open scientific literature is relatively empty of attempts at using nitrogen-rich materials to develop low erosivity propellants.

2.2.4 Nitrogen-rich Materials as Monopropellants

While the research into new energetic materials, especially nitrogen-rich species is flourishing to say the least, the peer reviewed literature is surprisingly scarce when it comes to nitrogen-rich materials used as monopropellants or as performance modifiers in propellant formulations. This can be explained in part by the quantities of materials required for burning rate characterization. Firing a propellant in a 700 cm^3 closed vessel at a loading density of 0.2 g·cm^{-3} as was performed for a few select nitrogen-rich species [92, 93] requires 140 g of propellant per test and multiple tests must be performed. Even at concentrations of 5% mass nitrogen-rich materials, syntheses at the multi gram scale are required. Higher nitrogen-rich content will require even more materials. On the other hand, the characterization of sensitivity, crystal structure, spectroscopy, etc. requires very little quantities of materials, even quantities below 1 g can be adequate [29, 50]. This fact could explain the current lack of characterization of nitrogen-rich materials as propellants. This is not to say that the scale-up of the synthesis of some nitrogen-rich materials has not been achieved, only that so far, it has been extremely limited in scope [43].

Thermochemical data on nitrogen-rich materials in propellants is more readily available as it requires no experimentation, but its usefulness is limited. The performance of a propulsion system, be it for rocket or gun applications is strongly dependent not just on the thermochemical properties of the propellant, but also on the burning rate of the latter.

Some nitrogen-rich materials TAGZT [73, 94], DAATO$_{3.5}$ [72], BTATz [63, 95], DAAF [63], DHT [63, 95], 3,6-bisnitroguanyl-1,2,4,5-tetrazine (NQ$_2$Tz) and its triaminoguanidine salt [55] have been characterized as monopropellants or with a small amount of binder by strand burner experiments. Triaminoguanidinium salts of 3,3'-dinitro-5,5'-azo-1,2,4-triazole and 3,3'-dinitro-5,5'-azoxy-1,2,4-triazole [56] and the mono, di and tri aminoguanidinium salts of 4,4',5,5'-Tetranitro-2,2'-biimidazolate have also been investigated as monopropellants [96]. Those experiments were carried at pressure ranges of roughly 1 MPa to 10 MPa which are more akin to rocket pressures than gun pressures. In these instances, specific impulse is also provided as a measure of performance rather than Impetus. All nitrogen-rich materials tested exhibited low pressure exponents and high linear burning rate coefficients. Figures 2.21 and 2.22 show some of those results.
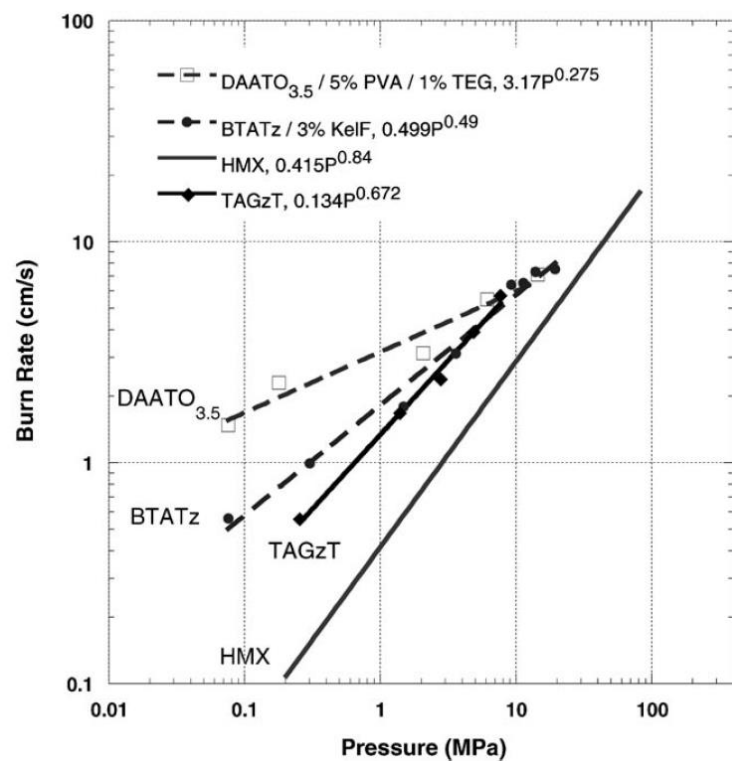
Figure 2.21: Burning rates of TAGZT, BTATz and DAATO [73]
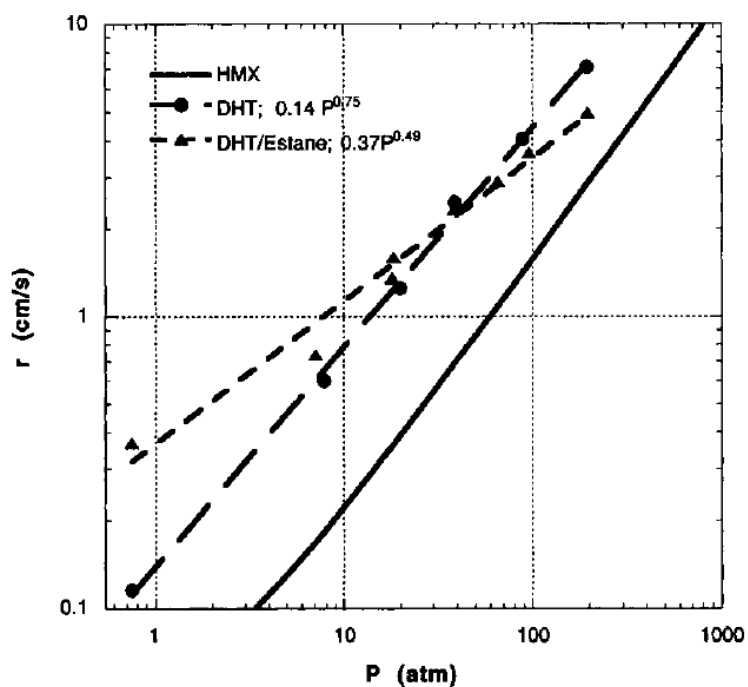
Figure 2.22: Burning rate of DHT [63]

Table 2.5 shows burning rate data for more pure nitrogen-rich materials at similar pressure ranges. All data was obtained using a strand burner setup. In most cases, the pressure rarely exceeded 10 MPa. HMX is provided as the reference energetic material in some of the works.

Table 2.5: Burning rates of nitrogen-rich materials as monopropellants

EM	I_{sp} [s]	β [cm·s^{-1}·MPa$^{-\alpha}$]	α	Range [MPa]
HMX [73]	266[1]	0.415	0.84	0.2-90
TAGZT [73]	217[1]	0.134	0.672	0.2-10
DAATO$_{3.5}$/5% PVA/1% TEG [72]	258[1]	3.17	0.275	0.2-20
BTATz/3% KelF [63]	219	1.78	0.49	0.2-20
DHT [63]	235	0.780	0.75	0.2-20
DAAF [63]	234	0.158	0.71	0.2-20
NQ$_2$Tz [55]	219[1]	1.31	0.163	0.2-7
TAGNQ$_2$Tz [55]	237[1]	1.14	0.366	0.2-7
DNAT [56]	-	0.073	0.760	0.21-7
TAGDNAT [56]	-	2.552	0.507	0.21-7
TAGDNATO [56]	-	1.592	0.566	0.21-7
MAGN4BIM [96]	194	0.087	0.753	2.4-8.6
DAGN4BIM [96]	206	0.293	0.618	2.4-8.6
TAGN4BIM [96]	214	1.301	0.413	2.4-8.6

These burning rate results are interesting as they show low pressure dependency and high linear burn rate coefficients for pure nitrogen-rich materials. This results in high burning rates even in the early stages of combustion and the low pressure dependency helps to avoid combustion instabilities that can occur in propellants with high pressure exponents [93]. Tetrazine compounds represent the most characterized family of energetic materials at rocket pressures along with some azoles.

2.2.5 Nitrogen-rich Materials in Gun Propellants

Literature on the effects of nitrogen-rich materials as and incorporated into gun propellants is even more scarce. There is some interesting thermochemical data that resulted from investigations into potentially low erosivity propellant formulations. These results are presented in Figure 2.23 where multiple nitrogen-rich materials were considered as partial RDX replacement in the EX-99 propellant formulation. The compositions of the various propellants are presented in Table 2.6, M1 is a highly used common propellant provided as a reference.

---

[1] Values of specific impulse reported in [94]
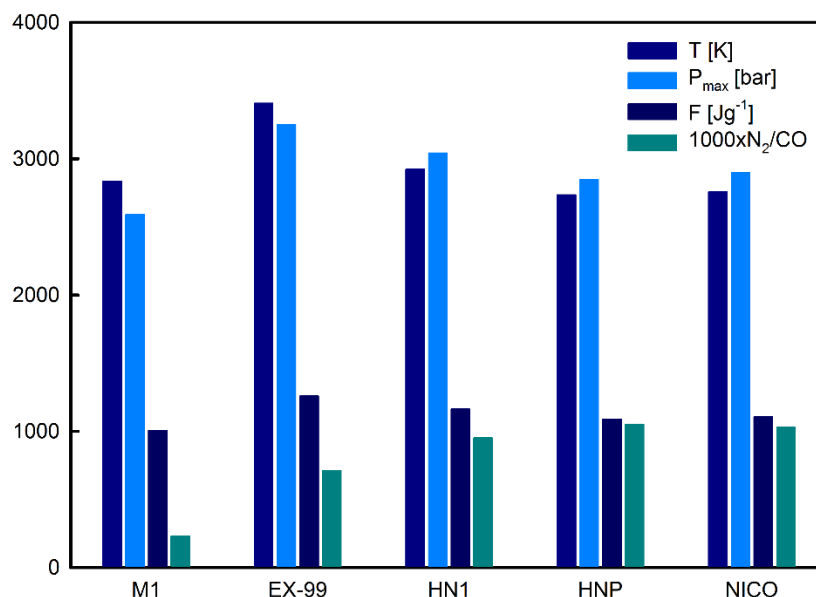
Figure 2.23: Thermochemical properties of some nitrogen-rich propellants, adapted from [26]

Table 2.6: Composition of the nitrogen-rich propellants in Figure 2.23, adapted from [26]

Propellant	Constituents	Weight ratio [%]
M1	NC 13.25%/2,4-DNT/DBP/DPA	86/10/3/1
EX-99	RDX/CAB/BDNPA/F/NC 13.25%	76/12/8/4
HN1	RDX/TAGZT/CAB/BDNPA/F/NC 13.25%	56/20/12/8/4
HNP	RDX/TAGZT/FOX-12/CAB/BDNPA/F/NC 13.25%	40/20/16/12/8/4
NICO	RDX/TAGBT/FOX-12/CAB/BDNPA/F/NC 13.25%	40/20/16/12/8/4

Other bistetrazolate salts were investigated as potential replacements for RDX in EX-99 with and without FOX-12 (thermochemical data not shown) [3]. The overall trend of the results is however the same: decrease in flame temperature, significant increase in N_2/CO ratio and a somewhat small decrease of the propellant's impetus.

There has been some work performed on burning rates of nitrogen-rich materials in gun CMDB propellant formulations including RDX as the reference propellant. The effects of BTATz on RDX based CMDB compositions were investigated both with and without ballistic modifiers [97]. The thermal stability, isoconvertional kinetics and pressure DSC behavior have also been investigated [98, 99]. The kinetics of propellant decomposition in DSC were found to follow second order reactions. In this case as well, the pressures at which the burning rates of these propellants was limited to an order of magnitude below the pressures observed in a gun system. The burning rate data is presented in Table 2.7.

Table 2.7: Burning rates of BTATz containing CMDB propellants, adapted from [97]

Propellant	β [cm·s^{-1}·MPa$^{-α}$]	α	Pressure Range [MPa]
NC/NG/RDX/Aux[2] (38/28/26/8)	0.189[3]	0.800[3]	8-22
	0.200[3]	0.781[3]	10-22
	0.194[3]	0.795[3]	14-20
NC/NG/BTATz/Aux[4] (38/28/26/8)	0.325	0.723	8-22
	0.333	0.714	10-22
	0.328	0.719	14-20
NC/NG/BTATz/Aux[5] (38/28/26/8)	0.658	0.522	8-22
	0.136	0.459	10-22
	1.069	0.353	14-20

Some nitrogen-rich salts have also been characterized in propellants. Firstly, TAGZT/RDX mixtures were investigated both experimentally [100] and numerically [101]. The results of the experimental characterization if RDX-TAGZT mixtures is shown in Table 2.8.

Table 2.8: Performance characteristics of RDX/TAGZT propellants [100]

Propellant	I_{sp} [s]	β [cm·s^{-1}·MPa$^{-α}$]	α
TAGzT	217	1.34	0.67
TAGzT/RDX (90/10)	220	1.66	0.66
TAGzT/RDX (50/50)	232	0.59	0.90
TAGzT/RDX (25/75)	251	0.45	0.86
RDX	267	0.25	0.80

Guanidinium 5-aminotetrazolate (GA), guanidinium nitrate (GN), triaminoguanidinium nitrate (TAGN) and triaminoguanidinium azide (TAGAZ) have also been investigated using a closed vessel at a loading density of 0.2 g·cm^{-3} [92, 93]. The propellant composition, thermochemical data and burning rate law parameters for the mentioned propellant formulations are presented in Table 2.9.

---

[2] The auxiliary ingredient is not mentioned in the original paper

[3] Burning rate law parameters were unavailable for the reference and were calculated from available burning rate data

[4] Auxiliary ingredients include dihydroyethylamine-dinitrate and other non-disclosed components

[5] A mixture of lead phthalate and carbon black, 3.5% mass fraction was added to the propellant

Table 2.9: Thermochemical and burning rate law parameters of nitrogen-rich salt containing propellants, adapted from [92, 93]

Propellant	F [J·g^{-1}]	T$_{ad}$ [K]	β [cm·s^{-1}·MPa$^{-\alpha}$]	α
NC 13.1%/RDX/DOP/EC (28/65/6/1)	1203	3210	0.14	0.84
NC 13.1%/RDX/GA/DOP/S^6 (28/60/5/6/1)	1185	3090	0.14	0.85
NC 13.1%/RDX/GA/DOP/S^6 (28/55/10/6/1)	1170	2980	0.14	0.85
NC 13.1%/RDX/GA/DOP/S^6 (28/50/15/6/1)	1160	2870	0.15	0.90
NC 13.1%/RDX/GA/DOP/S^6 (28/45/20/6/1)	1140	2760	0.13	0.80
NC 13.1%/RDX/GA/DOP/S^6 (28/40/25/6/1)	1120	2650	0.13	0.80
NC 13.1%/RDX/TAGN/DOP/S^6 (28/50/15/6/1)	1165	2995	0.30	1.40
NC 13.1%/RDX/TAGAZ/DOP/S^6 (28/50/15/6/1)	1160	2855	0.30	1.40
NC 13.1%/RDX/GN/DOP/EC (28/50/15/6/1)	1118	2815	0.13	0.80

BTATz propellants exhibit low pressure dependency compared to the reference propellant that has a higher pressure exponent. On the other hand, TAGN and TAGAZ show a marked increase in pressure exponent and this has been flagged as a potential issue [93]. There are however ways to design propellants around this if the other properties are desirable, such as changing the propellant's web [93]. GA on the other hand doesn't show the highly pressure dependent behavior shown by some triaminoguanidinium salts.

The burning rate data available on pure nitrogen-rich materials and nitrogen-rich materials in propellants show that in general, nitrogen-rich materials tend to have very high burning rates, even at low pressures. However, the pressure exponent α is highly variable between different materials and this behavior carries over to propellant formulations incorporating these materials. Furthermore, it has been shown that most of the burning rate data obtained was at relatively low pressures and that there is very little data available on nitrogen-rich materials at pressures above 20 MPa. The high burning rates is especially of interest since it shows that nitrogen-rich materials could be used in small quantities as modifiers for current propellants. Larger quantities may not lead to higher burn rates or the increase in burning rate could hit a plateau as was the case with TAGZT/RDX mixtures.

TAGZT is one of the most investigated nitrogen-rich materials. This is very likely due to the fact that production was scaled up to the multi-kilogram scale making the material readily available to a series of entities in the United States [43]. In fact, most of the nitrogen-rich materials which have

---

[6] S refers to a stabilizer mixture of 50% ethyl centralite and 50% resorcinol

been tested for propulsion applications are among the oldest discovered which left time for the scale-up of their synthesis.

In summary, while there has been an impressive amount of work focusing on the discovery of new nitrogen-rich materials. The amount of work performed with the goal of assessing the propulsion applications of nitrogen-rich materials is in comparison lacking. The little amount of work performed points to benefits in terms of performance, but this has yet to be fully established. More work is needed in order to understand the impact of nitrogen-rich materials on propellants. This is especially true of newer families of nitrogen-rich materials which have been synthesized in the 21st century. This type of work is more labor intensive than synthesizing new materials. This is due to concerns with the quantities of energetic materials necessary, the need of specialized facilities and qualified personnel to make the propellants. Not only are the performance aspects of nitrogen-rich materials poorly understood, but the safety aspects of such propellants are also missing from the available scientific literature aside from a few very specific cases. This type of research is necessary to better understand the advantages and drawbacks associated with nitrogen-rich materials.

CHAPTER 3   GLOBAL APPROACH AND METHODOLOGY

To remedy to the deficiencies identified in chapters 1 and 2, the research project presented in this thesis was initiated in partnership with Defense Research and Development Canada (DRDC) Valcartier, U.S. Army Armament Research, Development and Engineering Center (ARDEC) and General Dynamics Ordnance and Tactical Systems (GD-OTS) Canada Valleyfield. This section presents the methodological approach and motivations behind the choices of materials and experiments for the entire project. Additional precisions on the methodology is presented in the chapters associated with the resulting scientific articles.

3.1 Nitrogen-rich Materials

Four nitrogen-rich materials were chosen for this work. The choice of nitrogen-rich materials was performed using the following criteria:

- Explosive performance similar or better than that of RDX.

- Availability of chemical precursors.

- Synthesis of three or less steps for ease of scale-up.

- Reported sensitivity equal or lower than those reported for RDX.

- Intermediaries during the synthesis must also be relatively insensitive, no micro explosions in the reactor and safe handling of intermediaries must be ensured.

- Varied chemical structures.

This lead to the choice of the following nitrogen-rich materials: 5,5′-hydrazinebistetrazole (HBT); 5,5′-bis(1H-tetrazolyl)-amine (BTA); 5-aminotetrazolium nitrate (HAT-NO$_3$) and 3,6-dihydrazino-1,2,4,5-tetrazine (DHT). The synthesis methods for these materials are shown in Figures 3.1 to 3.4. A detailed list of the nitrogen-rich energetic materials that were considered is presented in Appendix A.
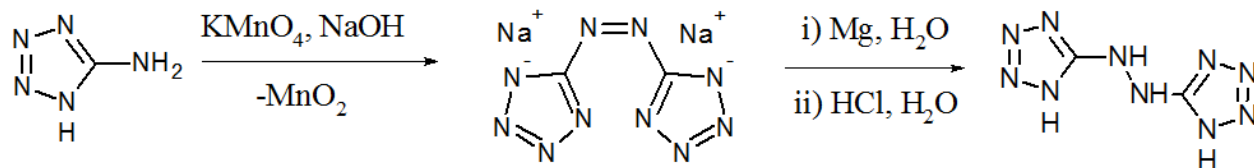
Figure 3.1 : Synthesis reactions of HBT

HBT was chosen due to its reported performance and sensitivity which are similar to those of RDX [3]. The synthesis was also previously optimized in our laboratories [102], this gave a good starting point with a molecule for which the feasibility of the synthesis was known.
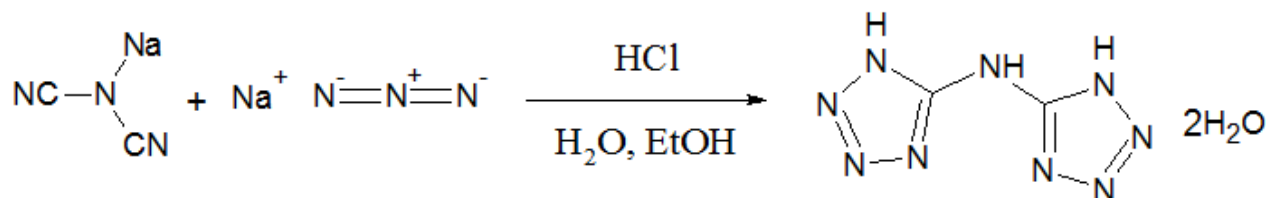
Figure 3.2: Synthesis reaction of BTA

BTA was also chosen for tis reported explosive performance which was deemed better than HBT and RDX [64]. BTA also provided a molecule similar to HBT which made for a good comparison of tetrazole type molecules with differing performance. The one-step synthesis also proved attractive and easy to perform. The synthesis yielded the monohydrate of BTA, reported as less sensitive which made its storage and transport safer. The molecule could be dehydrated to obtain BTA prior to its incorporation in propellants.
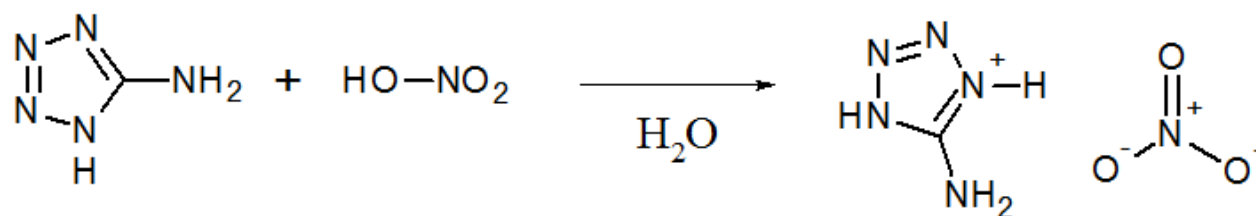
Figure 3.3: Synthesis reaction of HAT-NO$_3$

HAT-NO$_3$ was chosen as a tetrazole salt. The interest in tetrazoles for their balance between energetic content and stability was discussed in chapter 2. Its explosive performance and almost neutral oxygen balance along with the fact that it is an ionic molecule were the primary factor in choosing it [48]. The one-step synthesis from affordable and readily available reagents was also a

factor in its choice over 1,5-diaminotetrazolium nitrate which has good performance, but a complicated synthesis [103].
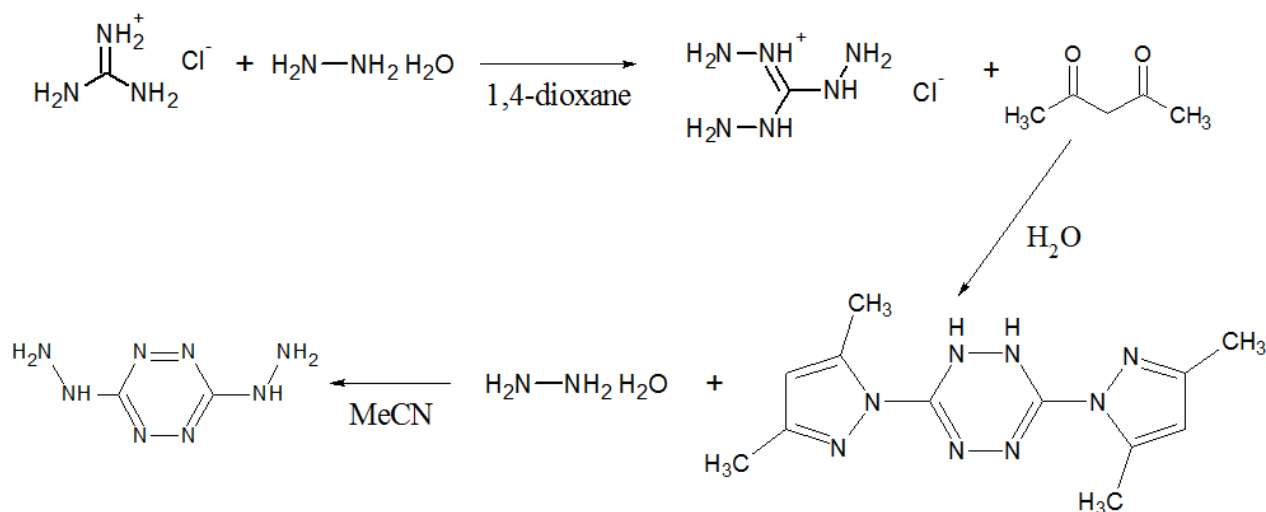
Figure 3.4: Synthesis reactions of DHT

DHT was chosen in part because it is a tetrazine based energetic materials. It is also one of the simplest tetrazines to synthesize [104, 105]. 1,2,4,5-tetrazines or *s*-tetrazines share the intermediary presented in Figure 3.4 and all *s*-tetrazines encountered in the literature followed the same reaction pathway up to 3,6-bis(3,5-dimethylpyrazol-1-yl)-1,2-dihydro-*s*-tetrazine (BDDT) [58, 65, 104-106]. The other factors that influenced the choice of DHT as a tetrazine were its reported monopropellant performance [63] and the fact that it had previously been synthesized at DRDC-Valcartier. In hindsight, this proved invaluable in troubleshooting issues encountered during the synthesis of DHT.

3.2 Reference Propellant

The reference propellant that was chosen for the nitrogen-rich materials to be incorporated in was a triple base propellant composed of nitrocellulose (NC), trimethylolethane trinitrate (TMETN) and triethylene glycol dinitrate (TEGDN). This propellant was chosen for its calculated thermochemical performance, its reported burning rate [71] and also the fact that it was a well-known gun propellant and not fielded by the CAF. Additionally, this would allow to determine if nitrogen-rich materials could provide the performance required of modern propellants. The availability of materials for the manufacturing of the propellants at DRDC-Valcartier was another motivation for using this propellant as the reference. The high plasticizer content also proved useful

in making the propellant easier to work with. It also helped to avoid cracking and the formation of porosity with the addition of nitrogen-rich materials.

3.3 Nitrogen-rich Propellants

It was decided to incorporate the nitrogen-rich materials in concentrations of 5%, 15%, 25% and 35% weight (m/m) in the reference formulations. The concentrations of nitrogen-rich materials were motivated by the desire to quantify the effects of these materials with increasing concentration. Furthermore, concentration higher than 20% were markedly absent from the literature in both rocket and gun conditions. Finally, time and material constraints were also considered. 250 g of each nitrogen-rich material was the required minimum amount of material to perform the experimental work. This quantity is non-negligible, and the synthesis had to be performed in much smaller quantities (25g or less) due to safety concerns should accidental initiation of any of the materials occur during their synthesis.

The nitrogen-rich materials were incorporated in the reference formulation in a way which kept the plasticizer to nitrocellulose ratio constant. This ensured that the plasticizer content would not be too low and cause plasticization of the nitrocellulose or high enough to desorb from the propellant. The former would cause the propellant to crack during the drying step and the latter would change the composition between different propellant formulations.

3.4 Propellant Characterization

Propellant performance was characterized using the Cheetah thermochemical computer code to obtain the performance data under adiabatic conditions. Experimental determination of performance was performed using a closed vessel apparatus. The performance calculated from the closed vessel results was done using standard MIL-STD-286C [107] and the BRLCB and XLCB burning rate computer codes [74, 108]. Additional performance simulations were using the IBHVG2 code to obtain internal ballistic data and muzzle velocities for the different propellants.

Error measurements on burning rate data was calculated as two standard deviations of the average of multiple closed vessel tests. A minimum of two tests were performed and if there was any significant difference between the calculated burning rates, additional tests were performed to identify outliers and the additional tests were factored into the average data. Error on burning rate

regressions was calculated as two standard deviations of the error on the regression parameters of the burning rate law equation.

The following section demonstrates how the burning rate of a propellant can be calculated using computer codes like BRLCB and XLCB [74, 108]. The pre-treatment of the pressure time data will not be discussed aside from the fact that the data is usually smoothed, and outlier data points removed prior to performing the burning rate calculations. The following additional assumptions are made:

- The closed vessel is treated as a well stirred vessel (properties are spatially invariant).

- Kinetic energy is negligible compared to thermal and chemical energy.

- The igniter is completely burnt upon ignition of the propellant.

- All thermochemical properties of the propellant are known.

- The Noble-Abel equation of state describes the state of the gases in the closed vessel adequately.

The fraction of propellant mass remaining in the closed vessel can be defined by equation 3.1.

$$\xi = \frac{m_p}{m_p^0} \tag{3.1}$$

Where ξ is the fraction of propellant remaining, m_p is the mass of propellant remaining in the closed vessel and m_p^0 is the initial mass of propellant that was present of the closed vessel.

The quantity of propellant burned is directly related to the "depth" of propellant that has undergone combustion (equation 3.2).

$$dV(x) = S(x)dx \tag{3.2}$$

Where $S(x)$ is the surface area of the propellant at depth x and x is the direction normal to the surface of the propellant. Integrating this equation and with the known density of the propellant known, the mass of propellant consumed can be calculated from equation 3.3.

$$(1 - \xi)m_p^0 = \int_{x_0}^{x} \rho(x)S(x)dx \tag{3.3}$$

This equation is the basic relation between the mass of propellant burn and the change in surface area or "form function" of the propellant. The density of the propellant $\rho(x)$ is assumed to be

variable with depth, but most of the time, the density of a propellant is uniform. Throughout the discussion on how to calculate the burning rate of a propellant from closed vessel data, the properties will be assumed isotropic. This form function can be defined in multiple ways, analytical solutions for some form functions can also be found in reference [20]. Mass conservation implies that the mass of gas in any given time in the closed vessel is the same as the mass of propellant that underwent combustion (equation 3.4).

$$m_g(t) = m_p^0(1 - \xi) \tag{3.4}$$

Where $m_g(t)$ is the mass of gas released by the combustion of the propellant. This quantity can be related to the pressure by a gas phase EOS. In this case, the equation used is the Abel-Nobel equation of state which can be defined according to equation 3.5. Equation 3.5 is a different form of equation 2.5 based on mass of gas instead of moles of gas.

$$P_{ch}(V_{free} - bm) = m\mathfrak{R}T_{ch} \tag{3.5}$$

Where P_{ch} is the pressure in the closed vessel, b is the covolume, m is the mass of gas, $\mathfrak{R}$ is the universal gas constant divided by the molecular weight of the gas mixture and T_{ch} is the temperature of the gases. V_{free} is the volume not occupied by the propellant in the closed vessel which is defined by equation 3.6.

$$V_{free} = V_{ch} - \frac{\xi m_p^0}{\rho_p} \tag{3.6}$$

Where V_{ch} is the overall volume of the closed vessel and ρ_p is the density of the propellant. Common closed vessel volumes are 90 cm^3, 200 cm^3 and 700 cm^3. Considering that in a closed vessel, an igniter, air and gases from the combustion of the propellant are present, the EOS can be rewritten as equation 3.7 to consider both the contributions of air and the igniter. The volume occupied by the igniter is assumed to be small enough that it has no significant impact on V_{free} and is therefore ignored. The mass of igniter is very small compared to that of the propellant which validates this assumption.

$$P_{ch}(V_{free} - m_p b_p - m_i b_i - m_{air} b_{air}) = (m_g \mathfrak{R}_p + m_i \mathfrak{R}_i + m_{air} \mathfrak{R}_{air})T_{ch} \tag{3.7}$$

Where the subscript "i" denotes the igniter (gas phase), the subscript "air" denotes air and the subscript "p" denotes the propellant. $\mathfrak{R}$ is the universal gas constant divided by the molecular weight of the gas specie denoted by the subscript.

The total energy in the closed vessel can be expressed by equation 3.8.

$$E_0 = E(t) + Q_w(t) \tag{3.8}$$

Where E_0 is the initial energy present in the system including the chemical energy stored in the propellant, $E(t)$ is the total energy contained in the closed vessel's volume and $Q_w(t)$ is the cumulative heat loss from $t = 0$ to t. E_0 is defined by equation 3.9.

$$E_0 = m_p^0 \theta_p^0 + m_i \theta_i^0 \tag{3.9}$$

Where θ^0 is the specific internal energy at the reference condition denoted as "0". This equation neglects the stored thermal energy of the material at the initial temperature. For any instant greater than $t = 0$, the igniter has completely burned and is in the gas state. The total energy can then be expressed as equation 3.10.

$$E(t) = m_p \theta_p^0 + T_{ch}(m_g C_{v_p} + m_{air} C_{v_{air}} + m_i C_{v_i}) \tag{3.10}$$

Where C_v is the specific heat at constant volume. Equation 3.8 can be rewritten as equation 3.11.

$$E_0 - Q_w(t) = m_p \theta_p^0 + T_{ch}(m_g C_{v_p} + m_{air} C_{v_{air}} + m_i C_{v_i}) \tag{3.11}$$

Solving equations 3.7 and 3.11 will allow the mass of propellant burned to be calculated for each $P(t)$ data point recorded. This however requires the cumulative heat loss $Q_w(t)$. From equation 3.11, it is clear that $Q_w(t)$ can have a large influence on the calculated burning rate of any given propellant. There is no consensus on how the heat losses should be calculated. The challenge stems from the fact that the time to full combustion of a propellant in a closed vessel takes only a few milliseconds making direct measurement of the temperature of the combustions gases extremely difficult. Measurement instruments need to have a very fast response time to keep track of the temperature which prevents the use of standard thermocouples. Furthermore, the combustion of the propellant can generate a significant amount of soot making optical measurements of temperature such as infrared difficult.

The treatment of the heat loss fraction in BRLCB and XLCB is handled according to equation 3.12 [74, 108].

$$Q_w(t) = \frac{P_{ch}}{P_{chmax}} Q_{max} \tag{3.12}$$

Where P_{chmax} is the pressure at propellant burnout, in other words the maximum recorded pressure in the closed vessel upon complete burnout of the propellant and Q_{max} is the maximum cumulative heat loss. By evaluating T_{ch} at P_{chmax} from equation 3.7, Q_{max} can be calculated from equation 3.11.

Once the mass of propellant burned over time is calculated, the burning rate of the propellant can be deduced from equation 3.13.

$$r = \frac{dm_p/dt}{\rho_p S(t)} \qquad (3.13)$$

Where dm_p/dt is the derivative of the mass of propellant burned over time and $S(t)$ is the surface area of the propellant. $S(t)$ can be related to the mass fraction of propellant burnt ξ by use of the appropriate form function. Once the burning rates calculated, the burning rate law can be calculated.

Given the assumptions made during the calculations of the burning rates of a propellant, the burning rate law is usually calculated over a given pressure interval. The dynamic vivacity can be used to select one or more appropriate pressure intervals. The dynamic vivacity is defined by equation 3.14.

$$A = \frac{dP/dt}{P(t) \cdot P_{max}} \qquad (3.14)$$

Where A is the dynamic vivacity, dP/dt is the derivative of the pressure over time, $P(t)$ is the pressure and P_{max} is the pressure at the propellant burnout. The dynamic vivacity should reflect the form function of the propellant if the burning rate data is accurate [109]. The dynamic vivacity is calculated from the pressure time data obtained during the closed vessel experiment and it is not subject to errors that may induced by the treatment of heat losses and other assumptions made during the calculations of the burning rate.

Other measurements of performance include the relative quickness (RQ), equation 3.16 and relative force (RF), equation 3.17. The relative quickness is calculated using a reference propellant and is a measure of how quickly the pressure increases over time as a function of the pressure (equation 3.15).

$$\frac{dP}{dt} = f(P) \qquad (3.15)$$

The methods that can be used to calculate the relative quickness are described in standard MIL-STD-286C [107].

$$RQ = \frac{1}{m}\sum_{i=1}^{m}\left(\frac{100}{n}\sum_{j=1}^{n}\frac{T_{ij}}{R_{ij}}\right) \times 100\% \qquad (3.16)$$

Where m is the number of reference test firings in a closed vessel, n is the number of data points per firing (usually four), T_{ij} is the value of dP/dt for the propellant tested taken at pressure "j" for test firing "i" and R_{ij} is the value of dP/dt for the reference propellant.

The relative force is simply the ratio of the maximum pressure of the propellant to that of the reference pressure.

$$RF = \frac{1}{m} \sum_{i=1}^{m} \frac{P_{\text{max},i}}{P_{max,ref,i}} \times 100\% \tag{3.17}$$

Where m is the number of test firings in a closed vessel, P_{max} is the maximum pressure observed in the closed vessel for the test propellant and $P_{max,ref}$ is the maximum pressure observed in the closed vessel for the reference propellant.

The relative force can be taken as a measure of the total energy stored in the propellant as the pressure will also depend on the molecular weight and flame temperature of the combustion gases of the propellant. Contrary to the impetus, this measure of performance is not under adiabatic conditions due to the heat losses to the closed vessel. Due to the time scale of the propellant combustion (milliseconds) and additionally if a volume reducing sleeve is used, completely adiabatic conditions are impossible to obtain. Heat losses can range from 5% without a volume reducing sleeve to 40% if a sleeve is used.

The principal advantage of the RQ and RF measurements is that they are derived from the pressure-time data of a closed vessel experiment. This avoids the effects of the heat loss modeling used to calculate the burning rate and does not require the assumptions made for those calculations either.

This section demonstrates well that propellant performance is dependent on multiple factors. Some of these factors, the thermochemical ones are relatively easy to predict and the methods to do so are well known. These parameters are far from the only ones affecting performance however. The burning rate has a large influence on the actual performance of the propellant when it is used in a rocker or gun system as it will affect how the chemical energy contained in the propellant will be released during its combustion. The burning rate can be deduced from pressure-time data with relative ease, although, care must be taken with how the treatment of the data is performed. It can then be modeled using Vielle's empirical law. More in-depth modeling involving detailed reaction kinetics are desirable, but pose significant challenges. These challenges are the number of competing reactions taking place, the lack of data available on how many energetic materials

decompose as single materials, let alone how they react with other energetics and the computational performance required to perform this type of analysis [110]. Kinetic modelling of even two energetic materials can involve hundreds of reactions and additional modeling of the heat transfer in the material and diffusion of the various participating species [101]. Modern propellants are composed of multiple energetic materials, plasticizers, stabilizers and other ingredients such as burning rate moderators, flash suppressants, etc. This means that multiple chemical species will participate in the decomposition of the propellant further complicating the modelling. These reactions will also be dependent on the temperature and pressure which will vary when ingredient proportions are changed as well. Lastly, the form of the propellant also has an influence on its performance. While this parameter is purely physical, the surface area of the chosen geometry and defects affecting said surface will influence the amount of gas generated by the propellant over time independently of how fast the propellant burns. The geometry is a direct result of the processing of the propellant and poor processing will result in defects that can lead to catastrophic failure of the system where the propellant is used. Care has to be taken to insure the desired geometry is achieved.

The stability of the propellants was measured using DSC and a vacuum stability (VST) apparatus. The DSC provided information related to the decomposition temperature of the propellants and the influence of the nitrogen-rich materials on short-term stability and decomposition temperature. The vacuum stability testing was used to provide information on the long-term compatibility of the nitrated esters present in the reference propellant and the nitrogen-rich materials.

3.5 Erosion

The main motivation behind the characterization of the erosivity of nitrogen-rich propellants was that no data on erosivity and nitrogen-rich materials was found in the scientific literature. Claims of significantly lower erosivity and barrel wear were however found [8]. Erosion modeling also agreed that higher nitrogen content should be beneficial [79, 83, 85]. The erosion of nitrogen-rich propellants part of the project was planned to be initiated after the initial characterization of the effects of nitrogen-rich materials on the performance and stability of propellants. Two nitrogen-rich materials were to be chosen based on these results. These two nitrogen-rich materials were HBT and BTA in large part due to stability and compatibility concerns.

The propellant formulation was to be chosen during the planning of the erosion experiments as it may have been judicious to use a different reference propellant. Thermochemical calculations however revealed that the reference propellant previously used with 35% (m/m) nitrogen-rich materials was adequate and offered a good comparative to M1 and JA2, two well known and fielded propellants. This also provided an opportunity to build upon the previous work related to the performance of nitrogen-rich materials in propellants.

The higher quantities of nitrogen-rich materials and the high quantities of propellant required for erosion testing also meant that scaling up the synthesis of HBT and BTA was necessary. This was performed using facilities at GD-OTS Valleyfield.

The characterization of the erosivity was performed using the vented vessel available at DRDC-Valcartier. The erosion was measured both as a loss of weight and a change in thickness of the erosion pieces. Additionally, scanning electron microscopy (SEM) coupled with energy dispersive X-ray spectroscopy (EDS) was chosen to obtain information on the erosion mechanisms and the reactions between the steel erosion pieces and the propellant combustion gases. This technique was chosen in part due to the geometry of the erosion pieces which were relatively easy to analyse using SEM-EDS comparatively to other techniques such as X-ray diffraction where the geometry of the sample is very important. Availability of the required apparatus was also a factor.

3.6 Resulting Scientific Articles

As a result of the planned work, three scientific articles were produced and published or submitted. The first article focuses on the performance and thermal stability of propellants incorporating HBT and BTA. The second article builds upon the foundation laid by the first and focuses on the performance aspects of HAT-NO$_3$ and DHT. It also presents the results of both long-term and short-term stability for all nitrogen-rich materials in gun propellants. Finally, the third article focuses on the effects of nitrogen-rich materials on the erosivity of propellants and additional performance data for higher content of HBT and BTA.

CHAPTER 4   ARTICLE 1: BURNING RATES AND THERMAL BEHAVIOR OF BISTETRAZOLE CONTAINING GUN PROPELLANTS

Jonathan Lavoie, Catalin-Florin Petre, Pierre-Yves Paradis, Charles Dubois

The aim of this article was to characterize the impact of increasing concentrations of two bistetrazole nitrogen-rich materials on a reference formulation of gun propellant. The short term thermal stability and decomposition activation energies were also calculated.

The scientific contribution of this work is threefold. Firstly, it is the first work to systematically look at the effects of nitrogen-rich materials in propellants and their concentration at pressures exceeding 30 MPa. It highlights how much an increase in nitrogen-rich materials can affect the kinetics of the propellant combustion by the determination of the empirical burning rate law presented in the literature review. Secondly, it also highlights how small changes in a molecule, in this case, the two bistetrazoles, can greatly affect the dynamics of the combustion of gun propellants. Finally, it firmly establishes the use of nitrogen-rich materials as burning rate modifiers for propellants, an effect that was anticipated, but never clearly demonstrated.

This article was published in Propellants, Explosives, Pyrotechnics [111]. The supporting information mentioned in this article is presented in Appendix B.

4.1 Abstract

The influence of two selected bistetrazoles, 5,5′-bis(1H-tetrazolyl)-amine (BTA) and 5,5′-hydrazinebistetrazole (HBT), on the combustion behavior of a typical triple-base propellant was investigated. Seven propellant formulations, one reference and six others incorporating 5 %, 15 %, and 25 % of either HBT or BTA compounds, respectively, were mixed and extruded into a cylindrical, no perforations, geometry. The resulting propellants showed high burning rates, up to 93 % higher than the reference formulation at 100 MPa. However, the increase in burning rates came at the cost of higher burning rate dependency on pressure, with a pressure exponent as high as 1.4 for certain formulations. HBT-containing propellants showed notably lower flame temperature when compared to the reference formulation, with a flame temperature reduction of up to 461 K for the propellant containing 25 % HBT. The thermal behavior of the propellants was

also investigated through DSC experiments. The addition of bistetrazoles provided lower decomposition temperatures than the pure nitrogen-rich materials, indicating that the two compounds probably react readily with the $-ONO_2$ groups present in the nitrocellulose and the plasticizers used in the formulation. The onset temperature of all propellants remained within acceptable ranges despite the observed decrease caused by the addition of the bistetrazole compounds.

4.2 Introduction

There are multiple challenges nowadays in the field of chemical propulsion. They range from increasing the performance, lowering the vulnerability, reducing the environmental impact, and minimizing the erosivity of the propellants, to name but a few. In recent years, a new family of energetic materials that has the potential to tackle these challenges has emerged in the form of nitrogen-rich molecules. These are often designated as nitrogen-rich materials due to their high nitrogen content, which can exceed 80 % of the total weight of the molecule. This shifts the source of the energy produced in the molecule from the oxidation of the carbon backbone to the production of nitrogen gas from materials with high enthalpies of formation. On the other hand, most of the current research has focused on the synthesis of these new nitrogen-rich compounds, the characterization of their physicochemical properties and their explosive performance, with little to no research on their effects when incorporated in actual propellants [3, 64, 110]. As an example, there has been some insight for the determination of the burn rates of some of the earlier nitrogen-rich materials, in their pure form, such as 3,6-dihydrazino-s-tetrazine (DHT), 3,6-bis(1H-1,2,3,4-tetrazol-5-ylamino)-s-tetrazine (BTATz), triaminoguanidinium-5,5′-azobis(1H-tetrazolate) (TAGZT), etc., under various pressure conditions [63, 94, 112, 113]. Those works showcased high burn rates accompanied by very variable pressure exponents and linear burn rate coefficients.

The limited amount of work from the literature on nitrogen rich materials incorporated into gun propellants has focused on the effects of triaminoguanidinium nitrates (TAGN) and triaminoguanidinium azide (TAGAZ) [93], BTATz [97, 98], and TAGZT [100, 101, 113] on nitramine based formulations. The formulations based on materials containing the triaminoguanidinium cation presented tremendously fast burning rates as well as increased pressure exponents. On the other hand, formulations incorporating BTATz showed lower pressure dependency, but high burning rates (at least 40 % higher). Similarly, investigations of DAATO3.5

and BTATz as monopropellants for micro-thruster applications also showed low pressure exponents and high burning rates [72]. With one exception (Damse *et al*. [93]), the burn rate characterization of the nitrogen-rich propellants was conducted on low pressure ranges more suited to rocket propellants, that is on the order of 0.1 to 10 MPa, which greatly differs from gun propellants where the pressure can reach upwards of 100 MPa while the combustion is still ongoing.

The past work on the burning behavior of nitrogen-rich materials demonstrated their potential usefulness as burn rate modifiers, which could also come with additional benefits, such as lower molecular weight combustion gases and lower flame temperature. It should however be noted that the amount of nitrogen-rich materials tested under such circumstances is fairly limited. The literature works previously performed also showed that the effects of such materials vary greatly from one nitrogen-rich material to another.

More recently, the number of nitrogen-rich materials based on the tetrazole ring that have been synthesized and characterized has significantly increased and they have shown desirable energetic content as well as fairly acceptable sensitivities. Tetrazoles are of particular interest as they strike the right balance between stability, nitrogen content and energy content through high enthalpies of formation. Among these materials, 5,5′-bis(1H-tetrazolyl)-amine (BTA) and 5,5′-hydrazinebistetrazole (HBT), shown in Figure 4.1, have demonstrated a great potential, as their performance has been compared to that of octahydro-1,3,5,7-tetranitro-1,3,5,7-tetrazocine (HMX) and 1,3,5-trinitroperhydro-1,3,5-triazine (RDX), two components often used in low vulnerability propellants [3, 64]. The synthesis of the precursor of HBT has been scaled up to the multi-kilogram scale [43]. Care was taken to choose nitrogen rich molecules, for which the synthesis could be scaled up with relative ease and with a small number of intermediaries.
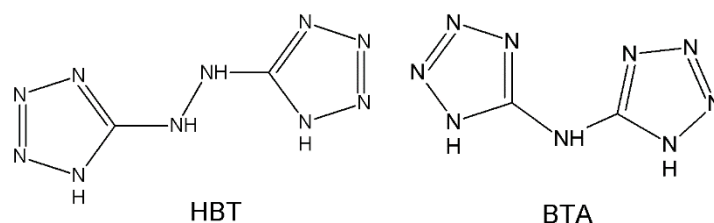
Figure 4.1 : Chemical structure of HBT and BTA

This work is concerned by the characterization of the effects of incorporating either BTA or HBT in a typical nitrocellulose-based triple base propellant. The burning performances of the resulted propellants were characterized via closed vessel tests. The thermal behavior of these propellants and their nitrogen-rich constituents has been investigated through differential scanning calorimetry (DSC) experiments. Furthermore, some of the properties of the bistetrazole molecules used such as the sensitivity and density are also presented.

4.3 Results and Discussion

4.3.1 Bistetrazoles

Due to safety concerns associated with the handling of energetic materials, the sensitivities to impact and friction of the synthesized bistetrazole compounds were tested prior to mixing the propellant formulations. Similarly, in order to provide accurate calculations of the thermochemical properties of the propellant formulations, the density of the materials was measured through gas (helium) pycnometry. These values are reported in Table 4.1. Some differences were observed between the properties previously reported in the literature and the properties measured through experimentation.

Table 4.1 : Selected Properties of the nitrogen rich materials, RDX and HMX

	ρ [g·cm^{-3}]	Impact [N]	Friction [N]
HBT	1.78	10	20
BTA	1.84	10	120
RDX	1.82	4	96
HMX	1.91	4	120

HBT proved to be much more sensitive than previously reported in the literature, as the reported sensitivities were greater than 30 J for impact and greater than 108 N for friction [3]. The impact sensitivity is still better than that of many energetic materials used in low vulnerability ammunitions, such as RDX and HMX (see Table 4.1). However, HBT proved to be much more sensitive to friction than anticipated based on the values reported in the literature. The 1H and 13C NMR performed on the HBT revealed no impurities, to which the increase in sensitivity could be attributed. However, impurities below the detection threshold of NMR would not have been detected. Both HBT and BTA were not recrystallized either. The sensitivity results are in

accordance with the testing previously done on HBT synthesized in much smaller quantities at our facilities.

BTA is less sensitive to friction than HBT and similarly sensitive to impact. Conversely, while BTA has proven to be more sensitive than previously reported (30 J, >360 N) [64], it still has lower sensitivity than materials with similar detonation parameters such as HMX (see Table 4.1). Both nitrogen-rich materials had slightly lower density than previously reported [3, 64], however, this could be attributed to the method used to calculate the density. Values previously reported in the literature were of 1.84 $g\,cm^{-3}$ and 1.86 $g\,cm^{-3}$ for HBT and BTA, respectively, and were measured through XRD. In contrast, the density measurements in this work were obtained by performing gas pycnometry on the dry powders.

The particle size of both bistetrazoles was summarily evaluated with an optical microscope and a particle size analyzer (details in the experimental section). The crystal size of HBT was found to be equal or lower than 35 μm. HBT did not tend to form crystal agglomerates. In contrast, BTA showed a wider particle size with agglomerates that were larger than 50 μm. Individual crystals were comparable to those of HBT. The agglomerates of BTA were easily disaggregated by the application of mechanical energy and it is expected that few of these remained in the propellants due to the shear in the mixer. Photos of crystals of both materials at 200× and 500× magnifications are shown in the Supporting Information. The results of the particle size analyzer confirmed the microscope observations. HBT has a surface weighted mean diameter of 23 μm and a volume weighted mean diameter of 33 μm. BTA has a surface weighted mean diameter of 0.4 μm and a volume weighted mean diameter of 19 μm. The higher polydispersity of the BTA particles is in part explained by the presence of a bimodal distribution with peaks at 0.18 μm and 46 μm and a maximum particle size of 138 μm with 90 % (vol.) of the particles having a diameter equal or lower than 59 μm. This corroborates the presence of both small particles and agglomerates as observed through the optical microscope. The size of the agglomerates after sonication proved to be acceptable for inclusion in propellants, which confirms the assumption that shear in a sigma type mixer is enough to break down the larger agglomerates. Particle size effects can therefore be excluded as a potential cause of the changes in the burning rates of the propellants. The crystal structure of both materials has been previously investigated through XRD [3, 64].

4.3.2 Thermochemical Data

A total of seven propellant formulations were manufactured, starting with the reference formulation containing no nitrogen-rich components and followed by three formulations for each bistetrazole compound. The reference propellant was composed of 53 % nitrocellulose, 39 % trimethylolethane trinitrate (TMETN), 7 % triethylene glycol dinitrate (TEGDN), and 1 % stabilizer. Ethyl centralite was used as the stabilizer. The plasticizers were chosen after multiple CHEETAH calculations, which demonstrated that in order to maintain performance only a minimum amount of oxygen was required in the propellant. To obtain the bistetrazole propellants, parts of the reference propellant constituents were replaced by, respectively, 5 %, 15 %, and 25 % of bistetrazoles on a mass basis and in such a way that the nitrocellulose to plasticizer ratio remained the same for all formulations. The calculated thermochemical properties of the resulted propellant formulations are presented in Table 4.2. Symbol definitions are the following: impetus (F), adiabatic flame temperature (T), maximum pressure (P_{max}), gas products molecular weight (M_g) and relative force (RF)

Table 4.2 : Thermochemical properties of the gun propellants

	Reference propellant	5% HBT	15% HBT	25% HBT	5% BTA	15% BTA	25% BTA
F /J·g^{-1}	1138	1121	1084	1040	1138	1137	1134
T /K	3224	3137	2954	2763	3187	3111	3032
P_{max} /MPa	211	209	204	197	212	214	215
M_g /g·mol^{-1}	23.6	23.3	22.7	22.1	23.3	22.8	22.2
RF /%	100	99.0	96.4	93.2	100	101	107

The thermochemical data provides some interesting insight as to the changes incurred from the addition of nitrogen-rich materials to the propellant formulations. One of the first changes concerns the flame temperature. The reference formulation was mildly hot with a flame temperature of 3224 K, while the formulation incorporating 25 % HBT proved to be what is considered a relatively cold propellant with a flame temperature of 2763 K, a reduction of 461 K. BTA yields hotter propellant formulations than HBT due to its higher enthalpy of formation (633 kJ·mol^{-1}) compared to that of HBT (414 kJ·mol^{-1}). However, all nitrogen-rich propellants yielded lower flame temperatures than the reference formulation. This probably resulted from the loss of oxygen content and the nature of nitrogen-rich materials, which shifted some parts of the gas generation from the oxidation of carbon backbones to the production of nitrogen. Despite this, the changes in oxygen balance were relatively moderate. The reference propellant has an initial oxygen balance of -36.7 %, while the

propellants containing 25 % of HBT or BTA, have an oxygen balance of -42.3 % and -42.4 %, respectively.

From the thermochemical calculations, both propellants generated final combustion products with lower molecular weight. These lower molecular weight combustion gases are believed to help offset the lower adiabatic flame temperatures, which in turn explains the relatively small loss of impetus. This is especially true for HBT, for which a reduction of impetus by 8.6 % was accompanied by a reduction of flame temperature of 14.3 % (almost double the decrease in impetus). Lower flame temperatures are of interest partly due to gun barrel erosion concerns. Not only does a lower flame temperature limit the reaction occurring between gun barrel steel and the hot combustion gases, it also limits thermal expansion and contraction during repeated firings, that were shown to lead to the cracking of the protective coatings generally used in gun barrels (i.e., hard chromium) [80]. In addition, when compared to the reference value (0.29), the N_2/CO ratio (a key parameter of the chemical erosivity of gun propellants) was found to be more than double (0.64 and 0.62) for, respectively, the 25 % HBT and the 25 % BTA propellants. It is well known that CO can react with steel of the gun barrel to form iron carbide, which results in higher chemical erosion of the barrel, whereas nitrogen gas it is believed to have the opposite effect [80]. Therefore, favoring the formation of the N_2 over CO during the propellant combustion will positively influence the span life of the gun barrel.

4.3.3 Burning Rates

The burning rate data was obtained from the pressure vs. time data recorded in the closed vessel, the thermochemical data calculated using CHEETAH, the propellant density and the geometrical dimensions of the propellant grains. In order to obtain good accuracy for the burning rate calculations, the density of the propellant grains was also measured using gas pycnometry rather than calculated using the density of the propellant constituents. The density of the reference was 1.56 g·cm^{-3}. The density of the propellants containing HBT varied from 1.57 g·cm^{-3} to 1.62 g·cm^{-3} and those of the propellant containing BTA from 1.56 g·cm^{-3} to 1.61 g·cm^{-3}. As both HBT and BTA are notably denser than the reference formulation main ingredient (NC), replacing the latter by one of the former resulted in an increase in density with the increased concentration of these molecules. Predicted density from theoretical maximum density values within less than 1% of measured values for the reference propellant and the HBT containing propellants, the measured

density for the 15% BTA propellant was within 4% and the two other BTA propellants within 2%. In order to confirm whether the burning rate changes were the result of the bistetrazoles or the result of porosity that was generated during the making of the propellants, the number of propellant grains calculated by BRLCB from the dimensions and density of the propellant was compared to the number of grains calculated through gravimetry. The error between the number of grains calculated using the software and through weighing the grains directly was 3.5 % for the reference propellant and 3.3 % for the formulation containing 15 % HBT. All other propellants had an error in the number of grains of the order of 1 % or below. This isn't expected to affect the calculated surface area and by extension the burning rate in any meaningful way. Porosity would have incurred a larger error in the number of propellant grains calculated by BRLCB and that calculated through weighing and numbering of the propellant grains. Micro porosity was characterized through gas pycnometry [120] and the number of closed pores was also found to be present only in negligible amounts.

The initial pressure rise caused by the igniter was subtracted from the pressure time data prior to the burn rate calculations. The burn rate laws were calculated in the 40–130 MPa range according to Vielle's law as shown in Equation (4.1).

$$r = \beta P^\alpha \qquad (4.1)$$

Where r is the burning rate in cm·s^{-1}, β is the linear burn rate coefficient, P is the pressure and α is the pressure exponent. The burn rate-pressure curves for the reference and nitrogen rich propellants are shown in Figure 4.2 and Figure 4.3.
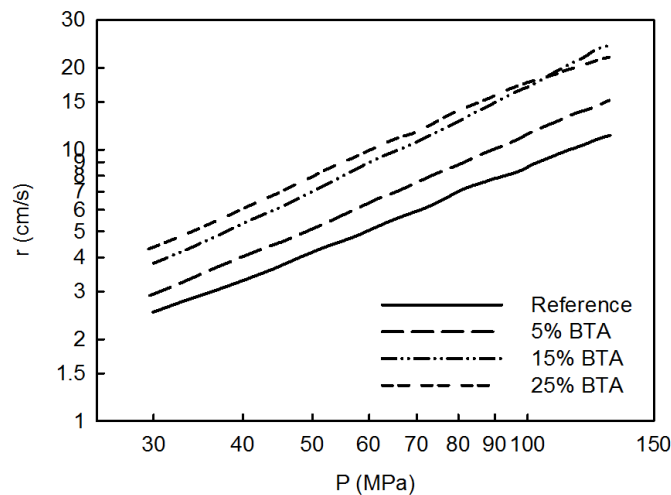
Figure 4.2 : Burning rates for the BTA containing propellants
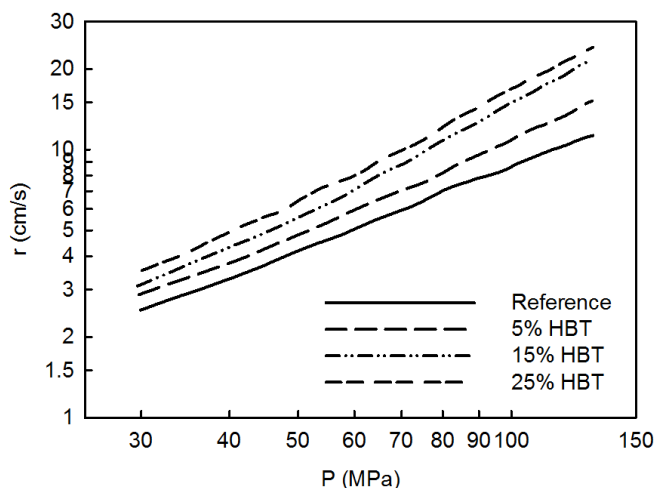
Figure 4.3 : Burning rates for the HBT containing propellants

As a first observation, all formulations containing nitrogen-rich molecules showed increased burn rates when compared to the reference propellant formulation. The reference was chosen from the literature for its reported relatively low pressure exponent, $\alpha=0.74$ [71] and also for its good oxygen content, most likely a result of the two nitrated esters used as plasticizers. However, the burn rate calculations performed showed a much higher pressure exponent than initially anticipated, $\alpha=1.037$ for the reference propellant. There are mainly three factors that are believed to have an influence on this: the heat loss data treatment applied for the closed vessel results has an impact on the burning rates and given the impact of the volume reducing sleeve on heat loss, this might have influenced the pressure exponent. However, given that the heat loss is comparable for every propellant, the validity of the comparison between the propellants is unchanged. Secondly, the nitrocellulose used in the propellant formulation had slightly different nitrogen content compared to the reference used: 13.25 % in this work compared to 12.56 % [114]. Finally, the reference from which the formulation was taken presented mostly strand burner results and some variation is to be expected between strand burner and closed data due to the difference in pressure. It is unknown, which factor or combination of these factors is responsible for the difference in pressure exponent. Despite the higher than initially anticipated burning rates, the positive effects of the bistetrazoles on the increase of the burning rate are clearly visible from Figure 4.2 and Figure 4.3.

The general effect of either of the two bistetrazoles on the burn rate of the propellants followed the same trend, which is an increase of the pressure exponent along with a decrease of the β coefficient at low concentrations. As the bistetrazole concentration increases, the pressure exponent stabilizes

at concentrations around 15 % and then decreases slightly at concentrations of 25 % (see Table 4.3). In the case of HBT, the β coefficient remained lower than that of the reference propellant and the pressure exponent α remained similar at concentrations of 15 % and 25 %. In the case of BTA, after an initial decrease of the β coefficient for the first two concentrations, the coefficient ended up being higher than that of the reference propellant with a pressure exponent equivalent to the reference propellant at 25 % concentration. Such high pressure exponents are generally indicative that the combustion of the propellant is driven by gas phase reaction of an order greater than one. In the case of the propellant containing BTA, the decrease in burn rate would indicate a greater contribution from reactions occurring in the condensed phase. These results are similar to those obtained by Damse *et al.* [92], where both TAGAZ and TAGN showed a high increase of the pressure exponent of the same order at concentrations of 15 %. On the other hand, the results from this study differ greatly from the burn rates measured for other pure nitrogen rich materials such as BTATz [63], where low pressure exponents and high burn rate coefficients were observed. The results also differ from the ones for propellants containing BTATz, where the addition of the nitrogen-rich compound yielded lower pressure dependency in the form of low α and high β coefficients [97]. In the case of the propellants containing BTATz, RDX was used as the main component, different decomposition pathways are likely occurring, resulting in the difference in pressure exponent. Pure BTATz also shows very low pressure exponent likely further contributing to the decrease in pressure exponent of the formulation. Obviously, such high pressure exponents may not be desirable as it could induce instabilities during the combustion process.

Table 4.3: Closed vessel data for the propellant formulations

	Reference propellant	5% HBT	15% HBT	25% HBT	5% BTA	15% BTA	25% BTA
↑[7]%, 30	2.6±0.1	7.3±7.3	19.1±6.6	35.7±6.5	11.3±6.3	47.8±8.1	66.8±7.5
↑%, 60	5.3±0.4	11.7±7.6	36.4±7.8	52.8±8.3	21.7±7.7	70.5±9.1	88.5±9.8
↑%, 100	9.1±0.7	19.2±7.9	64.6±9.8	88.7±10.9	25.8±8.1	89.8±10.5	92.5±12.5
β	0.07± 0.01	0.04± 0.00	0.02± 0.00	0.03± 0.00	0.06± 0.01	0.04± 0.00	0.11± 0.00
α	1.04± 0.03	1.21± 0.04	1.40± 0.01	1.39± 0.03	1.15± 0.02	1.30± 0.00	1.10± 0.01
RQ /%	100±0	110±4	142±1	150±1	118±1	159±1	166±2
RF /%	100±0	101±4	103±3	99±1	100±2	98±2	96±0

[7] Burning rate increase in % for all nitrogen-rich propellants, burning rate in cm·s^{-1} for the reference propellant.

Of note is the behavior of the propellant incorporating 25 % BTA. The pressure exponent is in the range of common values for gun propulsion applications and the linear burn rate coefficient also increases with the increase in nitrogen-rich concentration. As such, BTA could be used in high concentrations to generate quicker propellant formulations when needed while also reducing the flame temperature and probably increasing the performance. HBT on the other hand should likely be of use at lower concentrations, in slower propellant formulations, as a way of both reducing the flame temperature and increasing the burning rate. The decrease in the burn rate at higher pressure observed at 25 % BTA concentrations was also noted in the case of RDX-TAGZT mixtures [101] and the authors attributed this to an increase in the amount of hydrazine-like free radicals produced during combustion. It remains to be seen whether the effect observed at 25 % concentration of BTA could also be observed at higher (than 25 %) concentrations of HBT.

As a way to measure the dynamic vivacity and the amount of usable energy generated by the propellant formulations, the relative quickness (RQ) and relative force (RF) were also calculated. Both the RQ and RF were calculated according to a procedure similar to that prescribed by the MIL-STD-286C standard [107]; prescribed dP/dt values were interpolated when necessary. The four data points used were those prescribed by the standard as a function of the maximum pressure of the reference formulation, 27 %, 40 %, 53 %, and 66 % of the maximum pressure of the reference propellant. The relative force on the other hand was calculated as the average of the ratio of the maximum pressure for the firings of each propellant incorporating HBT and BTA to that of the reference propellant. The values of the relative quickness and relative force are shown in Table 4.3 and Figure 4.4.
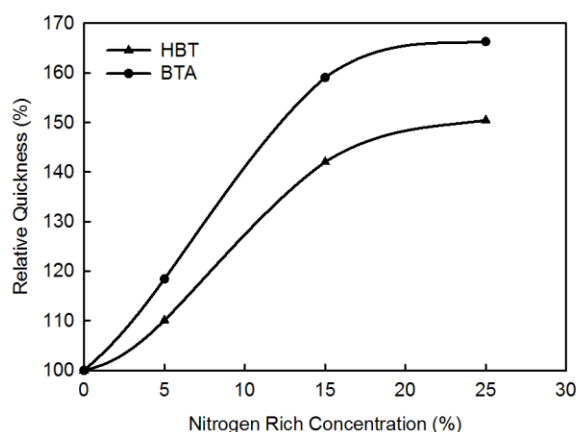
Figure 4.4: Relative quickness of the bistetrazole containing propellants

The *RQ* is a good way of comparing the rate of pressure increase of new propellants to a reference. In this case, both nitrogen-rich materials showed great potential as quickness enhancers. The addition of either of the two bistetrazole compounds showed a similar trend. The increase in *RQ* happens at a much higher rate in the 0 to 15 % concentration range and starts to plateau afterwards. Of the two materials, BTA gives the higher *RQ* of the two. This clearly shows the potential of both bistetrazoles as quickness enhancers for slow-burning propellant formulations. However, as mentioned above, the increase in quickness came at the cost of an increased BR dependency to pressure.

The *RF* calculated from the closed vessel tests is close to the one calculated from the thermochemical data. However, HBT propellants were found to yield a slightly higher *RF* when the closed vessel data is used for calculations, while the BTA propellant yielded slightly lower values (Table 4.2 versus Table 4.3). This could be attributable to the difference in propellants flame temperature. While the heat losses in the closed vessel were all in the same range, the propellants containing HBT showed slightly lower heat losses (evaluated using BRLCB v3.0). The maximum pressure calculated from the thermochemical data assumes adiabatic conditions while the closed vessel test did not ensure adiabatic conditions. Lower flame temperatures are expected to have lower heat losses to the jacket of the closed vessel and, as a result, the actual maximum pressure in the closed vessel would be closer to the theoretical adiabatic value. The same effect should be observed in an actual gun.

4.3.4 Thermal Behavior

DSC was performed on low mass samples (ca. 0.5 mg) in order to avoid the effect of propellants self-heating from interfering with the heating rate of the apparatus. Initial tests were conducted at heating rates of 2, 5, 7, and 10 K·min^{-1} in order to determine the activation energy for the decomposition process observed. The Arrhenius plots used for the calculation of the activation energy are available in the Supporting Information. The DSC curves for each propellant are presented in Figure 4.5 and Figure 4.6 for the heating rate of 5 K·min^{-1}. All other presented values were also evaluated at this heating rate. Also, the results derived from the DSC experiments are presented in Table 4.4. To avoid gas losses if any gas-phase reaction occurred, hermetic aluminum pans were used for the DSC experiments.
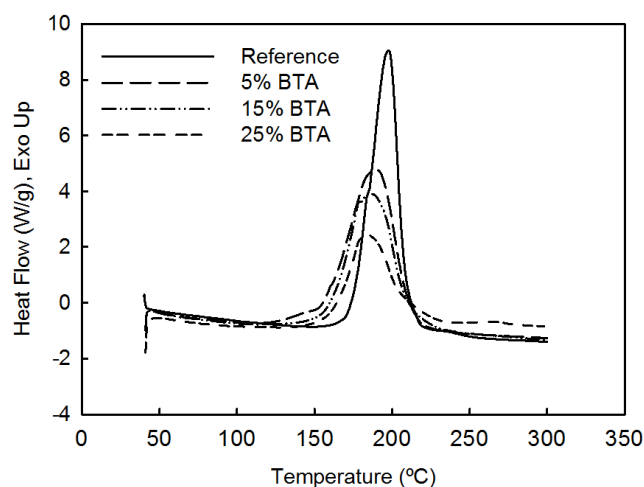
Figure 4.5 : DSC curves of the BTA containing propellants
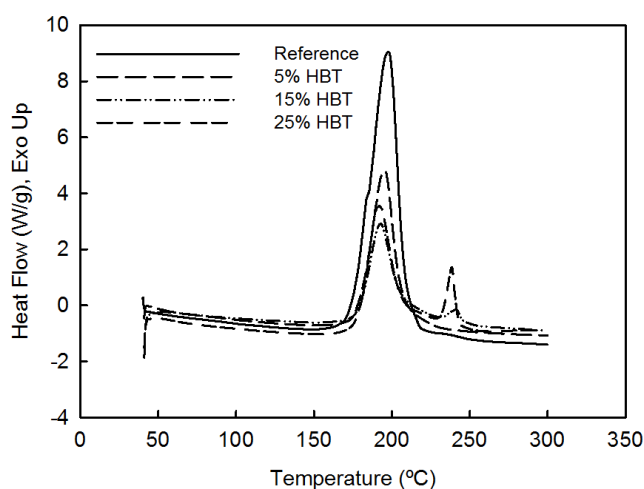
Figure 4.6 : DSC curves of the HBT containing propellants

Table 4.4: DSC data on the propellants

	Reference propellant	5% BTA	15% BTA	25% BTA	5% HBT	15% HBT	25% HBT
Onset [°C]	177	157	162	160	179	179	179
Peak [°C]	198	190	186	186	196	192	192
E_a [kJ·mol^{-1}]	170	148	141	N/D	174	197	213

The activation energy needed for the decomposition of the propellants was calculated according to the Ozawa-Flynn-Wall method [115] as prescribed by ASTM standard E698 [116]. In order to verify the applicability of the method, the term E_a/RT used for the approximation of the integral

was evaluated and it was verified that it remained in the 20–60 range, which verifies the applicability of the method. The activation energy for the propellant containing 25 % BTA (312 kJ·mol^{-1}) was found to fall outside of the applicability range of the method ($E_a/RT \approx 80$). Therefore, the value may not be accurate; however, it is presented as a qualitative comparison to the other activation energy values.

The onset temperature of the decomposition process is a good indicator of the thermal stability of a propellant. The onset temperatures were measured for all seven propellants. The propellants containing BTA presented the lowest values for the onset temperature among the tested propellants. This is probably indicative that BTA readily reacts with the other constituents of the propellant formulations, most likely the $-ONO_2$ groups present both in the nitrocellulose and the plasticizers. Pure BTA showed an onset temperature much higher than that of any propellants studied herein, with an onset at 246 °C and decomposition peak temperature of 257 °C. Propellants containing HBT on the other hand, showed no noticeable increase of the onset temperature meaning that the decomposition of the propellant is initiated by the decomposition of its other constituents. This would be indicative that HBT does not react as readily as BTA with the other constituents of the propellant formulations. The lower peak temperature for the propellants containing HBT probably indicates that while HBT doesn't play a part in initiating the decomposition of the propellant, it still reacts with the other constituents and causes the propellant to undergo faster decomposition. From the safety concerns and thermal stability standpoints, HBT proved to be the more interesting of the two tested molecules.

Given the similarity between the two bistetrazole compounds, one can conclude that the chemical group present between the tetrazole cycles, in this case amine for BTA and hydrazine for HBT, has a direct effect on the thermal stability of the propellants. A similar trend can be observed with the activation energies of the main decomposition of the propellants. The activation energy for the HBT-containing propellants increases with the increase of the HBT content, which corroborates the high thermal stability provided by HBT. In contrast, for the BTA-containing propellants due to their lower thermal stability, the calculated energy of activation was found to decrease with the increase of the BTA content (see Table 4.4), which is also in agreement with the measured lower onset temperature of these propellants.

For the cases of the propellants containing 15 % and 25 % HBT, a second decomposition peak can be observed at higher temperatures (Figure 4.5). This peak is very small for the propellant containing 15 % HBT, but becomes significant for the propellant containing 25 % HBT. This second peak cannot be attributed to the decomposition of unreacted pure HBT. HBT's decomposition peak occurs at lower temperatures (226 °C) than the decomposition peaks observed in Figure 4.5 (237 °C). In contrast, the propellants containing BTA do not show any additional decomposition peaks, except maybe for a very small peak at 25 % concentration. It is likely that multiple decomposition reactions also occur for the propellants containing BTA, but they occur simultaneously rather than sequentially. Once again, the difference in the decomposition mechanisms can be attributed to the different chemical groups lodged between the two tetrazole rings.

While the exact decomposition mechanisms resulting from the addition of HBT and BTA remain unknown for now, a difference between the decomposition of the two bistetrazole compounds in the condensed phase can be observed through the DSC experiments. One interesting fact is that the decomposition mechanisms of bistetrazole containing propellants can be easily influenced by the presence or absence of certain chemical groups present between two tetrazole rings. This also suggests that the decomposition pathways of both compounds are probably different. As a result, the burning properties of bistetrazole containing propellants could be altered to a certain extent through the use of different chemical groups linking the two tetrazole rings, while the nitrogen and energetic content still remains high. This could also explain the difference observed in the burning behavior of HBT and BTA containing propellants compared to that of BTATz containing propellants [97] where BTATZ presents a s-tetrazine between two tetrazole rings rather than an amine or hydrazine group. This approach could be an alternative to the use of ionic nitrogen-rich compounds, where the various cations and anions are generally used to change the burning properties and the composition of the resulting molecules. Of course, both approaches can be used in conjunction, with a good example being the use of salts of bistetrazole and azotetrazole.

4.4 Experimental

HBT and BTA were synthesized according the procedures previously described by Klapötke *et al*. [3, 64]. The purity of all materials was verified through hydrogen, carbon, and nitrogen nuclear magnetic resonance spectroscopy (^{1}H NMR and ^{13}C NMR). BTA: ^{1}H NMR (400 MHz,

[D$_6$]DMSO, 25 °C)=11.92 ppm (s, 3 H, NH) ^{13}C NMR (400 MHz, [D$_6$]DMSO, 25 °C)=154.16 (s, 2 C, CN3). HBT: ^{1}H NMR (400 MHz, [D$_6$]DMSO, 25 °C)=9.67 ppm (s, 4 H, NH) ^{13}C NMR (400 MHz, [D$_6$]DMSO, 25 °C) 159.48 ppm (s, 2 C, CN3). All materials were synthesized with high yields as well as good purity. Precursors for the synthesis of these materials were procured from Sigma-Aldrich and used as is with the exception of sodium 5–5′-azobis(1H-tetrazolate) (Na$_2$ZT), which was synthesized on site according to the procedure described by Radack *et al*. [43]. In the case of HBT and its azotetrazolate precursor, the syntheses were performed at higher concentrations than reported in the literature in order to reduce the reactor volume required; the other experimental conditions remained the same as those reported in the literature. The particle size of both bistetrazole was characterized with an optical microscope and using a Malvern Mastersizer 2000 particle size analyzer using ethanol as the eluent. The materials were sonicated in the solvent prior to analysis. Grade C nitrocellulose, nitrogen content of 13.25 %, wetted with ethanol was used as the polymeric binder and as an energetic component.

The propellant manufacturing facility was described previously in detail by Petre *et al*. [76]. The propellants were mixed in a sigma blade mixer using the solvent incorporation method until a dough judged to be adequate for extrusion was obtained. The dough was subsequently extruded, cut in cylindrical geometries with no perforations and dried until the weight loss due to solvent evaporation was negligible.

Closed vessel tests were conducted on the propellant grains to evaluate their burning characteristics. For this study, a RARDE (model CV21, V=700 cm^3) closed pressure vessel was used with an internal metallic sleeve in order to bring the volume down to 188 cm^3. The closed vessel can be operated at pressures up to 248 MPa. A piezoelectric pressure transducer was used to measure the pressure-time relationship for each sample. Ignition of the propellants was achieved using an electric match and a small quantity of black powder. All formulations were fired at a loading density of 0.155 g·cm^{-3}. The use of the sleeve increased the heat loss in the vessel to an estimated 30–35 % for all firings. The burning rate coefficient (β) and pressure exponent (α) as well as the dynamic vivacity were calculated from the pressure-time data recorded in the closed vessel and the use of the impetus and flame temperature data simulated through the use of the CHEETAH thermochemical code using the virial equation of state (BLAKE compatibility). The BRLCB v3.0 computer code was used to perform the burning rate regressions. The closed vessel temperature was maintained at 21 °C through the use of a jacket where cold water was circulated.

The sensitivity of the nitrogen rich materials was assessed using a Julius-Peters BAM friction apparatus and impact sensitivity was evaluated using a Julius-Peters drop hammer. The sensitivity threshold for both materials was defined as the force or energy where no reaction, be it smoke, crackling, spark, or other occurred for six consecutive tests.

Differential Scanning Calorimetry was carried out with a TA Instruments Q2000 DSC with auto sampler and aluminum hermetic pans at various heating rates in a nitrogen flow of $50 \, mL \cdot min^{-1}$.

Supporting Information (see footnote on the first page of this article): additional data on the kinetic calculations from DSC and the particle size of the synthesized nitrogen-rich materials.

4.5 Conclusions

Both bistetrazole compounds tested in this work (BTA and HBT) have shown high potential as burn rate modifiers, even when only small quantities were added to the propellant. In addition, both bistetrazoles studied here can easily be synthesized from commercially available materials with good yields and purity which will be helpful in scaling up the synthesis if desired. Furthermore, the synthesis of the precursor of HBT was scaled up to the multi-kilogram scale [43].

By adding 5 % of HBT or BTA to the triple base propellant formulation used in this work, the relative quickness was found to increase with 10 % and 18 %, respectively. Furthermore, by adding 15 % of either HBT or BTA the relative quickness increased with 42 % and 59 %, respectively. On the contrary, at higher concentrations (>15 %), the burn rate modification effects slowed down, and it is probable that, for this particular propellant formulation, higher concentrations of bistetrazoles will only yield small increases of the burning rate. While the increase in burning rates may not be as significant at high concentrations, other advantages such as lower flame temperature and less erosive combustion gases for similar relative force can be obtained with the use of these nitrogen-rich molecules. This could be especially expected for HBT, where a sensibly lower flame temperature and a higher amount of nitrogen gas produced could lead to interesting reduction in gun barrel wear, with no significant performance losses.

The main disadvantage of the two chosen bistetrazoles is probably their effect on the pressure dependency of the burning rates. The presence of these materials was found to increase the pressure exponent (α) by a non-negligible amount and this is not desirable as it could yield combustion instabilities.

Of the two bistetrazole, HBT provided the better thermal stability to the resulting propellant. This in turn could result in safer propellants, despite the fact that HBT itself was found to be more sensitive than its counterpart, which in turn provided a greater increase of burning rate properties. It is also important to note that the compatibility of the materials used in the propellant formulations was summarily evaluated. No short term compatibility issues were observed; however long term stability was not investigated.

Finally, the DSC experiments brought to light that, despite their similarities, both bistetrazole lead to different decomposition mechanisms when incorporated into the same propellant formulation. However, more work is needed in order to determine the exact decomposition pathways favored by these two molecules.

4.6 Acknowledgements

CHAPTER 5 ARTICLE 2: STABILITY AND PERFORMANCE OF GUN PROPELLANTS INCORPORATING 3,6-DIHYDRAZINO-*S*-TETRAZINE AND 5-AMINOTETRAZOLIUM NITRATE

Jonathan Lavoie, Catalin-Florin Petre, Simon Durand, Charles Dubois

This article is a continuation of the work performed in the first paper published in Propellants, Explosives, Pyrotechnics. Its contribution builds on the first one by solidifying the use of nitrogen-rich materials as burning rate modifiers with two additional materials. Additionally, it takes an in-depth approach to the analysis of the stability of nitrogen-rich materials in propellants. Incompatibilities with certain families of nitrogen-rich materials were discovered and a family of nitrogen-rich materials compatible with nitrated esters was also discovered.

5.1 Abstract

The addition of either 3,6-dihydrazino-s-tetrazine (DHT) or 5-aminotetrazolium nitrate (HAT-NO$_3$) to nitrocellulose-based propellants were investigated. At 25% (m/m) concentration, DHT and HAT-NO$_3$ had significant impact on the burning rate of the propellant, up to 80% higher than that of the reference propellant. DHT was found to have very poor compatibility with nitrocellulose and the nitrated esters used in the formulation despite the presence of stabilizer. This lead to a rapid autocatalytic decomposition reaction resulting in a deflagration. HAT-NO$_3$ also had poor compatibility with the same materials. On the contrary, non-ionic tetrazoles were found to be fully compatible with nitrocellulose and nitrated esters based propellants.

5.2 Introduction

Nitrogen-rich energetic materials are being investigated to address current challenges in the field of chemical propulsion [26]. Requirements for new energetics for propellants include lower sensitivity to external stimuli, lower environmental impact, less erosive and less toxic combustion gases [9, 26]. For low vulnerability (LOVA) propellants applications, requirements for new energetics can be defined as: impact sensitivity ≥ 7.5 J, friction sensitivity ≥ 120 N and good thermal stability [9]. Furthermore, materials such as 1,3,5-trinitroperhydro-1,3,5-triazine (RDX) used in

current LOVA propellants exhibit high toxicity while the toxicity of some nitrogen-rich materials is promising [9, 39].

These new safety and environmental concerns have grown in importance, but performance remains important for researchers in the field of chemical propulsion. New safer and greener propellants will have to provide performance from stored chemical energy in the form of impetus equivalent to the propellants they are to replace. This can be achieved by lowering the molecular weight of the combustion gases, increasing the flame temperature or both.

Another aspect of gun propulsion that can be tackled with the use of nitrogen-rich materials is muzzle flash [38, 117]. Combustion gases containing more nitrogen gas and carbon dioxide rather than fuel rich gases such as carbon monoxide will result in less flash which is desirable when reduced signature and stealthy characteristics are important.

The development of gun propellants containing high concentrations of nitrogen-rich materials is challenging due to the high quantities of propellants required for closed vessel experiments. Whereas the characterization of nitrogen-rich materials as an explosive necessitates samples of a few grams, strand burner experiments demand quantities of a few dozen grams at most and closed vessel testing requires a few hundred grams of material. As a result, there has been very little work published to date focusing on the effects of nitrogen-rich materials in propellants under closed vessel conditions. Strand burner data for some nitrogen-rich materials is available, but the pressure range is limited (up to ~10 MPa) [63, 72, 94, 96, 113]. These results show very variable pressure exponents, even for chemically similar materials. This illustrates the potential of nitrogen-rich materials as burn rate modifiers. It also highlights a dire need for characterization of such materials as both monopropellants and burning rate modifiers. There have been some low-pressure investigations of nitrogen-rich materials as burning rate modifiers [97, 100], where faster burning rates with low pressure exponents were observed. Closed vessel experiments allow the characterization of a propellant over a pressure range that can reach a few hundred MPa. Despite some work performed [92, 93, 111], there is in practice very little work done under those conditions.

In this study, two nitrogen-rich materials were incorporated in a high-energy gun propellant based on nitrocellulose. The first, 3,6-dihydrazino-s-tetrazine (DHT) was chosen for its strand burner performance ($r = 0.14P^{0.75}$) [63] and potential as a burning rate enhancer in nitrocellulose based

compositions [118]. Thermochemical calculations showed no performance loss compared to the reference propellant. The second nitrogen-rich material, 5-aminotetrazolium nitrate (HAT-NO_3), was selected based on its oxygen balance (-10.8%) and high-nitrogen content. HAT-NO_3 has good reported explosive performance (P_{det} = 35.7 GPa; V_{det} = 8898 m·s^{-1}) [48], but has yet to be characterized as an additive in propellants. Both materials were chosen due to their ease of synthesis where one or two steps synthesis can be achieved from commercially available reactants [48, 65, 104]. The chemical structures of DHT and HAT-NO_3 are shown in Figure 5.1.
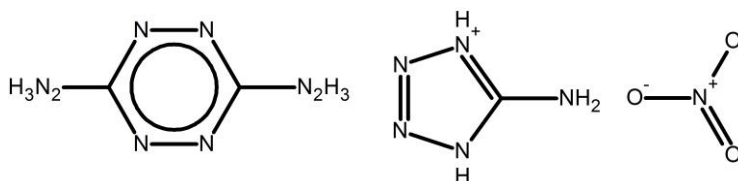
Figure 5.1: DHT (left) and HAT-NO_3 (right)

5.3 Experimental

HAT-NO_3 was synthesized according to the procedure reported in the literature [48]. ^{1}H NMR (400 MHz, DMSO-d_6, 25°C) = 11.5 ppm (bs, 4H, NH); ^{13}C NMR (400 MHz, DMSO-d_6, 25°C) = 155 ppm (s, 1 C, CN_3). HAT-NO_3 was recrystallized in water and ethanol (non-solvent). The recrystallization gave particles suitable for gun propellants (platelets of up to 80 microns in length with a length to width ratio of 4), the use of ethanol helped remove potential impurities. DHT and its intermediates were partly synthesized using the procedures previously reported in the literature [13, 105, 106]. The remainder of the DHT was synthesized from triaminoguanidine nitrate (TAGN) to yield the tetrazine intermediary [65] reducing the number of synthesis steps and then reacted to DHT as described by Chavez & Hiskey [105]. ^{1}H NMR (400 MHz, DMSO-d_6, 25°C) = 4.25 ppm (bs, 2H, NH) 8.39 ppm (s, 4 H, NH_2); ^{13}C NMR (400 MHz, DMSO-d_6, 25°C) = 163.4 ppm (s, 2 C, CN_3). Both methods resulted in comparable purity and particle size (1 to 25 microns). DHT had to be further purified using tetrahydrofuran and toluene or methyl acetate extractions. All reactants were purchased from Sigma-Aldrich and used as received. TAGN was supplied by Explosia and recrystallized in water and ethanol prior to use.

Nitrocellulose grade C was used as an energetic binder. Trimethylolethane trinitrate (TMETN) and triethylene glycol dinitrate (TEGDN) were used as energetic plasticizers. The propellants were manufactured in solvent using a Bayer-Perkins sigma mixer, 1 USG (3.7 L) capacity. The

propellant dough was subsequently ram extruded. The facilities have been previously described [76].

Thermochemical data was calculated using Cheetah [23]. Closed vessel tests were conducted using a RARDE (model CV21, V = 700 cm³) closed vessel with an internal metallic sleeve, reducing the volume to 180 cm³. Black powder and an electric match were used as the igniter, the loading density was 0.155 g·cm⁻³. Burning rates (equation 5.1) and dynamic vivacity (equation 5.2) were calculated with the XLCB software [74].

$$r = \beta P^\alpha \tag{5.1}$$

Where r is the burning rate, β is the linear burn rate coefficient, P is the pressure and α is the pressure exponent.

$$A = \frac{dP/dt}{P \cdot P_{max}} \tag{5.2}$$

Where A is the dynamic vivacity, dP/dt is the derivative of the pressure-time curve from the closed vessel experiment, P is the pressure and P_{max} is the maximum pressure observed in the closed vessel.

The sensitivity of the nitrogen-rich materials was tested using a Julius-Peters BAM hammer and Julius-Peters BAM friction apparatus. BAM tests were conducted based on UN Test 3(b) and measurements were determined by the recording of six negative results (no reaction). RDX and HMX were tested to provide reference values.

Densities were measured using a Micrometrics Accupyc II 1340 gas pycnometer with helium; and a 10 cm³ chamber.

DSC was performed using a TA Instruments Q2000 DSC equipped with a refrigerated cooling system under a 50 ml·min⁻¹ nitrogen purge. Hermetic aluminium pans were used, and sample mass was kept below 0.5 mg to avoid self heating effects and overpressure. The maximum absolute pressure supported by the pans was 400 kPa. An empty pan was used as the reference. An indium calibration was used. Kinetic parameters were determined according to ASTM standard E698 [116] at 1 K·min⁻¹, 2 K·min⁻¹, 4 K·min⁻¹, 5 K·min⁻¹ and 7 K·min⁻¹.

The long term chemical stability was tested at 90°C by vacuum stability test (VST) according to STANAG 4147 [119]. Tests ran for 70 h or more if stability was judged good or stopped as soon as compatibility was found to be poor.

5.4 Results and Discussion

5.4.1 Performance

The measured densities (DHT: 1.68; HAT-NO$_3$: 1.80) agreed with previously reported values [48, 104]. The sensitivity values are reported in Table 5.1 along with those of HMX and RDX and were measured out of safety concerns for the handling of the nitrogen-rich materials.

Table 5.1: Sensitivity of DHT, HAT-NO$_3$, RDX and HMX

	DHT	HAT-NO$_3$	RDX	HMX
Impact [J]	7.5	7.5	4	4
Friction [N]	240	120	96	120

Seven (7) propellant formulations were manufactured. The composition of the reference propellant was: NC (53%), TMETN (39%), TEGDN (7%) and ethyl centralite (1%). The other six propellants incorporating 5%, 15%, 25% (m/m) of, respectively, DHT or HAT-NO$_3$ were formulated in a manner to keep the plasticizer to nitrocellulose ratio constant. Table 5.2 shows the thermochemical parameters (calculated with Cheetah software) of the propellants including the impetus (F), flame temperature (T), adiabatic pressure (P_{max}) and gas molecular weight (M_g).

Table 5.2 : Thermochemical data

	Reference	5% HAT-NO$_3$	15% HAT-NO$_3$	25% HAT-NO$_3$	5% DHT	15% DHT	25% DHT
F [J·g^{-1}]	1138	1146	1163	1179	1138	1135	1127
T [K]	3224	3252	3308	3364	3148	2996	2843
P_{max} [MPa]	210	212	215	218	212	213	214
N$_2$/CO	0.292	0.348	0.473	0.620	0.351	0.467	0.590
M_g [g·mol^{-1}]	23.57	23.60	23.66	23.72	23.00	21.94	20.98
ρ [g·cm^{-3}]	1.56	1.60	1.61	1.62	1.56	1.57	1.58

From Table 5.2, HAT-NO$_3$ provides an increase of the propellant's impetus whereas DHT causes a slight decrease. HAT-NO$_3$ differs from DHT in part due to its oxygen content. HAT-NO$_3$ has an oxygen balance (CO$_2$) of -10.8%, quite high compared to molecules such as RDX (-21%). The higher oxygen content is probably also responsible for the increase in flame temperature, due to a

more complete combustion of the carbon and hydrogen present in the composition(s). This increase in flame temperature is believed to be responsible for the increase in impetus for HAT-NO$_3$ propellants, while the lack of oxygen in DHT is responsible for the decrease in both flame temperature and impetus. HAT-NO$_3$ also differs from DHT as it produces higher molecular weight combustion gases than DHT. It is believed here that this is a result of the oxygen content that favors heavier products such as CO_2 and H_2O rather than CO and H_2. Given the high amount of hydrogen in DHT, the decrease of the molecular weight for the combustion gases of the DHT propellants is due to an increase in N_2 and H_2 produced.

The N_2/CO ratio increases for all propellants along with nitrogen-rich content. This parameter is believed to be one of the main factors influencing the erosivity of gun propellants [3]. This parameter has an impact on gun barrel wear and thus the cost associated with weapon system maintenance. An increase in the amount of nitrogen produced will have an impact on maintenance and barrel replacement costs, making nitrogen-rich materials prime candidates for next generation propellants. Higher N_2 content in the gases generated can also reduce muzzle flash. The increase of the N_2/CO ratio is mainly driven by the increase in N_2 produced during combustion for propellants containing DHT. HAT-NO$_3$ containing propellants show an increase in the N_2/CO ratio driven by the increase in N_2 and the decrease of CO in favor of CO_2.

The measured densities of the propellants (Table 5.2) were found to be very close to the theoretical maximum densities, indicating porosity did not affect the burning rate calculations [120]. Heat loss upon complete combustion of the propellant was estimated to be of the order of 30% to 35% due to the use of the volume reducing sleeve. Figures 5.2 and 5.3 show the burning rates (*r*) of the propellants used in this work. Error bars were omitted due to being small. The relative standard deviation was equal or below 3% across all burning rate data. The pressure range used to calculate the burning rate law parameters was selected based on the calculated dynamic vivacity to ensure that combustion proceeded according to the geometry of the propellant grains [75, 109]. The ranges are 40-130 MPa for the Reference and DHT propellants, and 60-130 MPa for the HAT-NO$_3$ propellants. The narrower range for the dynamic vivacity of the HAT-NO$_3$ propellant is attributable to slower flame spread. Figures C1 to C7 in Appendix C show typical dynamic vivacity and d*P*/d*t* curves.
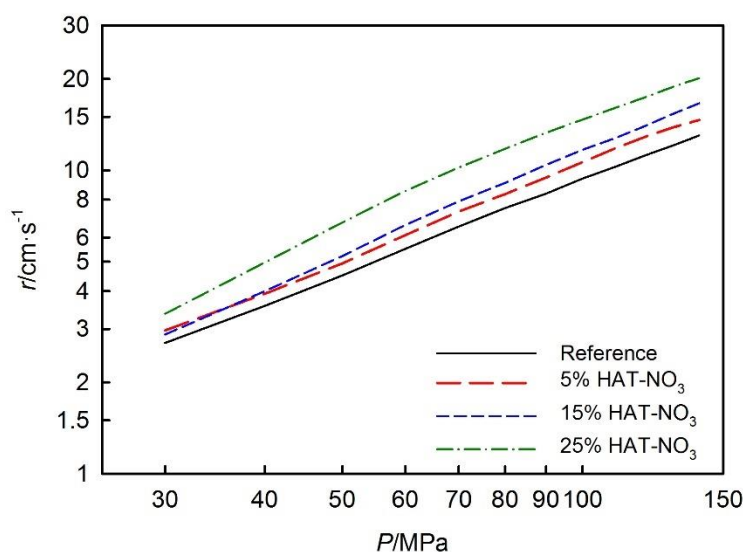
Figure 5.2 : Burning rates of DHT propellants

Another potential source of error in the calculated burning rates is poor estimation of the initial surface area of the propellant. To quantify this source of error, the number of propellant grains was calculated using gravimetry and using the measured densities and dimensions. In the case of the reference, it was found that the surface calculated with the latter method, which is used by the XLCB code underestimated the number of propellant grains by 4% or less.
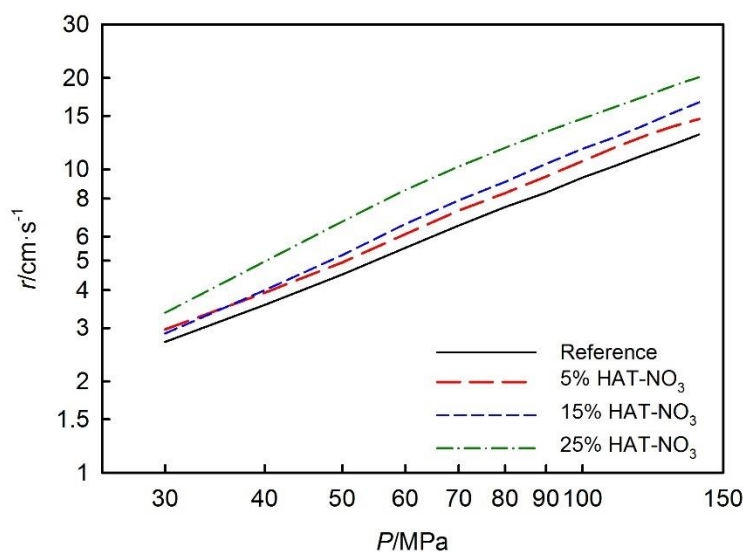
Figure 5.3 : Burning rates of HAT-NO$_3$ propellants

Tables 5.3 and 5.4 show the calculated burning rate data and relative force (*RF*) according to equation 5.3.

$$RF = \frac{P_{max}}{P_{max,ref}} \times 100\% \tag{5.3}$$

Where *RF* is the relative force, P_{max} is the maximum pressure of a given propellant and $P_{max,ref}$ is the maximum pressure of the reference propellant. It is important to note that the maximum pressure measured in the closed vessel is not under adiabatic conditions.

Table 5.3 : Burning characteristics of DHT propellants

| DHT [% (m/m)]	0	5	15	25
BR, 40 MPa [cm·s^{-1}]	3.58±0.04	4.21±0.02	5.00±0.07	6.18±0.38
BR, 80 MPa [cm·s^{-1}]	7.51±0.12	8.67±0.07	9.44±0.14	11.66±0.23
BR, 120 MPa [cm·s^{-1}]	11.22±0.14	13.28±0.39	14.03±0.07	19.86±0.94
α	1.04±0.013	1.05±0.01	0.95±0.01	1.09±0.00
β [cm·s^{-1}·MPa$^{-\alpha}$]	0.08±0.00	0.09±0.00	0.15±0.01	0.11±0.00
RF [%]	100	95.0±0.9	97.6±1.0	98.0±0.2

Table 5.4: Burning characteristics of HAT-NO$_3$ propellants

HAT-NO$_3$ [% (m/m)]	0	5	15	25
BR, 40 MPa [cm·s^{-1}]	3.58±0.04	3.93±0.07	4.01±0.02	4.98±0.05
BR, 80 MPa [cm·s^{-1}]	7.51±0.12	8.36±0.09	9.17±0.13	11.78±0.22
BR, 120 MPa [cm·s^{-1}]	11.22±0.14	12.94±0.03	14.10±0.10	17.45±0.12
α	1.04±0.01	1.06±0.00	1.09±0.03	1.01±0.00
β [cm·s^{-1}·MPa$^{-\alpha}$]	0.08±0.00	0.08±0.00	0.08±0.01	0.14±0.00
RF [%]	100	97.8±2.3	100.5±0.2	101.0±0.5

Table 5.3 and 5.4 show that incorporating nitrogen-rich materials yields higher burning rates even at low concentrations. From this standpoint, DHT is a better burning rate enhancer than HAT-NO$_3$, especially at low concentrations (of the order of 5%). Whereas the increase in burning rate of propellants incorporating HAT-NO$_3$ is relatively modest at low pressures, the increase reaches as high as 80% for the propellant incorporating 25% DHT. This makes DHT very interesting for use as a burning rate modifier in propellants used at low charge density in a large caliber gun application.

As reported previously [92], high pressure exponents are somewhat undesirable leading to hazards due to combustion instabilities resulting from small pressure variations. DHT exhibits a behavior where the increase of the linear burn rate coefficient and overall pressure exponent indicate burning rates less dependent on pressure. These results differ from the burning rates observed when

incorporating salts of triaminoguanidinium in LOVA propellant formulations, where pressure exponents as high as 1.4 were observed [92, 93]. In these cases, an increase in burning rates was also observed which further consolidates the claim that nitrogen-rich materials are excellent burning rate modifiers.

The behavior of the propellants in this work also differs from that of propellants where the incorporation of BTATz (a s-tetrazine based compound) lead to a decrease of the pressure exponent and an increase in burning rate [97].

HAT-NO$_3$, the increase in burning rate is mostly a result of higher pressure exponents at concentrations of 5% and 15%. However, just like DHT, at higher concentrations (25%), there is a significant increase in the linear burn rate coefficient. This observation is demonstrated by the significant increase in burning rate of the modified propellants at 40 MPa. The burning rate law calculations point to an optimal concentration in the 15% to 20% range for DHT and over 25% for HAT-NO$_3$, which would yield a low-pressure exponent and a high linear burn rate coefficient. A similar effect was observed in strand burner experiments with triaminoguanidinium 5,5'-azotetrazolate (TAGzT)/RDX mixtures [100], where an optimal concentration of TAGzT was found to reduce the pressure dependency of the propellant while maintaining high burning rates. However, the exact concentration is material and propellant dependent.

A slight shift in the burning rate curves of the propellant containing 25% DHT is observable in Figure 5.2. As a result, additional burning rate laws were calculated between 30 to 80 MPa and 90 to 130 MPa for that propellant, equations 5.4 and 5.5.

$$r = (0.23 \pm 0.03)P^{(0.89\pm0.02)}; 30 \leq P \leq 80 \ MPa \qquad (5.4)$$
$$r = (0.03 \pm 0.00)P^{(1.37\pm0.02)}; 90 \leq P \leq 130 \ MPa \qquad (5.5)$$

Formulations often exhibit a complex burning rate dependency on pressure, which can be described by a various "burning laws" under different ranges of pressure. This could be due to melting of DHT during burning, particle size or a change in the flame front due to increasing pressure. Regardless of the cause, it can be attributed to the addition of DHT in the propellant as it is pronounced at higher DHT concentrations. The melting point of DHT has previously been assessed as 160°C [104]. Melt is expected to occur during combustion. Melting of one or more components of the propellant can form a foam layer which induces an additional mass transfer component to

the combustion reactions which will influence the burning rate of the propellant[8]. The exact causes for this shift in pressure exponent are yet unclear and require further investigation to understand fully.

Both propellants show excellent potential as quickness enhancers. Figure 5.4 shows the relative quickness (*RQ*) compared to the reference propellant. The relative quickness is a good indicator of how fast the burning of a propellant proceeds compared to a reference. The *RQ* is calculated from the derivative of the pressure-time data and is unaffected by any of the error sources that can occur during the calculation of burning rates. The *RQ* was calculated according to the MIL-STD-286C standard [107]. The relative quickness all propellants tested here increased almost linearly with increasing nitrogen-rich molecule concentration, DHT having the higher gains. Whether these gains would similarly increase at higher nitrogen-rich content remains to be determined. The increase in *RQ* would be expected to plateau eventually as the nitrogen-rich fraction approaches unity, the burning behavior of the pure nitrogen-rich material would dominate the combustion of the propellant. The concentration at which this happens would have to be determined through further testing and is propellant formulation specific.
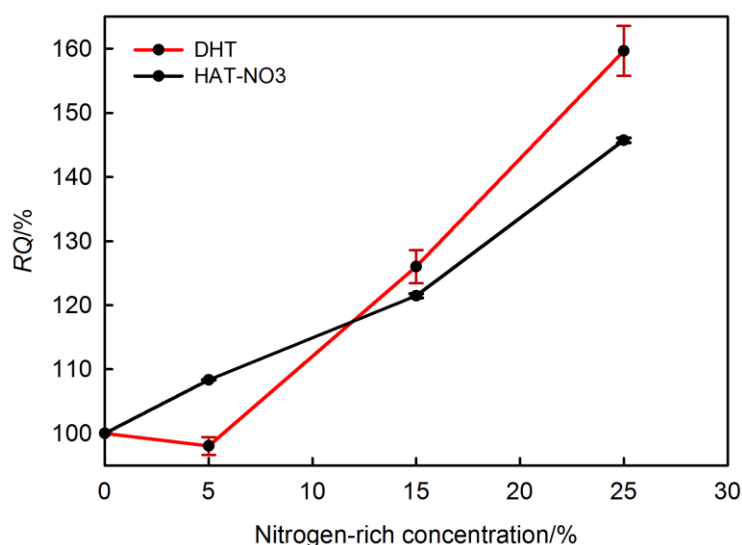

Figure 5.4 : Relative quickness as a function of nitrogen-rich content

---

[8] This sentence was added at the request of one examiner and was not part of the original manuscript

The lower RQ of the propellant containing 5% DHT can be explained by its lower dP/dt values at higher pressures. dP/dt values were taken at 27%, 40%, 53% and 66% of $P_{max,ref}$. Therefore, the RQ is representative of the early to middle stages of the propellant's combustion rather than the full pressure range. Given the burning rate law parameter of the 5% DHT propellant (Table 5.3), three of the dP/dt values ended up being lower than those of the reference propellant, therefore resulting in lower RQ. There is the possibility that the propellant batch was flawed, but this is not the preferred explanation for the calculated RQ value. The presence of DHT can easily be confirmed due to its effect on the color of the propellant which acquired the deep red color associated with DHT. It should also be noted that the triple-base reference is already a fast burning composition.

Preliminary experiments to this work conducted on a modified single base propellant, composed of mainly nitrocellulose, incorporating 3% (m/m) DHT had a RQ of 113±9.7%. However, the burning rate of the non-modified single base propellant was much lower than event that of the reference propellant used in this work with a burning rate of 3.29±0.21 cm·s^{-1} at 40 MPa and 3.88±0.21 cm·s^{-1} at 80 MPa. This result is in line with low RQ for a faster burning reference propellant.

The changes in relative force are minimal for all propellants. This is in accordance with the thermochemical data, the changes in impetus are minimal with the addition of nitrogen-rich molecules. This coupled with the high heat losses in the closed vessel could easily explain the similar P_{max} for all propellants. An interesting observation is that this occurs despite an important decrease in flame temperature for propellants incorporating DHT. A reduction of 381 K to the flame temperature at 25% DHT comes at virtually no energy loss, which is quite significant for a gun propellant. Coupled with the fact that DHT has positive effects on both burning rate law parameters and RQ, it is a promising candidate to generate faster burning propellants.

In the case of HAT-NO$_3$, the more complete combustion of the propellant was previously mentioned as an advantage. A more complete combustion of the propellant coupled with an increase in nitrogen content is likely to reduce muzzle flash which would reduce the need for flash suppressors. Consequently, adding nitrogen-rich molecules with an oxygen balance higher than that of the base propellant merits further exploration.

It is believed here that the decomposition of nitrogen-rich propellants is driven by the nitrogen-rich compounds. Further experiments with different reference formulations than the one used in this work are necessary to confirm this.

5.4.2 Stability

Figures 5.5 and 5.6 show the DSC results at 5 K·min^{-1}. Figure 5.7 shows the calculated activation energies. Numerical values, details on the calculations and Arrhenius plots are presented in Appendix A (Table C1 and Figures C8 to C21).
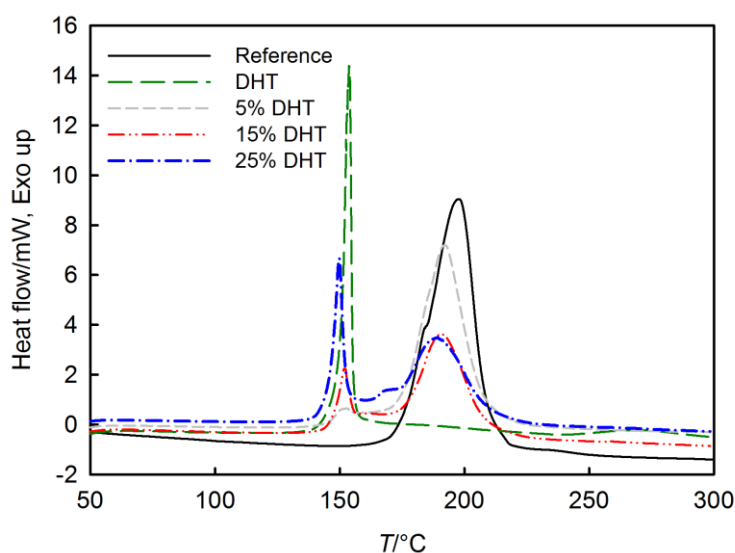
Figure 5.5: Stability of DHT propellants in DSC

The decomposition of the propellants containing DHT appears to be initiated by the DHT in the propellant. This is evidenced by the first decomposition peak which is the same for pure DHT. The second decomposition peak occurs at a slightly lower temperature than that of the reference propellant. The lack of a return to the baseline between the two decomposition peaks for the propellants containing DHT also clearly demonstrates that the decomposition of the DHT propellants is not described by the separate de composition of DHT and the reference. This can be attributed to the effects of the remaining DHT and its decomposition products accelerating the decomposition of the other energetics present in the propellant.

The activation energy of DHT was evaluated at 128±13 kJ·mol^{-1} in accordance with values previously reported, same for the onset and peak temperatures [95]. For the 5% DHT propellant,

the activation energy of the first decomposition is equivalent to pure DHT, indicating that DHT dominates that decomposition reaction. The activation energy of the second degradation reaction is also different from the reference propellant. This illustrates that remaining DHT and its decomposition products influence the reaction kinetics of the decomposition of the second reaction. As the DHT content increases, the activation energy for the first decomposition increases indicating a change in the kinetics of the decomposition reaction. A change in the decomposition kinetics of the second degradation process is also observable with an activation energy increase (195 ± 8 kJ·mol^{-1}) at 15% DHT, and a decrease (157 ± 13 kJ·mol^{-1}) at 25% DHT. The decomposition temperature of the first decomposition reaction indicates that nitrocellulose, TMETN and TEGDN have a limited effect on the thermal stability of DHT, but that the reverse is not true. This will be further evidenced with the vacuum stability tests. Hermetic DSC pans allowed for the measurement of solid and gas phase reactions. Gas phase reactions are pressure dependent. This makes a direct comparison with closed vessel experiments difficult. However, the variation of burning rate law parameters with DHT content is also indicative of changes in reaction kinetics meaning that both DSC and closed vessel experiments point to the same behavior. The peak temperatures are indicative of which material characterises best the bulk of the decomposition reaction. The first degradation is likely characterized by DHT, while the second degradation likely a combination of the degradation of the other energetics and the degradation products of DHT.
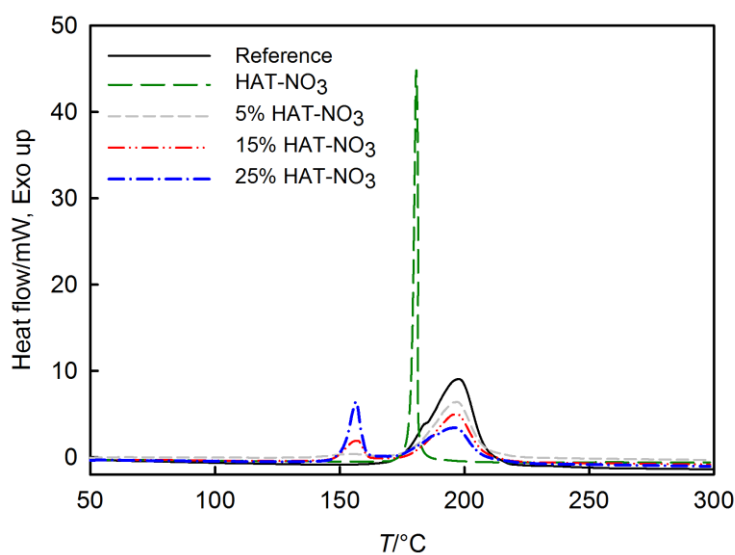

Figure 5.6: Stability of HAT-NO$_3$ propellants in DSC

For the HAT-NO$_3$ containing propellants, the decomposition is below those of the reference formulation and pure HAT-NO$_3$. This indicates that HAT-NO$_3$ and the other energetics in the propellant might react together. This usually results from poor compatibility between HAT-NO$_3$ and other energetic materials. Further experiments in DSC of mixtures of HAT-NO$_3$ and individual plasticizers demonstrated that TMETN and TEGDN are responsible for the decrease in decomposition onset. The same onset temperature (140°C) was observed for a mixture of TMETN and HAT-NO$_3$ equivalent to the contents of the 5% HAT-NO$_3$ propellant. A mixture containing HAT-NO$_3$ and TEGDN had an onset of 161°C. Pure TMETN and TEGDN have onset temperatures of 176°C and 171°C respectively. The thermal stability of the HAT-NO$_3$ propellants remains acceptable, but it is quite far from stated criteria for new energetic materials of > 200°C [9].
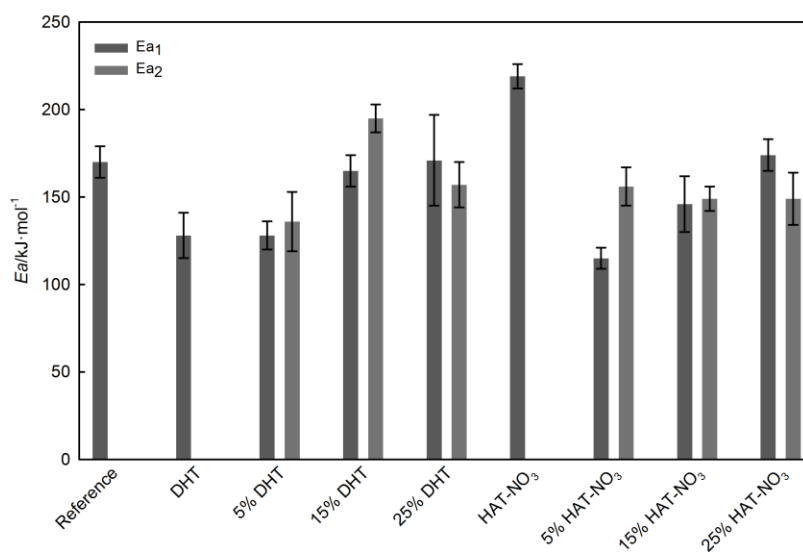
Figure 5.7 : Activation energies of the propellants decomposition in DSC

The activation energy of the first degradation peak for the HAT-NO$_3$ propellants increases with HAT-NO$_3$ content towards the activation energy of pure HAT-NO$_3$. This supports the hypothesis that the bulk of the degradation of HAT-NO$_3$ proceeds separately from the degradation of the other energetic materials in the propellant. If this was not the case, effects like those seen with DHT and two previously studied nitrogen-rich materials [111] would be observed. The similar activation energies between the decomposition of the reference propellant and the second decomposition reaction of the HAT-NO$_3$ propellant also support this.

An important aspect of new energetic molecules is the thermo-chemical compatibility of these molecules with other energetic materials. The long-term stability is especially interesting from a safety perspective. Nitrogen-rich materials have been put forward as replacement for nitramines [3, 64] and proved to be excellent burning rate enhancers [111]. Current research into environmental impact of azoles is also promising [9]. This demonstrates the potential of tetrazoles as environmentally friendly energetics. In addition to the propellants presented in this work, the stability of the reference propellant and of two previously reported propellants [111], containing 25% of 5,5'-bis(1H-tetrazolyl)amine (BTA) or 5,5'-hydrazinebistetrazole (HBT) nitrogen rich materials were also investigated. The results are shown in Figure 5.8 and Table 5.5.

For the vacuum stability experiments, Figure 5.8 and Table 5.5 show that HAT-NO$_3$ propellants exhibited a strong gas release after only 40 hours indicating most probably that HAT-NO$_3$ and nitrated esters like TMETN and TEGDN exhibit poor long-term stability which may result in auto ignition. This accelerated decomposition is attributed to the ionic nature of HAT-NO$_3$ which is expected to partly dissociate into its acid and base, nitric acid and 5-aminotetrazole. This is reflected in the similar activation energy of the second decomposition of all HAT-NO$_3$ propellants (Figure 5.7). The worst results were recorded for the propellant with 25% DHT. A steep increase in the pressure was observed after only 10 hours after which a deflagration strong enough to damage the VST cell occurred. This behavior is indicative of an autocatalytic reaction resulting from chemical incompatibility (the materials cause a decrease in stability or a self-accelerating reaction) between DHT and one or more of the other constituents of the formulation. DHT has been reported to decompose under oxidizing conditions [54]. The depletion of the stabilizer within the propellant due to the accelerated ageing in the VST likely resulted in the formation of decomposition products that were partly oxidizing in nature; this plus the high nitro group concentration already present in the formulation likely contributed to the fast decomposition of DHT. This event was followed by the quick decomposition of the entire propellant which lead to the observed deflagration event.
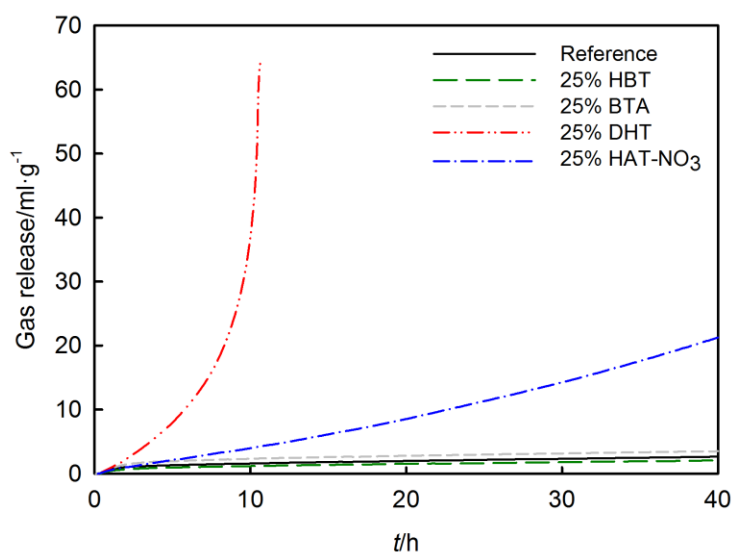
Figure 5.8: Vacuum stability at 25% (m/m) nitrogen-rich content

Table 5.5: Vacuum stability at 90°C

Propellant	t [h]	Gas volume released[9] [ml·g^{-1}]
Reference	116	1.91 (compatible)
25% HBT	70	0.93 (compatible)
25% BTA	70	1.37 (compatible)
25% DHT	11	Deflagration[10]
25% HAT-NO$_3$	40	12.6 (poor compatibility)

Isothermal DSC experiments of the three propellants containing DHT (Figure C22), confirmed that all propellants exhibited an autocatalytic decomposition. Further experiments are requited to assess which of TEGDN and/or TEMTN are chemically incompatible with DHT.

On the other hand, HBT and BTA exhibited excellent compatibility with the reference propellant formulation.

The results of the DSC experiments and the VST experiments may appear to disagree for the DHT propellants. This however, is not the case, the time scale of the DSC experiments is short enough that the autocatalytic behavior does not have time to appear and the decomposition is driven by the heating of the propellant. The time scale and temperature of the VST experiments lend themselves

---

[9] At end of experiment after return to room temperature

[10] Due to the apparatus breaking, a value at room temperature could not be obtained

better to measuring the autocatalytic nature of DHT and nitrated esters. The VST and DSC experiments agree that HAT-NO$_3$ is has poor compatibility with nitrated esters. The nitric acid from partial dissociation of the salt likely depletes the stabilizer faster because of its poor compatibility which leads to the increased gas release in the VST test. This may possibly be countered with other stabilizers. A higher amount of stabilizer would help alleviate this, but would also remove energy from the propellant. The autocatalytic nature of DHT makes it unsuitable for nitrocellulose based composition. Based on previous DSC results [15] and the current VST data, the more practical solution to using nitrogen-rich materials in nitrocellulose based compositions is the use of neutral tetrazoles like HBT and BTA for good stability.

5.5 Conclusions

The addition of low quantities of DHT and HAT-NO$_3$ to a triple base propellant provided significant burning rate improvements. Both nitrogen-rich materials were found to be excellent quickness enhancers while retaining similar force.

The results show that there is an optimal concentration of nitrogen-rich materials which will yield the highest burning rates with the lowest pressure dependency. This concentration is dependant of the overall propellant formulation.

The nitrogen-rich materials have a significant effect on the degradation processes of the propellant compared to the reference formulation.

The long term thermal stability of the propellants containing both DHT and a nitrated ester results in autocatalytic decomposition. Therefore, care must be taken when formulating DHT containing propellants to avoid combining it with chemically incompatible materials. HAT-NO$_3$ was also found to have poor long-term compatibility in the propellants, but no DHT-like autocatalytic behavior was observed. Finally, neither BTA nor HBT affected the stability of the triple-base propellants tested here. It is proposed that neutral tetrazoles are the best candidates for nitrocellulose based formulations.

These nitrogen-rich materials show promise as environmentally friendly energetics for use in future generations of propellants. Scale-up efforts are being made on BTA and HBT molecules for further environmental, performance and toxicity assessment.

5.6 Acknowledgements

5.7 Funding

CHAPTER 6   ARTICLE 3: EROSIVITY AND PERFORMANCE OF NITROGEN-RICH PROPELLANTS

Jonathan Lavoie, Catalin-Florin Petre, Simon Durand, Charles Dubois

This article continues the investigation into the uses of nitrogen-rich materials in propellants. It is the first work focusing erosivity of propellants incorporating nitrogen-rich materials. It illustrates the potential of nitrogen-rich materials to form a protective barrier to erosion by analyzing the changes in composition of steel resulting from the use of nitrogen-rich materials. It also builds upon the previous two articles by using similar propellants with even higher proportions of nitrogen-rich materials. Finally, this article builds a good case for the performance of future propellants that use nitrogen-rich materials.

6.1 Abstract

Five propellant formulations were test fired both in a vented vessel and a closed vessel. Two formulations contained 35% weight of nitrogen-rich materials. The erosion by weight of the propellants ranged from 0.53 g to 1.31 g after two consecutive test firings of a given propellant. The addition of nitrogen-rich materials resulted in reduced erosion. Scanning electron microscope and energy dispersive X-ray spectroscopy revealed nitrogen in the erosion pieces for one of the reference propellants (SB) and the two nitrogen-rich propellants. The two hottest propellants cause melting of the erosion pieces. The presence of nitrogen-rich materials has a tremendous impact on the burning rates with the burning rate increase at 100 MPa reaching up to 2.4 times that of the formulation used as the base for the nitrogen-rich propellants.

6.2 Introduction

Since World War II, it is common knowledge for gun systems users/manufacturers that the erosion of gun barrels leads to two types of problems: (i) barrel replacement costs over the lifespan of fielded weapon systems, and (ii) reduced operational effectiveness due to variable gun performance and availability [79-81, 84, 90]. This is due to the effects of repeated firings on gun barrels, that even under normal firing conditions, are generally manifested in damage to the bore surface and a progressive increase of the bore diameter. The costs are not limited to the replacement of the barrel

itself, but transportation of the gun barrel from its production facility to the location of the gun system is another contributing factor. These are non-negligible logistic costs that depend on distance and fuel prices.
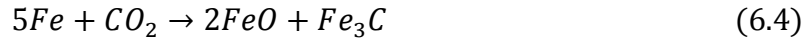
There are three main approaches to mitigate gun barrel erosion: development of less erosive propellants, the use of coatings, treated barrel materials and liners, and erosion-reducing additives and lubricants. The most widely used approach is the use of protective coatings or surface treatments on the bore of the gun barrel. Normally, this is either done by depositing a thin layer of hard chromium inside the gun barrel or by nitriding (hardening) the interior of the barrel [84, 90]. These coatings/treatments are designed to mitigate all mechanisms of erosion, which are detailed below.

Multiple phenomena are responsible for gun barrel erosion, but they can usually be divided into three categories: mechanical action, heat transfer effects and changes in chemical composition. These phenomena are designated as mechanical, thermal and chemical erosion and they are tightly interdependent acting in concert to erode the barrels [79-81]. Mechanical erosion is caused by the friction from a projectile (or its driving band) moving through a gun barrel and is out of the scope of this work.

Thermal erosion is caused by the morphological changes of the gun barrel steel, i.e. austenite and martensite phase transformation of steel and by the melting of the barrel material. Depending on the propellant used in the gun system and the rate of fire of the system, the steel temperature can get as high as 1800 K in a matter of milliseconds [81]. This is high enough to cause partial melting of the gun steel. The melting temperature of typical gun steel is 1723 K [84]. While temperatures of up to 1800 K can be attained, this is for very hot propellants and usually, the temperature of the gun barrel will be lower. For example, the barrel surface temperature for a Navy 5"/54 gun has been evaluated at 1450 K for XM-39 propellant which has a flame temperature of 2654 K [80].

Chemical erosion refers to the effects of chemical reactions occurring between the gun steel and the combustion gases generated by the propellant. The main combustion gases generated by a gun propellant are carbon monoxide (CO), carbon dioxide (CO_2), water (H_2O), hydrogen (H_2) and nitrogen (N_2). While other gaseous species are also formed, they are in small quantities and are usually lumped together or simply ignored in erosion modeling [78, 79, 85]. Each of these gases

can react with gun steel to form various compounds. Some of these reactions are shown in equations 6.1 to 6.4 [82, 83].

$$Fe + CO_2 \rightarrow FeO + CO \tag{6.1}$$
$$3Fe + 2CO \rightarrow Fe_3C + CO_2 \tag{6.2}$$
$$4Fe + CO \rightarrow FeO + Fe_3C \tag{6.3}$$
$$5Fe + CO_2 \rightarrow 2FeO + Fe_3C \tag{6.4}$$

Iron carbide, formed due to the presence of CO and CO_2, has a melting point around 1420 K, and other low melting point ferrous compounds are to be avoided to minimize erosion [84]. For the moment, there is no consensus on which combustion gas is the most erosive. Lawton has proposed a robust model with an erosion parameter based on the combustion gas composition of propellants commonly fielded in the United Kingdom, equation 5.5 [79].

$$\ln(A) = \ln(114) + 0.0207(f_{CO} - 3.3f_{CO_2} + 2.4f_{H_2} - 3.6f_{H_2O} - 0.5f_{N_2}) \tag{6.5}$$

Where "f" represents the volume fraction in percentage of the gas species in subscript and A is the erosivity in m·s^{-1}. Jaramaz et al. also proposed a propellant erosivity coefficient based on the gas composition, equation 5.6 [85].

$$\ln(A \cdot 10^3) = -0.27f_{CO_2} + 0.079f_{CO} - 0.14f_{H_2} + 0.35f_{H_2O} - 0.019f_{N_2} + f_R \tag{6.6}$$

Where "f" represents the fraction in % of the associated gas species, "R" standing for the remainder of the gas species and A is an erosion mass loss coefficient. Kimura proposed the following order for propellant combustion gases from the most chemically erosive to the least chemically erosive, equation 5.7 [83]. The difference in these models likely comes from the propellants and the experimental setup used given their empirical nature.

$$CO_2 > CO > H_2O > H_2 > 0 > N_2 \tag{7}$$

Kimura's observation on CO_2 is also in agreement with erosion data from Conroy et al. [121]. Claims have also been made that high nitrogen content in the combustion gases could contribute to re-nitridation of the gun barrel and increase lifetime up to a factor of four [8]. The formation of iron nitride due to propellant combustion gas has been observed [84], but the propellants tested were limited to formulations made of conventional energetic materials. The research and modeling performed on the erosivity of combustion gases show a lack of consensus as to which gas is the most erosive. Despite the lack of consensus, there is agreement between various works that CO

and H_2 increase the rate of gun barrel wear associated with the propellant. Comparatively, nitrogen gas is considered to have a lowering effect on gun wear.

The interdependence between the propellant and the thermal and chemical erosion becomes apparent. The propellant combustion is responsible for the heat generated in the gun. The composition of the combustion gases of a propellant depend on its molecular composition and its flame temperature. Finally, the reactions occurring between the combustion gases and the steel depend on the gas composition and temperature. As such, it stands to reason that adjustments to the flame temperature and combustion gases composition should have a direct impact on the erosivity of a propellant. While the amount of CO generated could be mitigated by a shift in the oxygen balance of the propellant, this would lead to a higher CO_2 and H_2O content while the nitrogen content remains constant. Given that nitrogen is not considered an erosive combustion gas, its generation should be prioritized. In fact, since it can be obtained from thermochemical calculations without experiments, the N_2/CO ratio has been used as an estimation of how erosive a propellant could be [26].

Based on the above, in order to design a low erosivity gun propellant, emphasis should be put on lowering the flame temperature and increasing nitrogen content in the combustion gases. This makes nitrogen-rich materials very interesting as they are mostly composed of nitrogen, often exceeding 80% by weight. It goes without saying that new propellants designed to have lower erosivity should also provide similar or better performance than the propellants they are designed to replace. The positive effects of nitrogen-rich materials on the burning rate of propellants have already been demonstrated by Mason *et al.* and Lavoie *et al.* [100, 111]. It was shown that in certain cases, despite the lower flame temperature, the experimental maximum pressure observed for nitrogen-rich propellants in a closed vessel remained highly similar to comparable formulations that did not incorporate nitrogen-rich materials, an indication that similar performance is attainable [111]. This work is a follow up on the previous one [111] and focuses on the effects of two nitrogen-rich materials on the erosivity of gun propellants comparatively to standard formulations with matching impetus.

6.3 Results and Discussion

6.3.1 Erosivity

. An erosivity vented vessel allows observing the effects of the thermo-chemical erosion mechanisms, isolating their effects from the mechanical erosion mechanism. As such, two parameters are very important when conducting erosivity vented vessel experiments: the flame temperature and the composition of the combustion gases of the propellants investigated. Therefore, the propellant formulations from this study were all chosen based on the simulated thermochemical properties. Ideally, the burning rate of propellants should also be matched, or the geometry adapted to insure similar pressure-time profiles. However, it is currently not feasible to predict the burning rates of complex propellants [110]. Insuring that the amount of energy contained in a propellant remains constant requires the design of complex propellants which is what motivated the use of thermochemical properties which can be predicted contrarily to burning rates.

Thermochemical data, calculated with Cheetah 7.0 is shown in Table 6.1. One can notice that propellants SB and MTB15 provide similar impetus and flame temperature. This affords the opportunity to observe in detail the effect of the gas composition on the erosivity of propellants with similar thermochemical properties. For example, the N_2 to CO ratio of MTB15 is four times greater that of SB which should in theory help reduce the erosivity of the MTB15 propellant. In the case of MTB16, it provides the same amount of energy than JAM with increased nitrogen content and reduced flame temperature. The quantities in Table 6.1 are as follow: impetus (F), flame temperature (T), molar ratio of gases (N_2/CO; CO/CO_2), adiabatic pressure ($P_{max,ad}$), experimental pressure ($P_{max,exp}$).

Table 6.1 : Thermochemical properties of the propellants, calculated from Cheetah

Propellant	F/J·g⁻¹	T/K	N₂/CO	CO/CO₂	Pmax, ad/MPa	Pmax, exp/MPa
SB	960	2602	0.20	9.75	246	220 ± 1
MTB15	987	2569	0.80	18.23	258	260 ± 1
JAM	1128	3305	0.30	3.96	282	265 ± 2
MTB16	1125	2951	0.77	21.5	293	246 ± 3
MTB17	1139	3229	0.29	4.55	286	266 ± 2

The maximum pressure observed experimentally in the vented vessel was 89% or more of the maximum adiabatic pressure (Table 6.1). This indicates that venting during combustion of the propellant and heat losses are minimal. Therefore, the composition of the combustion gases determined by the thermochemical calculations represents a good estimate of the combustion gases flowing through the erosion pieces.

The mass loss resulting from the erosivity of the propellants is show in Figures 6.1 to 6.4. The measured erosion resulted from several phenomena: the chemical erosion resulting from reactions between combustion gases and steel, heat transfer including possible melting of the steel and friction from the flow of high pressure gases. The erosion on steel from a decommissioned M68 105 mm artillery gun was evaluated for the JAM propellant to compare with 4340 AISI steel. Mass loss for the erosion pieces made of gun steel was 1.58 g $\pm$ 0.15 g (one test firing) and 1.28 g (two consecutive test firings). Mass loss for the 4340 AISI steel was 1.52 g $\pm$ 0.20 g (single test firing per piece) and 1.31 $\pm$ 0.37 g (two consecutive firings per piece) which is very comparable to the M68 gun steel.

The absence of a rupture disc results in a different pressure history once an erosion piece is used more than once due to the change in diameter of the channel through which the combustion gases flow. To compare results between tests and propellants, the data was normalized according to equation 8. Equation 8 was chosen because a complete modeling of the transient flow of the gases was not possible. The use of pressures avoided further mathematical treatment of the pressure-time data that could potentially induce errors or require additional assumptions. The principal limitation of this treatment is that significant differences in action time will not be entirely factored into the analysis. Normalized erosion will likely be overestimated for fast action times due to increased gas flow rates and underestimated for slow action times. This only affects SB and MTB15, the other propellants remain unaffected. This will be elaborated on in the discussion of the erosivity results.[11]

$$E_{norm} = E\left(\frac{P_m}{P_{ref}}\right)^{-1} \tag{6.8}$$

---

[11] The discussion of the limitations of the equation was added at the request of the original examiner, it will be added to the manuscript for the final submission of the article to the scientific journal.

Where E_{norm} is the normalized erosion, E is the measured erosion, Pmax is the maximum pressure for any given test and Pref is a reference pressure. The reference pressure was chosen to be 265 MPa due to it being among the highest pressure observed across all propellants. The erosion data was normalized to partially remove the effects of friction from high velocity gas flow compared to flame temperature and gas composition on the data. Higher pressure gas will have higher erosion due to higher velocity gas flow. This approach was verified using the results of JAM fired at respectively 0.1 g·cm^{-3} and 0.2 g·cm^{-3} which resulted in comparable normalized erosion. A total of three erosion pieces were tested per propellant. One piece was subjected to three consecutive firings, another to two and the last piece was subjected to a single firing. This explains the lack of error bars on the data for three firings as the results are for a single test piece. The pieces were weighed between each test firing. It was decided to measure the diameter of the erosion test pieces

after most of the JAM propellant had been tested which is the reason why it is excluded from the thickness erosion results.

Figures 6.1 to 6.4 show the erosion by mass loss between consecutive firings and by the change in diameter between consecutive firings. Both values were measured as the change in mass loss will be influenced by changes in the steel composition due to gas species reacting with the steel.
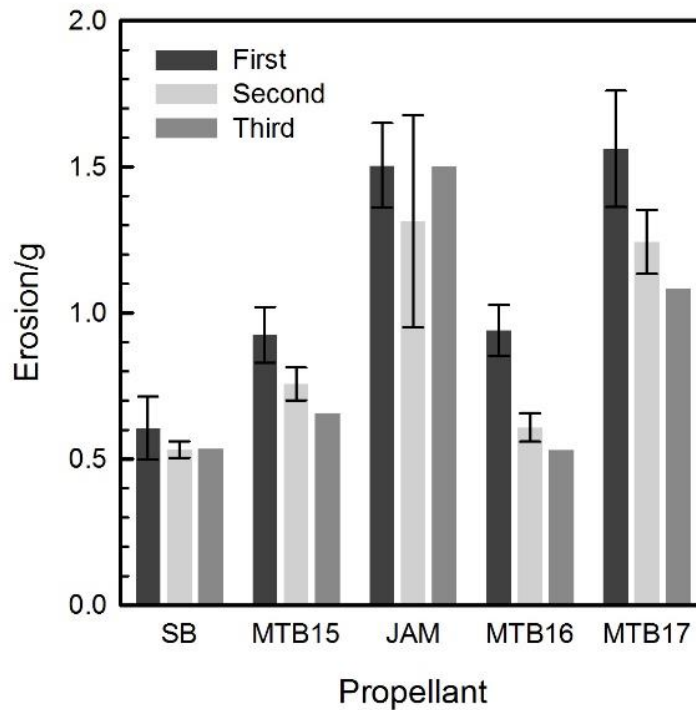

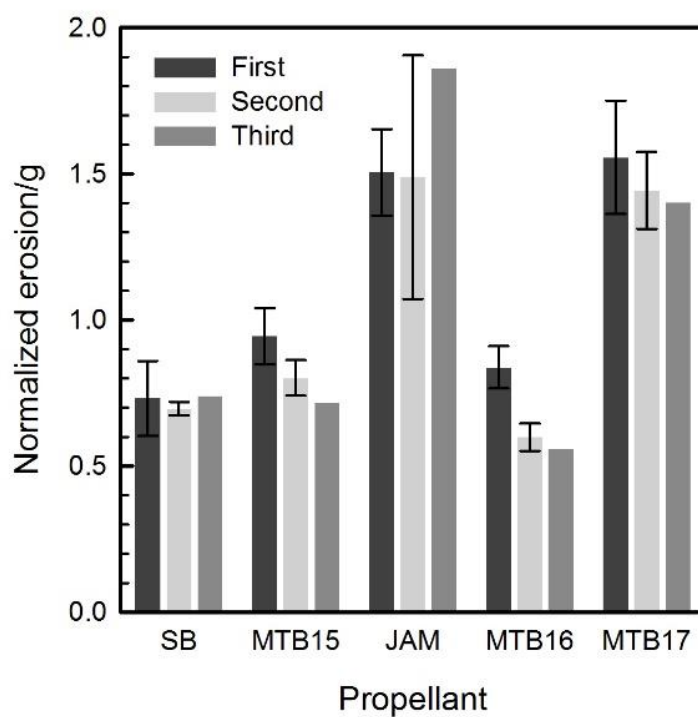Figure 6.1 : Erosion by weight loss between firings

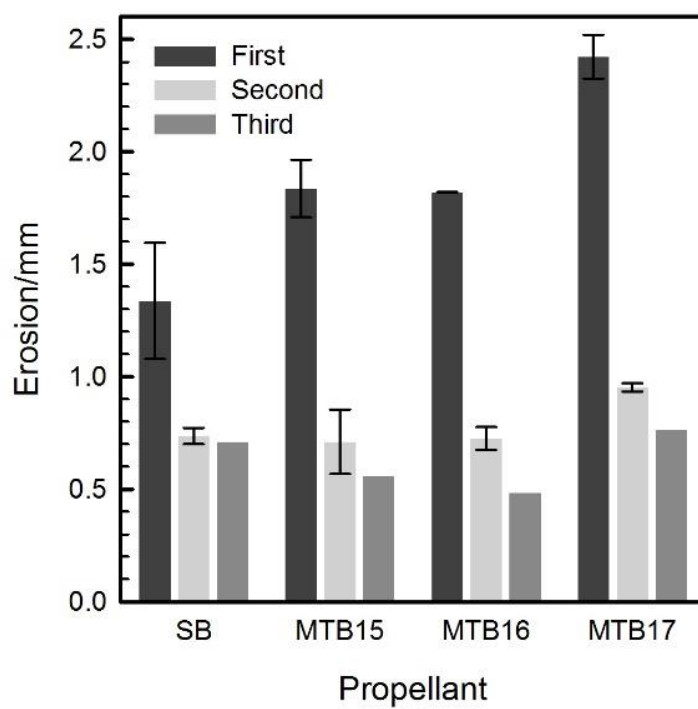Figure 6.2 : Normalized erosion by weight loss between firings

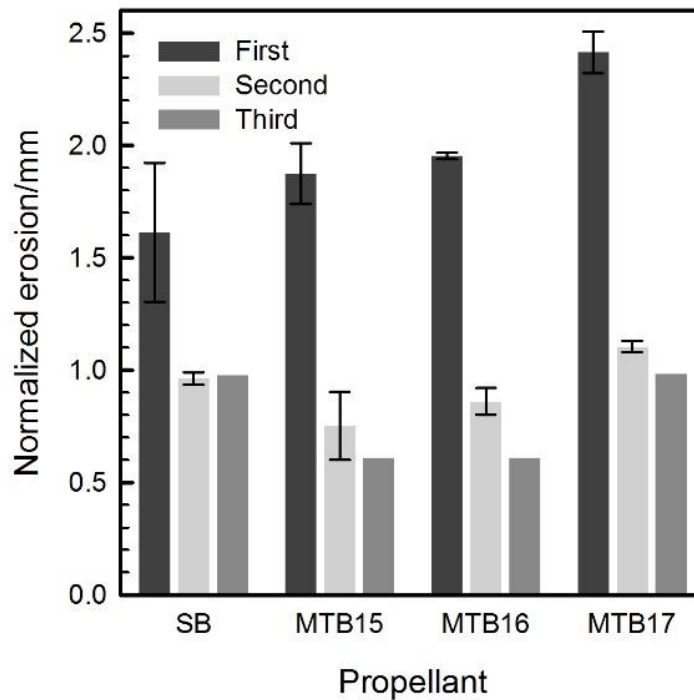Figure 6.3 : Erosion by diameter change between firings

Figure 6.4: Normalized erosion by diameter change between firings

Figures 6.1 to 6.2 shows that JAM and MTB17 are the two most erosive propellants tested. This was expected based on composition of the combustion gases and adiabatic flame temperature. SB is a generally considered a cold propellant and as such was expected to show lower erosivity. Even when using normalized data, MTB15 proved to be more erosive than SB, mainly because it has a burning rate that is roughly four times faster than that of SB. The burning rates will be discussed in the section on performance. The approach used to normalize the erosivity is solely based on the maximum pressure and as a result, does not account for the flow pattern history of the combustion gases. It was found that MTB15 exhibited significantly faster pressure rise in the vented vessel than all the other propellants and SB had a slower pressure rise (Figure 6.5).
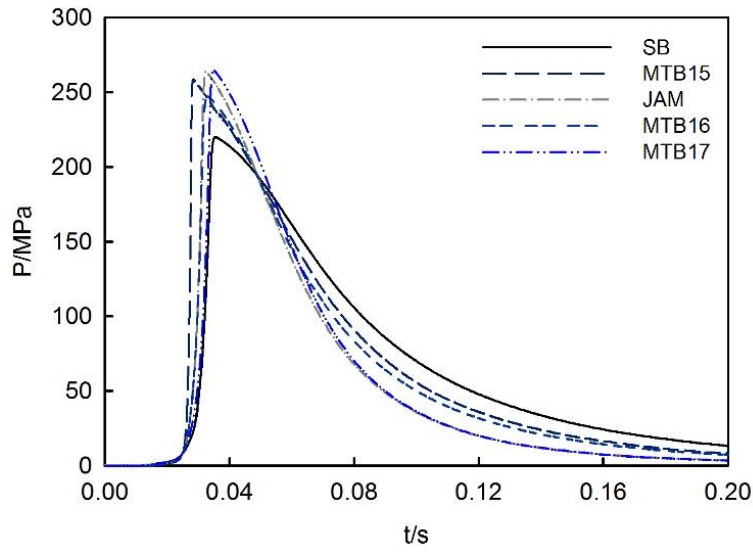
Figure 6.5 : . Pressurization of the vented vessel during a first test firing

It is expected that this behavior will significantly increase the erosion due to the mechanical action of the gas flow. The SEM micrograph of the piece subjected to three firings of MTB15 showed significant cracking in the flow direction at a higher degree than any of the other propellants (this will be elaborated on the next section). This is indicative of a high mechanical stress which likely amplified the erosion significantly and would explain the higher erosivity comparatively to the SB propellant. The higher erosion for the first test compared to pieces that were subjected to two or three tests supports the idea of strong flow erosion effects for MTB15. The change in diameter for MTB15 is similar to the change in diameter for SB on pieces subjected to two or three test firings. The change in the shape of the channel of the steel pieces compared to other pieces where no melting occurred also supports strong gas flow effects (Figure 6.6).

Interestingly, MTB16 was the least erosive propellant despite a temperature of 2951 K, higher than that of MTB15 (2569 K) and SB (2602 K). This can be attributed to the higher nitrogen content of the combustion gases. The photos sectioned erosion pieces for MTB16 also show no evidence of melting and uniform erosion along the whole channel (Figure 6.6).

JAM and MTB17 are the two propellants that show evidence of the erosion pieces melting. For JAM, the melting occurred only after three test firings and was quite pronounced. For MTB17, melting was observed after two firings, but is less pronounced than it was for JAM. The high normalized erosion of JAM after three tests agrees well with the observed melting.

A behavior that was observed for all propellants was that the erosion for the first test was much higher than for any subsequent tests. This results from the small initial diameter of the erosion pieces which is small enough to experience a large amount of mechanical erosion from the flow of combustion gases. The effects of gas flow are also evidenced by the formation of a curvature at the entry point of every erosion piece as easily evidenced by Figure 6.6.
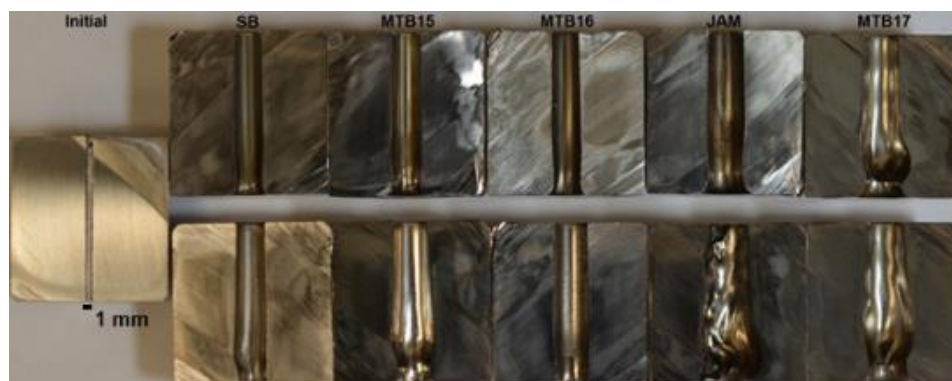

Figure 6.6 : Cut erosion test pieces after two (top) and three (bottom) test firings

Changes in erosion for three consecutive test firings are shown in Table 6.2 relative to the erosion of SB, JAM and MTB17, the three reference propellants. Table 6.2 shows that from a mass loss standpoint, MTB16 is the least erosive propellant after three consecutive firings and that MTB15 remains less erosive that any of the reference propellant. The changes in diameter show that both propellants show similar erosivity between the second and third test firings. The likeliest explanation for the discrepancy between the changes in mass and diameter is that the reaction of the combustion gases with the steel results in the formation of ferrous compounds that have an influence on the final mass of the erosion piece. The pieces subjected to three consecutive firings were weighed after being thoroughly washed to ensure that combustion residue had no influence on the calculated data. The amount of combustion residue present in the channel of the erosion pieces was also found to have a negligible influence on the change in weight before and after washing the erosion pieces for all tests (two orders of magnitude lower).

Table 6.2: Normalized erosion relative to the reference propellant formulations

	SB	JAM	MTB17
MTB15 (weight)	0.97	0.39	0.51
MTB16 (weight)	0.76	0.30	0.40
MTB15 (diameter)	0.62	N/A	0.62
MTB16 (diameter)	0.62	N/A	0.62

It is also interesting to note that the molar concentration of hydrogen in the propellants was the highest for the two nitrogen-rich propellants at 22% compared to 19% for SB, 12% for JAM and 13% for MTB17. Hydrogen has been postulated to promote heat transfer and often results in higher erosion by weight loss at lower flame temperatures [9]. A linear relationship between the logarithm of the erosion and the square root of the ratio of the flame temperature to the molecular weight of the combustion gases was previously observed, illustrating the influence of hydrogen content on increased heat transfer which results in higher erosion [9]. The normalized erosion of the three conventional propellants follows this trend well across all tests for any number of firings on the same erosion piece. The exception was the JAM test where important melting and higher erosion occurred. MTB15 appears to follow the same tend to some degree, however MTB16 is a clear divergence from this trend with a much lower erosivity at similar $\sqrt{(T/M_w)}$ to the other propellants (Figure 6.7).
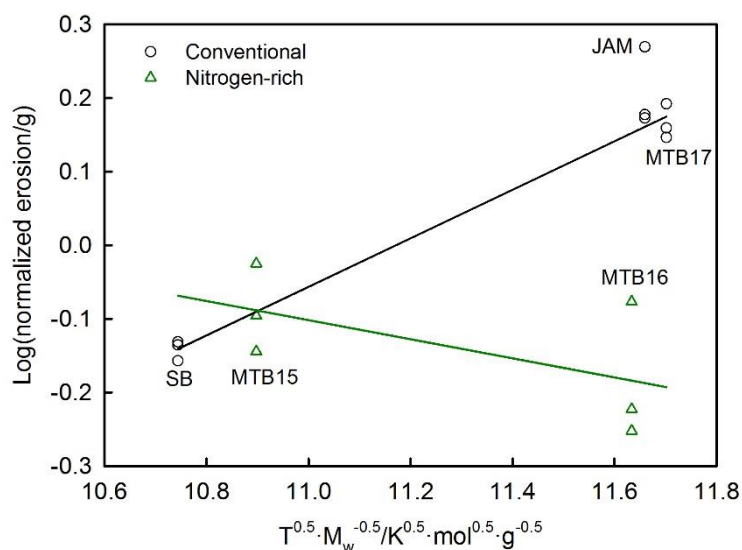

Figure 6.7 : Effects of flame temperature and gas weight on erosion[12]

As previously discussed, MTB15 firings resulted in pressurization of the vented vessel roughly three times as fast as SB and twice as fast as the other propellants. The normalization of the erosion data is therefore likely to have less of an impact on MTB15 and the effects of the gas flow will remain higher compared to the other propellants. The chemical and thermal erosion effects are

---

[12] Figure was modified from the originally submitted manuscript

expected to be lower than the ones presented in Figure 6.7. Another hypothesis that could explain, at least partially, the lower erosion as a function of $\sqrt{(T/Mw)}$ is the improved heat transfer that results in two opposing effects: reactions of steel with carbon and oxygen which increase erosion competing with nitriding of the steel which decreases erosion. Depending on the quantity of nitrogen in the combustion gases, nitriding of steel should be the dominant reaction. This could lead to hot propellants with low erosivity to a certain extent. Propellants hot enough to cause bore temperatures of 1700 K or more would still result in melting of gun steel regardless of the nitrogen content. More experimental work is needed to confirm whether this would be the case, but the results of this study highlight this possibility.

6.3.2 Scanning Electron Microscopy

Carbon contamination from sample handling and organic compounds present in the laboratory is difficult to avoid completely. A composition analysis on the non-reacted steel outside of the channel where gas flow occurred gave 2% to 4% weight carbon which gives an approximation of the carbon content from contamination. Therefore, any carbon content at those levels with no apparent change in morphology was not considered as Fe_3C in the analysis.

Unexpected traces of contamination were found by the EDS detector during the SEM experiments. This was puzzling at first and made interpreting the results of the EDS detector more difficult. Figure 6.8 shows examples of the contamination observed. The left image shows droplets from what was identified to be weld contamination on the piece subjected to 3 test firings of SB. These droplets were identified to be either mainly tin (50+ % weight) or a lead-tin alloy, 3:4 weight ratio. The droplets were thin enough for some iron to be detected by the EDS detector. Iron, carbon, oxygen and other elements composed a minority of what was detected. The middle image taken from the piece subjected to 3 tests with MTB15 is splatter from lead at 21% weight, the layer was thin enough to detect 59% weight of iron along with some carbon (9%) and oxygen (8%). Part of the carbon is expected to come from combustion residue rather than having reacted with the steel. Potassium, sulfur, copper or a combination of these elements were always present with the contamination. This contamination is expected to come from the igniter where copper, black powder and the electric match charge and support is the likeliest source for the contamination.
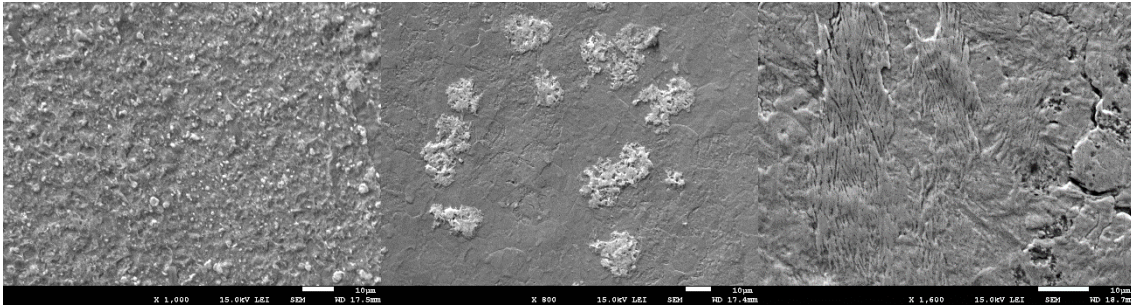
Figure 6.8: Contamination from the ignition system, from left to right: lead and tin droplets, lead and tin splatter and copper splatter.

Any location where significant amounts of contamination were detected were not factored into the analysis and discussion of the effects of the combustion gases on the erosion pieces that follows.

The erosion mechanisms of the two hottest propellants (JAM and MTB17) appear to differ significantly from the other three. Table 6.3 shows the atomic content of iron, carbon, oxygen and nitrogen found in the erosion pieces after two test firings. For comparison, a non-tested piece parts of the segmented erosion pieces not exposed to the propellant gases is shown.

Table 6.3 : Atomic composition after two test firings

	Fe [atomic %]	C [atomic %]	O [atomic %]	N [atomic %]
Non-exposed steel	82-84	10-14	0-6	0
SB	57-58	25-30	10-13	0
MTB15	62-70	20-25	4-9	2-5 (at 5 kV)
JAM	62-70	22-27	5-9	0
MTB16	55-64	24-29	7-15	3-7
MTB17	68-78	14-20	3-5	0

After two test firings, what is believed to be chemical etching appears on the test pieces subjected to SB, MTB15 and MTB16. Figure 6.9 shows images of erosion pieces subjected to two test firings of propellants SB, MTB15 and MTB16 at low and high magnification. The "needle" like structures formed by the reaction with the combustion gases are visible for all three propellants, but are much more pronounced for SB than the other two propellants. Sites free of visible igniter contamination on the piece in contact with the combustion gases of SB exhibited atomic oxygen content of around 10%-13%, higher carbon content (25%-30%) with 57%-58% iron. The balance was a very small amount of igniter contamination and nickel which is present in AISI 4340 steel. This indicates it is more likely that SB results in the formation of iron carbide (Fe_3C) than oxides. The flame temperature of SB is low enough that the formed Fe_3C is not expected to melt. Small amounts of

nitrogen were sometimes also detected. Composition analysis of pieces in contact with MTB15 after two firings showed no distinct oxide layers and the chemical attack appears to be less important than for SB. Any layer found on the erosion pieces was due to igniter contamination. Atomic concentrations varied between 62%-70% Fe, 20%-25% C and 4%-9% O. This is indicative of some amount of Fe_3C with only a very small amount of oxide, given that manganese, chromium, nickel and the other components of 4340 AISI steel were usually detected on these sections, it is expected that not all steel was converted to Fe_3C and that some of the carbon content is combustion residue and organic compounds. At 15 kV, a nitrogen peak was observed, but the deconvolution algorithm used by the software resulted in a negative peak area giving it an erroneous concentration value of 0%. Scans taken at 5 kV yielded better results and puts the nitrogen atomic content between 2% to 5% in areas where no igniter contamination was observed. The electrons can penetrate approximately 1 micron at 15 kV and only 0.16 microns at 5 kV. Interestingly, where layers of metal splatter from the igniter were detected, higher nitrogen content was also observed. This is either due to unburnt propellant buried under the contamination or other nitrided species like Cu_3N.
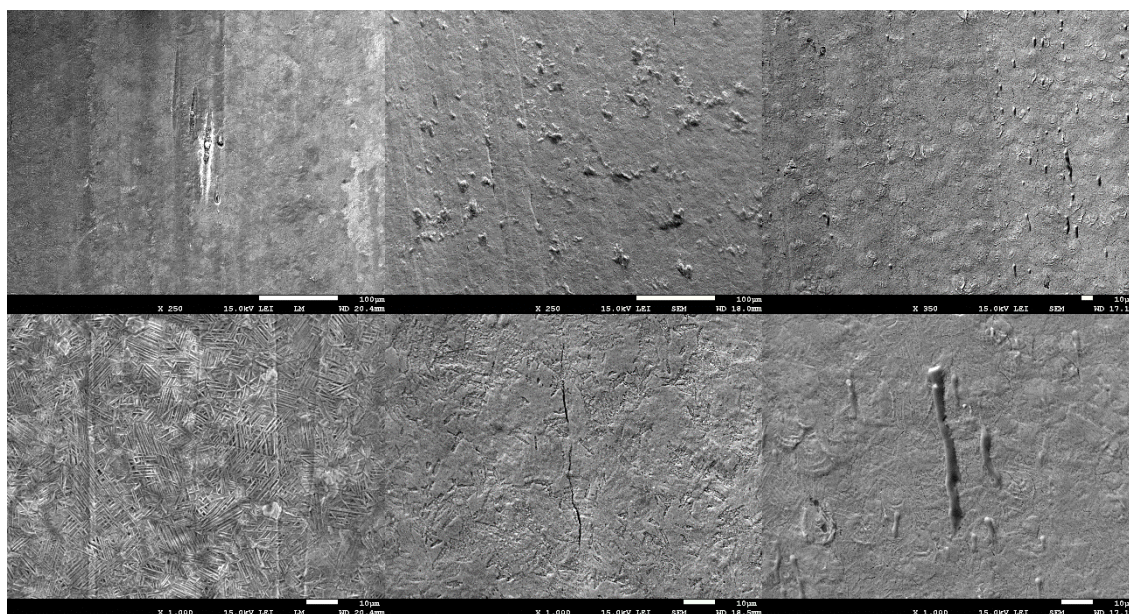

Figure 6.9 : Erosion pieces after two test firings, from left to right: SB, MTB15 and MTB16

MTB16 shows similar results to MTB15 with an atomic composition in areas free of contamination of 55%-64% Fe, 24 %-29% C, 7%-15% O and 3%-7% N. In this case, the nitrogen could be detected even at 15 kV. The preferred hypothesis for the higher oxygen and carbon content is the

flame temperature of MTB16 favoring the reaction between the combustion gases and the steel. This would also favor higher nitrogen content which as observed. This higher nitrogen content is line with the lower relative erosivity of MTB16 compared to all the other propellants. The chemical attack of the combustion gases which in this case is evidenced by the change to a needle like structure was also lesser for MTB16 compared to SB. The exact cause of the shape of the structure are currently unknown. The overall carbon content is also lower for the nitrogen-rich propellants than it is for SB. The handling of all samples was kept identical, therefore, any change in atomic content is expected to be a result of the effect of the propellant composition.

Also, visible on Figure 6.9 are the impact from impinging particles, contamination from the igniter and stress cracks in the flow direction from the gas pressure. The fact that cracks do not follow the grain of the steel is attributed to the stress imparted by the high pressure during the tests rather than thermal expansion and contraction.

Test pieces subjected to JAM and MTB17 firings exhibited significant cracking as evidenced Figure 6.10. This cracking follows the grain of the steel and is attributable to rapid heating and cooling of the material which results in rapid thermal expansion and contraction of the material. The resulting stress causes the formation of cracks along the grain of the steel. The higher magnification images for MTB17 also easily show that the temperature of the steel was high enough for a change to austenite and subsequently martensite upon cooling. These phase transitions are accompanied with changed in density and cause additional stress in the material. The change in chemical composition also results in density changes. The cracking suggests that the erosion mechanism for the two hotter and more erosive propellants is clearly different than for the other three propellants. Cracking of this nature was present on the entirety of the erosion piece and on the pieces tested after three firings as well.
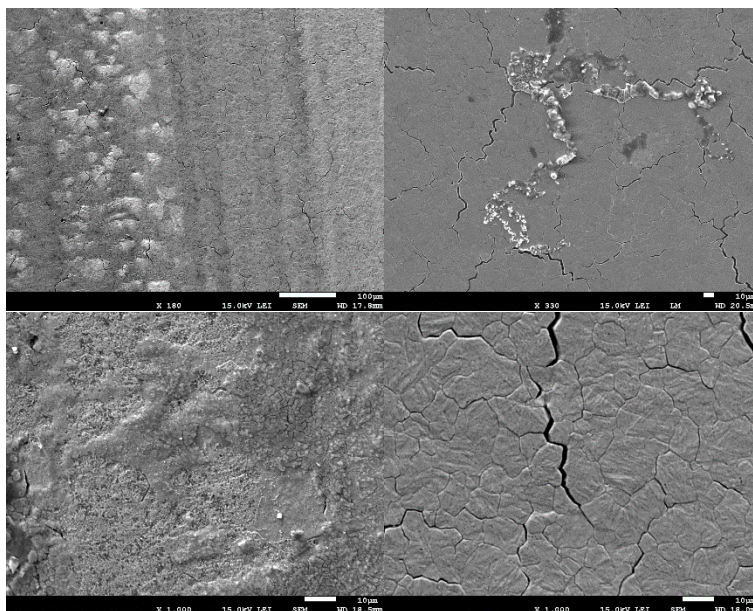
Figure 6.10 : Erosion pieces after two test firings: JAM (left) and MTB17 (Right)

Iron oxide is also visible on some of the micrograms in Figure 6.10 as a darker, often cracked layer, while the lighter deposits are the usual contamination from lead and/or tin. Oxide layers for both erosion pieces subjected to JAM and MTB17 firings had atomic proportions close to 1:1 Fe:O which is consistent with a layer composed mainly of FeO with other oxides making up the remainder. Atomic carbon content relative to iron varied between 0.25 and 0.5, part of this carbon content is attributable to small portions of Fe_3C, combustion residue trapped in the oxide, especially where cracks are present and contamination from organics which despite best efforts could not be entirely avoided and make up the reminder of the carbon content. Any pits or cracks would limit the effectiveness of washing the erosion pieces and leave combustion residue with high carbon content. This was observed across all samples where any composition analysis locations that could easily trap combustion residue resulted in higher carbon content. Analysis on what appeared to be steel with no igniter contamination or oxide layers yielded an atomic composition of 62%-70% Fe, 22%-27% C and 5%-9% O for JAM and 68%-78% Fe, 14%-20% C and 3%-5% O. This indicates that MTB17 results in lower F_3C content than JAM. This is also consistent with the observed pronounced melting of the erosion piece exposed to three firings of JAM (Figure 6.6) where high Fe_3C content explains the significant melting of the material. What appears as melt was also observed for MTB17, but on a much smaller scale. Smaller amounts of localized melting which could partially solidify before exiting the erosion piece would explain the overall lower carbon

content after two firings as part of the formed Fe₃C would be wiped by the gas stream. This is consistent with the observed area where there is a widening of the channel for MTB17 which was not observed for the other propellants including JAM. The irregularity of the widening also points to partial melting of the material instead of a purely flow induced phenomena as would be the case for the other propellants after two test firings.

A summary of the atomic composition where morphological changes were not significant for test pieces subjected to three consecutive test firings for all propellants is shown in Table 6.4.

Table 6.4 : Atomic composition after three test firings

	Fe [atomic %]	C [atomic %]	O [atomic %]	N [atomic %]
Non-exposed steel	82-84	10-14	0-6	0
SB	69	21	2	0-5
MTB15	82-87	11-16	0	0
JAM	34-40	11-20	38-44	0
MTB16	66-68	22-29	0-11	4 (at 5 kV)
MTB17	29-34	14-21	49-52	0

After three test firings, formation of Fe₃C accompanied by a distinct change in morphology was also observed for SB. The atomic composition was evaluated at 67% Fe and 27% C. Carbon content is easily influenced by organic contamination that is present in the air and could be deposited during handling of the samples. Combustion residue is also a potential source of contamination although, a layer of residue was not observed with the SEM. The change in morphology as evidenced in Figure 6.8 also supports a change in chemical composition. In locations where no morphological changes were observed for three SB firings, the iron content was higher than the piece after two firings at 69% and the overall carbon and oxygen content were lower, 21% and 2% respectively. This would be indicative of the reacted layer being removed and that reaction of the steel with the combustion gases takes places over more than one test firing until it reaches a point where a significant portion of the reacted material is ablated. The Fe₃C also exhibits signs of stress cracking which was not observed in the bulk of the material after two firings. In the case of MTB15 after three test firings, the atomic composition of the piece was 82%-87% iron, 11%-16% carbon with no traces of oxygen, the other elements present in 4340 AISI steel, even those not often detected in areas where high carbon content was observed like molybdenum were detected in this case. The exposed layer, Figure 6.9, was observed to a much lower degree than after two firings, cracks in the flow direction were also observed throughout the surface of the erosion piece (Figure 6.11). No

nitrogen was detected. The formation of nitrides after two firings would help form a barrier to limit the reactions between CO and CO_2 and the steel. The reacted hard layer however is ablated by the very high velocity gas stream resulting from the high burning rate of MTB15 in the subsequent (and third) test exposing what is essentially virgin steel. After three test firings, content for the piece exposed to MTB16 was evaluated at 66%-68% Fe, 22%-29% C and 0%-11% O. The overall higher iron content and lower oxygen content seem to indicate that the presence of nitrogen formed nitrides that partially protected unreacted steel. Nitrogen was detected at 15 kV, but suffered from the same issues mentioned previously where the deconvolution algorithm gave it a negative peak area. At 5 kV, the atomic nitrogen content was evaluated at 4%. The presence of nitrogen indicates that the protective nitrides generated by the propellant during each shot which was not the case for MTB15. This agrees with the lower erosion of MTB16 compared to MTB15 and the other propellants.
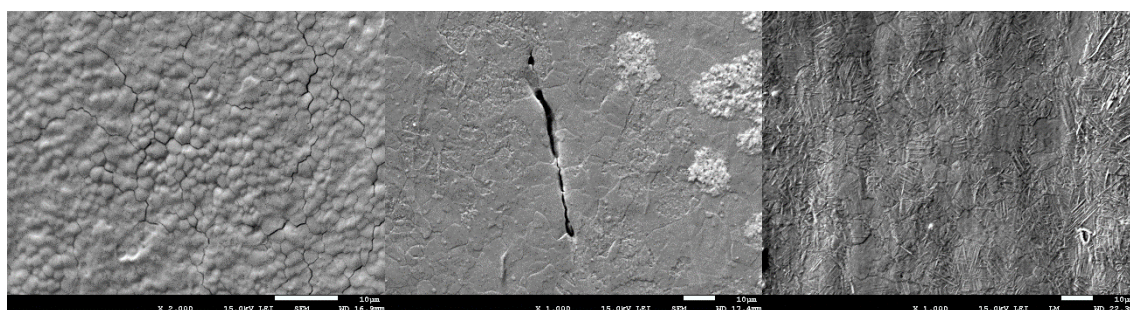

Figure 6.11 : Three tests with M1 (left) MTB15 (center) and MTB16 (right)

A significant amount of oxygen was found on the erosion piece subjected to three tests with JAM. Atomic proportions of 34%-40%% Fe, 38%-44% O and 11%-20% C were detected. This is consistent with a mixture of FeO, other oxides such as Fe_3O_4, likely some Fe_3C and trapped combustion residues, FeO and Fe_3O4 have previously been observed in erosion testing [9]. The oxide was visible with the naked eye for the piece exposed to JAM and the dark color is indicative of oxides different from Fe_2O_3. The oxide layers caused by MTB17 had a different atomic composition with 29%-34% iron, 49%-52% oxygen and 14%-21% carbon. The higher oxygen content is likely to result from a different proportion of oxide species than for JAM given the difference in gas composition and flame temperature. The oxide layers, shown in Figure 6.12, were cracked and partially ablated for both propellants. This is another good indication that cracking and subsequent ablation of the ferrous species by the gas flow plays a more important role in the erosion caused by JAM and MTB17 compared to the other three propellants.
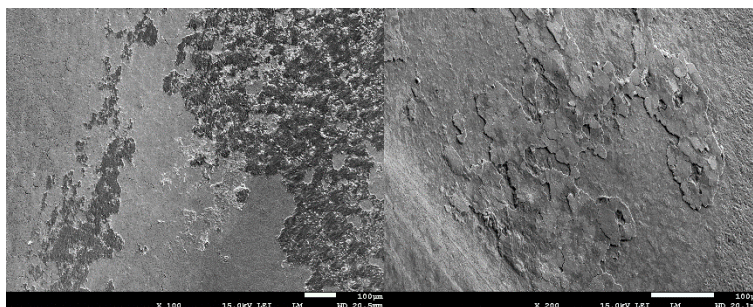
Figure 6.12 : Following three tests: iron oxide from JAM (left) and MTB17 (right)

While the composition of individual elements could be measured using the EDS detector, it is difficult to identify the specific species of ferrous compounds present given that multiple species coexist together. However, the increase in carbon and oxygen content confirm the formation of Fe_3C and oxides. The presence of nitrogen on pieces tested with MTB15 and MTB16 is encouraging in validating the hypothesis that nitrogen-rich propellants form protective nitride species when used. These do not prevent the formation of carbides and oxides, but help in limiting the erosion resulting from the propellants nonetheless. X-ray diffraction analysis also confirmed the presence of a cubic structure of iron nitride, especially on the MTB16 samples (data not shown). More tests will be in the future done to couple the SEM/ESD and XRD results. No iron nitride was observed on MTB17, the propellant on which the nitrogen-rich formulations are based. As previously reported for SB [16], some nitrogen was found by EDS on SB samples, but not consistently across reacted surfaces like in the case of MTB15 and MTB16. The presence of nitrogen associated with SB may be a result of its flame temperature compared other two propellants which may favor diffusion of nitrogen in the steel to some extent.

The effects of the presence of nitrogen-rich materials in the propellant are clearly visible in the erosion results and the composition analysis of the testes pieces. It can be concluded that nitrogen-rich propellant formulations are an effective way to combat erosion and the claims that nitrogen-rich materials promote the nitriding of steel are indeed verified. The presence of nitrogen in the steel observed using the EDS detector and the reduction in erosion of MTB15 and MTB16 compared to the reference propellants demonstrate the protective effects of nitrogen well.

6.3.3 Performance

The addition of either BTA or HBT to the baseline formulation (MTB1&2 and MTB17) resulted in a significant increase in the burning rate of the propellant. Comparing the grains of the same geometry at 100 MPa showed a burning rate increase of 1.5 times for MTB16 and 2.4 times the burning rate for MTB15. The combined data of MTB17 and MTB1&2 was used to calculate the burning rate law parameters of the baseline formulation. Figure 6.13 presents the burning rates of all 5 propellants used in this work. The calculated burning rate law parameters for all propellants are presented in Table 6.5 with the burning rates of the SB and JAM presented for comparison.
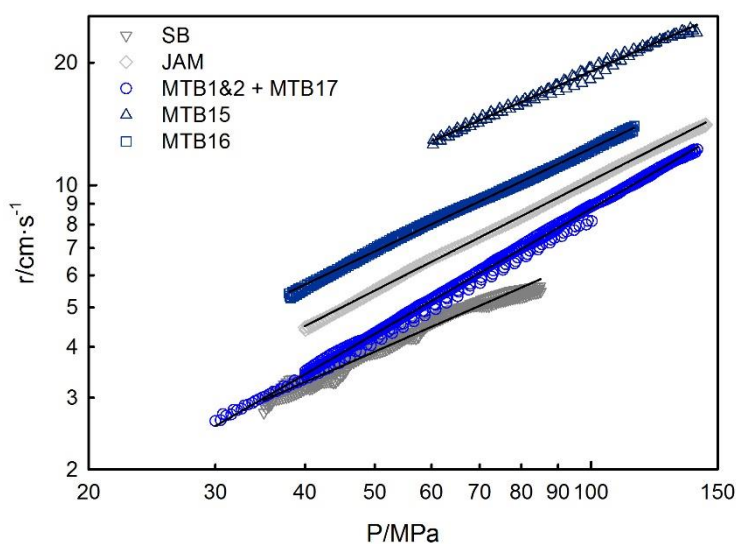
Figure 6.13 : Burning rates of the propellants

In addition to the increased burning rates, there is also a significant change in the linear burn rate coefficients and pressure exponents. This is different from the previously reported burning rate law parameters for propellants containing BTA and HBT where an increase in pressure exponent was observed rather than a decrease [14]. This agrees with the statement that mixtures of nitrogen-rich materials with other energetics can show an increase in pressure exponent and a decrease in linear burn rate coefficient followed by the reverse when the nitrogen-rich content increases. The same type of phenomena was also observed for RDX and triaminoguanidinium azotetrazolate mixtures [13].

Table 6.5 : Burning rate parameters of the propellants

Propellant	β/cm·s^{-1}·MPa$^{-\alpha}$	α	Range/MPa
SB	0.19±0.01	0.77±0.01	35-85
JAM	0.16±0.0	0.90±0.00	40-145
MTB1&2 + MTB17	0.08±0.00	1.02±0.00	(30-100) + (40-140)[13]
MTB15	0.53±0.03	0.78±0.01	60-140
MTB16	0.26±0.01	0.84±0.00	40-115

Internal ballistic simulations were conducted using IBGHV2 software for three particular test cases using large caliber gun. The gun parameters were determined from experimental data so that the simulated results would match them. The simulated muzzle velocity with the SB propellant was within 10% available experimental data. The first test case was where the propellants were used with their current geometries and the propellant weight charge was adjusted to match the muzzle velocity provided by SB. Case 2 is a geometry optimization of case one to fit, as much as possible, the simulated pressure curve generated by SB propellant. The third test case is where the charge weight was set to the maximum allowable by the size of the simulated gun and the pressure was limited to one serviceable by the gun to see how much the muzzle velocity could be improved with the maximum propellant charge. The grain geometry was varied to achieve the maximum serviceable pressure. The results are presented in Table 6.6. All results are presented relative to the simulation of the experimental data for the SB propellant.

Table 6.6 : Ballistic performance

	Case 1	Case 2	Case 3
Propellant	$m_{prop, rel}$	$m_{prop, rel}$	$v_{m, rel}$
SB	1.00	1.00	1.00
JAM	0.66	0.58	1.26
MTB17	0.94	0.76	1.12
MTB15	0.79	0.96	1.05
MTB16	0.84	0.80	1.13

MTB15 and MTB16 require less propellant to obtain the same muzzle velocity. MTB16 has higher energetic content, so this is expected, but MTB15 has energy content similar to SB and achieves similar performance with less propellant. This can essentially be explained by its different burn

---

[13] The first range is for the MTB1&2-1 data and the second range is for the MTB17 data. The burning rate law parameters were calculated using the data from both propellants.

rate as the geometry of the grains are very similar to that of SB. Case 2 was chosen to demonstrate that geometry optimization would yield satisfactory performance at lower charge weight and also insure that the pressure-distance profile in the gun system remained within the operating parameters of. This was indeed the case and demonstrates that it is possible to decrease the propellant charge for a higher performance formulation without having to sacrifice the lifespan of the gun system by using a conventional high-performance, high erosivity propellant formulation such as MTB17 or JAM. Test case 3 also illustrates that it is possible to increase performance with the maximum allowable propellant charge and to reduce erosivity altogether. It is particularly interesting that the performance of MTB16 equals that of MTB17 which is a hotter and more erosive propellant in both test cases. BTA is a very promising nitrogen-rich material for use in gun propellants. JAM was designed to be very similar to JA2, a propellant currently used in high performance applications, this explains the higher muzzle velocity compared to the other high energy propellants.

6.4 Experimental

The nitrogen-rich materials used in this work were synthesized at the General Dynamics Ordnance and Tactical Systems (GD-OTS) Valleyfield facilities in kilogram batches using a 30 L glass reactor. The facilities available at GD-OTS Valleyfield allowed for the safe scale-up of energetic materials. 5,5'-bis(1H-tetrazolyl)amine (BTA) was synthesized according to the experimental protocol already described in the literature [17] and was performed with ease. The synthesis of 5,5'-hydrazinebistetrazole (HBT) was modified from the original protocol [18] due to issues appearing during the scale-up operations. The purity of the materials was assessed using 1H NMR and 13C NMR, no impurities were detected.

Five propellants were used in this work: a standard simple base propellant (SB), a formulation similar to JA2 triple-base propellant (designated JAM), the same reference triple-base used in a previous work (MTB17) [14] and two propellants each incorporating one nitrogen-rich crystal at 35% weight concentration, either BTA (MTB16) or HBT (MTB15). Table 6.7 shows the composition of the propellants.

Table 6.7 : Propellant constituents

Propellant	Constituents
SB	NC (13.4%N); DNT; DBP; DPA
MTB15	NC (13.25%N); TMETN; TEGDN; HBT; EC
JAM	NC (13%N); NG; TEGDN; AK II
MTB16	NC (13.25%N); TMETN; TEGDN; BTA; EC
MTB17 and MTB1&2	NC (13.25%N); TMETN; TEGDN; EC

JAM is a good benchmark for erosivity as it is a very hot propellant, generally known for being highly erosive. JAM propellant was designed to match the thermochemical properties the propellant incorporating BTA (MTB16) and was manufactured at the GD-OTS Valleyfield pilot plant. SB was also provided by GD-OTS Valleyfield. Finally, the two propellants incorporating nitrogen-rich materials were manufactured using the facilities available at DRDC-Valcartier in a 1 USG (3.7 L) Bayer-Perkins sigma blade mixer, as described previously [13, 14]. All propellants were extruded to a cylindrical 7 perforations geometry. MTB15 was extruded to have 7 perforations cylindrical geometry equivalent to that of SB. MTB16, MTB17 and JAM were extruded using a larger 7 perforations cylindrical geometry. MTB1&2 was a previously manufactured reference propellant batch with a geometry similar to that of MTB15.

The pressure-time data used in the determination of the burning rates was acquired using a RARDE closed vessel, model CV21, V = 700 cm3. An internal sleeve was used to reduce the volume of the closed vessel to approximately 180 cm3. The exact volume was measured prior to each test. All propellants were fired at a loading density of 0.2 g·cm-3. 1 g of black powder was used to achieve ignition of the propellant. The burning rate data for each closed vessel firing was calculated using the XLCB software. Burning rate law parameters were calculated by performing regression on the logarithm form of Vielle's law. The pressure range to which the regressions were applied was chosen by analysis of the dynamic vivacity curves. The use of vivacity to validate the data range over which regressions can be performed has previously been discussed [19, 20].

The erosivity was measured using a vented vessel of custom design. The erosion pieces were made of 4340 AISI steel and had an initial opening diameter of 1 mm. The vessel was not equipped with a rupture disc; hence the combustion gases were free to escape the vented vessel as soon as combustion of the propellant occurred. A diagram of the vessel is presented in Figure 6.14.
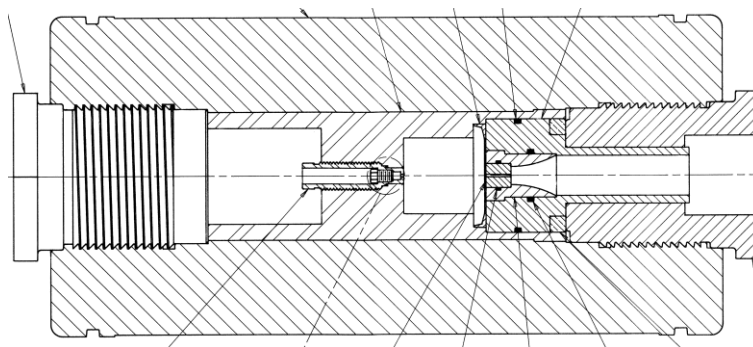
Figure 6.14: Vented vessel apparatus

In order to assess the cumulative effects of combustion gases on the same erosion piece, each propellant was fired 1 to 3 times per erosion piece. Scanning electron microscopy (SEM) coupled with energy dispersive X-ray spectroscopy (EDS) was performed using a JEOL JSM-7600TFE scanning electron microscope equipped with an Oxford Instruments EDS detector. Erosion pieces were cut in half prior to SEM-EDS experiments. Compositions at 15 kV (1 micron depth penetration) and 5 kV (0.16 micron penetration depths) were taken. An analysis of an erosion piece that was not submitted to testing was used as the baseline for carbon contamination from handling and organics. It was also used to determine if cutting resulting in the presence of impurities. Each erosion piece was washed with acetone, hexanes and methanol using both an ultrasonic bath and cotton swabs.

The ballistic performance was calculated with the IBHVG2 software. The software was calibrated using experimental data for the simulated gun prior to performing any simulations on the experimental propellants.

6.5 Conclusions

The addition of nitrogen-rich materials decreases the erosivity of gun propellant formulations. The effects of nitrogen-rich materials are important enough to yield hotter propellants that are less erosive than conventional ones. Part of the reduction in the erosivity is due to nitrogen diffusion in and reacting with the steel compared to the reference conventional propellant. The higher nitrogen content limits, but does not prevent the formation of Fe_3C and oxides resulting from the presence of CO and CO_2. The addition of nitrogen-rich materials had a significant impact on the burning rate of the reference propellant with significantly higher burning rates and lower pressure dependency. The increased burning rates had an effect on the erosivity results for the fastest

burning propellants due to higher velocity gas flow. The simulated ballistic performance of the nitrogen-rich propellants was as good as the initial test case or better.

6.6 Acknowledgements

CHAPTER 7   ADDITIONAL RESULTS

This section contains additional results related to the research objectives that were excluded from the scientific articles due to being out of scope or due to time constraints. In this case, the additional results are associated with the performance of nitrogen-rich propellants and the thermal stability of some of the propellants.

Additional internal ballistic simulations were performed under same conditions as those mentioned in the experimental section of the third article (chapter 6). The simulations were performed on all other propellants incorporating nitrogen-rich materials and M1 was still used to normalize the data and yield the relative muzzle velocities. The results of the simulations are shown in Figure 7.1.
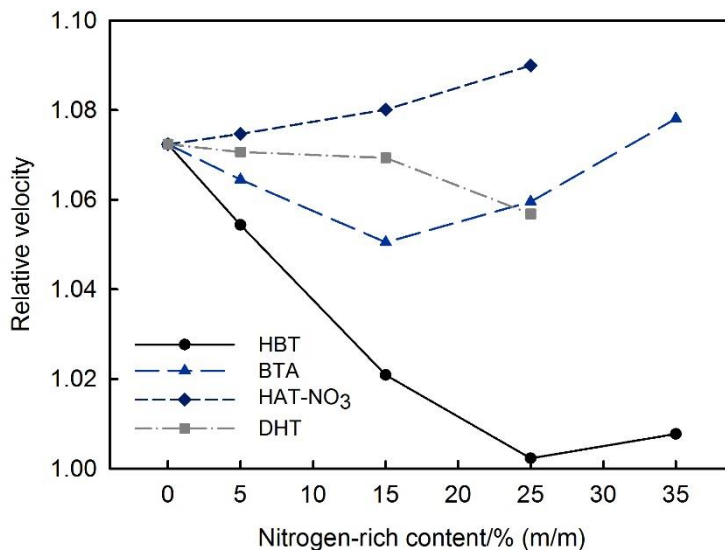
Figure 7.1: Relative muzzle velocity of nitrogen-rich propellants in a large caliber gun system

A potential improvement brought by nitrogen-rich materials that was mentioned in the article on erosion was reduced signature of the muzzle flash. While this was not characterized in a completely controlled environment and the results were not shown in the article, high speed camera recordings of one vented vessel test were taken for each propellant tested. Single frames of these videos are shown in Figures 7.2 to 7.5. The flash for the reference propellant used as the basis for the nitrogen-rich formulations was quite significant and during the venting of the gases, three distinct flashes were observed. The primary flash is the one shown in Figure 7.2, the secondary and tertiary flash observed were of the same type as the first one.

Figure 7.2: Reference propellant vented vessel flash

Figure 7.3: 35% BTA propellant vented vessel flash

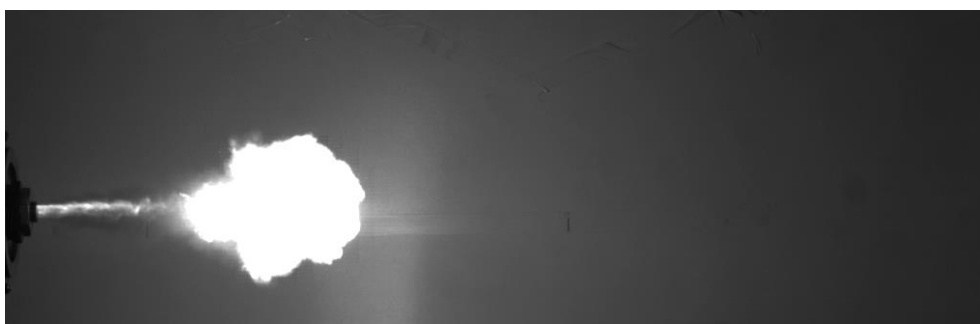Figure 7.4: 35% HBT propellant vented vessel flash

Figure 7.5: SB propellant vented vessel flash

From Figures 7.3 and 7.4, it can easily be seen that the magnitude of the flash is reduced by the addition of nitrogen-rich materials. While the flash is not as small as for M1, the reduction

compared to the reference propellant is still significant. What is also of interest is that the internal ballistic performance of the propellant containing 35% BTA is equivalent to that of the reference propellant. This confirms the statement that nitrogen-rich materials offer gains in terms of weapon signature. These preliminary results show that the avenues of nitrogen-rich materials for reduced signature should be investigated further. This could also provide a starting point for future research as specialty applications where characteristics other than cost are an important factor make it likelier to further the development of nitrogen-rich propellants as the cost of these materials is currently high due to their experimental nature and the lack of any industrial scale production.

CHAPTER 8   GENERAL DISCUSSION

One of the main conclusions that can be drawn from all propellant burning rate data is that nitrogen-rich materials increase the burning rate of conventional propellants. This was observed both in this work and in the literature [93, 97, 100]. This confirms the initial hypothesis formulated that nitrogen-rich materials are excellent performance enhancers. The large variation in the impact of nitrogen-rich materials on propellant performance across different structures and concentrations was not anticipated. The survey of the literature resulted in an anticipated decrease in pressure exponent for every nitrogen-rich material.

One of the aims of this work was to demonstrate the usefulness of nitrogen-rich materials in high performance propellant formulations. These formulations come at the cost of increased complexity. In this work, a triple base propellant was used as the reference propellant. The choice of a NC based propellant was motivated by the fact that nitrocellulose has been a key component of propellants for over a century and will likely remain in use for some time. Other energetic materials, especially energetic binders have difficulty competing with nitrocellulose from an economic perspective. This makes the introduction of new energetic materials in propellant formulations a difficult proposition. The work presented in this thesis demonstrates the potential usefulness of nitrogen-rich materials, even in more high-performance propellants. Not only this, the choice of using small concentrations of nitrogen-rich materials as burning rate enhancers shows a path to introduce those materials to the propellant industry with limited cost increases.

Despite the lack of detailed kinetics, the burning rate laws parameters can be taken as a form of apparent kinetics. Some trends can also be deduced from the experimental results as well as the small amount of literature data available.

- Tetrazoles and tetrazines have different effects on the burning rate modification of propellant formulations.

- Tetrazoles exhibit a significant change in both pressure exponent and linear burn rate coefficient at the 25%-35% molar concentration (Figures 8.1 and 8.2).

- Nitrogen-rich materials are all good quickness enhancers even in small quantities
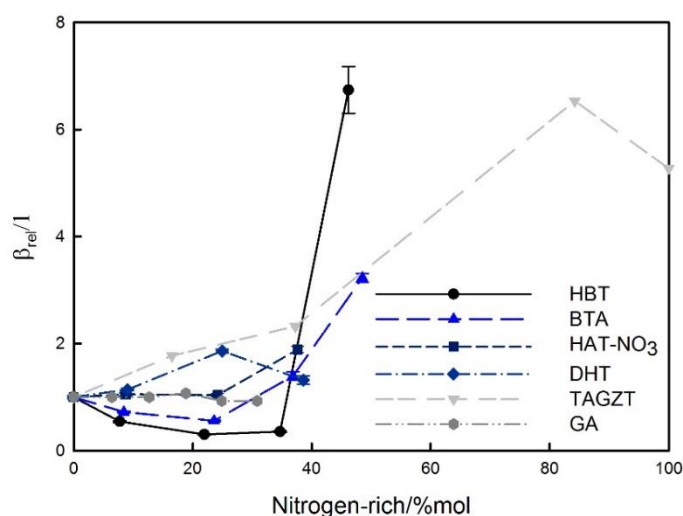
Figure 8.1: Relative linear burn rate coefficients of nitrogen-rich propellants, data for TAGZT, taken from [100] and data for GA taken from [92]

The data available on the burning rate modification of tetrazole based nitrogen-rich materials is relatively small which makes it hard to predict the behavior general to all tetrazole molecules. However, all data points to similar behavior, this includes the data for TAGZT/RDX at rocket pressures. It appears that there is a significant change in the kinetics of the combustion reactions taking place at similar tetrazole molar concentration (25%-35%) for all tetrazole materials when they are used with either nitrated esters (NC, TMETN, TEGDN) or nitramines (RDX). The observed behavior is the same in that the linear burn rate coefficient increases past that point and the pressure exponent decreases. The magnitude of the impact varies between different molecules, but the trends remain the same for every tetrazole for which data was available or that were part of this work.
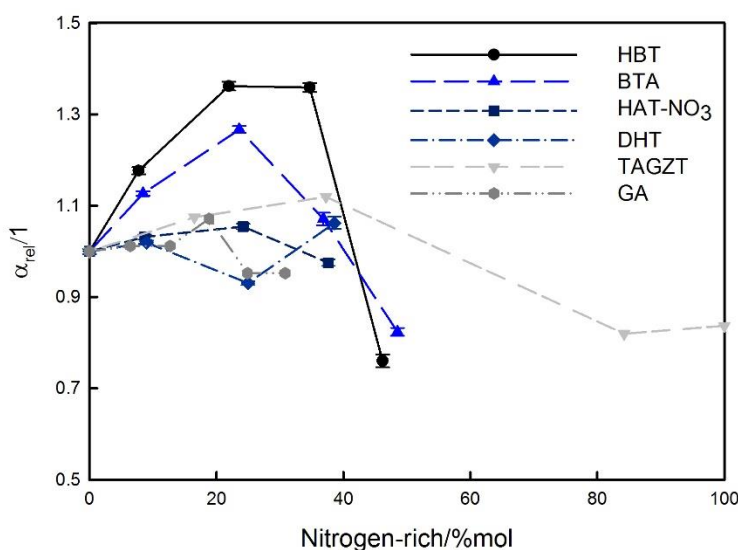
Figure 8.2: Relative pressure exponent of nitrogen-rich propellants, TAGZT data from [100], and data for GA taken from [92]

One of the principal limits of the burning rate analyses performed is the lack of detailed kinetics that describe the burning rate of the propellants from first principles. This is unfortunate, however, given the complexity of the propellants used in this work, it is not unexpected. Chemically simple model systems that can be used in a closed vessel are difficult to obtain. The propellant needs to be able to withstand the deflagration and pressure resulting from its combustion. This means that a binder and a plasticizer are necessary as a matrix to hold the nitrogen-rich materials in place. A stabilizer is also necessary for safety reasons. This will lead to at minimum a propellant with four components already making the system difficult to model with detailed kinetics as can be demonstrated from the work done on kinetics of RDX and TAGZT [101]. As a result, the typical burning rate law was used to model the burning rates of the propellants. There remains a tremendous amount of work necessary for detailed kinetics modeling to be achieved. However, the current work is expected to provide a good amount of experimental data that can be used to validate eventual models.

The work also suffered from what can be described as a "chicken and egg" problem. The nitrogen-rich materials used in this work were never used before in propellant systems and their effects were unknown. For interest in synthesizing large amounts of these materials to be present, the nitrogen-rich materials would have to have demonstrable benefits in propellants. However, any complete

research on the effects of these nitrogen-rich materials required quantities of a few hundred grams experiments on propellants incorporating these materials.

From the combined results presented in the different article, the following set of heuristics for incorporation of nitrogen-rich materials in propellants is proposed:

- From the *RQ* values: Quickness enhancement without significant modification of burning rates should remain in the 1% to 10% molar of nitrogen-rich materials. This is expected to hold true for most nitrogen-rich materials as this behavior was observed for all tetrazoles and tetrazines.

- From the burning rate law parameters: Significant modification of burning rates occurs once past around the 10% molar range, in favor of higher pressure exponents and once more in the 25% to 35% molar range towards reduced pressure dependency. This is confirmed for tetrazole type molecules. Further experimentation is necessary to confirm this behavior holds true for other nitrogen-rich heterocycles.

- From the stability results: Neutral tetrazoles are highly compatible with nitrated esters like NC and should be the materials of choice for nitrocellulose based compositions.

- From the stability results: Tetrazines should be used in compositions without materials with oxidizing effects.

- From the stability study: Nitrogen-rich salts should be limited to formulations with energetic materials not sensitive to acids or bases. This should be observed especially for nitrate or nitro-containing ions.

- From the erosivity experiments: Low erosivity formulations should be designed with at least one third of the formulation as nitrogen-rich materials. Lower concentrations would still yield a reduction in erosivity; however, the effects will be limited.

These heuristics should form a good basis to guide the selection of nitrogen-rich materials for future experimental propellant formulations to better target specific combustion behaviors and to limit compatibility issues. They should prove particularly useful to target future propellant formulations for research purposes.

The scale-up of the nitrogen-rich materials to the 1 kg scale also presented an opportunity to perform a rough estimation of the material costs of the nitrogen-rich materials. At this moment and acquiring most materials from specialty chemical suppliers, the cost per kilo of BTA are expected to be of the order of 345 USD and the cost per kilo of HBT is of the order of 875 USD. The increase in life expectance of gun barrels at 35% weight nitrogen-rich materials is estimated at roughly 40% (40% reduction in thickness erosion) without loss of performance. With economies of scale and synthesis process refinements, the cost of BTA especially would be expected to fall within the range of nitramines like HMX. This would make it attractive from a financial perspective both as an energetic and for its increase in gun barrel lifespan. Further refinements of propellant formulations tailored to specific applications could also yield higher erosivity gains.

Additionally, the synthesis of BTA was easier to scale-up. The synthesis of BTA is a single step reaction. The reaction is per se not exothermic, and the only exothermic step is the addition of HCl to the reaction media. This can easily be controlled with cooling and the mixing enthalpy can even be taken advantage of to bring the reaction media to the required temperature. The principal limiting factor is the reaction time of 48 hours. Sodium azide also poses certain risks due to its reactivity to some metal which forms explosive metal azides. This limits the materials with which the reaction vessel can be constructed to glass, polymers and stainless steel. The scale-up of this reaction to the pilot plant was easy to execute from a technical standpoint and the hazards can easily be mitigated or eliminated.

The synthesis of HBT was more complex to scale-up. The synthesis of NaZT is exothermic and requires careful temperature control. The subsequent step which requires adding magnesium to an aqueous media is also exothermic and temperature control can be difficult. This is a classic scale-up problem when there increase in reaction vessel size makes heat transfer between the reaction media and a heat transfer fluid less efficient due to a higher reaction volume to heat exchange surface ratio. No issues were encountered at the laboratory scale, but at the pilot scale, both steps required careful control of the addition of at least one reactant to limit the amount of heat generated. Nevertheless, the feasibility of scaling up NaZT has been demonstrated [43]. The scaling up of the synthesis of HBT is more technically challenging than that of BTA, but remains feasible.

In summary, BTA is a more interesting molecule than HBT for use in propellants due to the excellent performance it provides, its significant reduction to propellant erosivity and ease of

scaling up production. It provides a good candidate to further the development of nitrogen-rich propellants.

CHAPTER 9   CONCLUSION AND RECOMMENDATIONS

This work has demonstrated the usefulness of nitrogen-rich materials as combustion modifiers in gun propellants, something that previous work hinted at, but could not be affirmed with certainty due to the scarcity of data available in the scientific literature. This was also demonstrated for high concentrations of nitrogen-rich materials. Most of the work previously performed focused either on low pressure data on pure nitrogen-rich materials or gun propellants incorporating concentrations below 20%, and most often even below that. One limitation of the current work was that it focuses solely on nitrocellulose based propellants, the effects of nitrogen-rich materials with other energetic materials such as azided polymers and nitramines remains largely unknown. It is recommended that some research efforts be focused on the incorporation of nitrogen-rich materials in energetic polymers and in LOVA propellant formulations based on nitramines. Another recommendation is research into propellants formulations composed principally of nitrogen-rich materials.

The long-term stability of nitrogen-rich gun propellants was investigated and published in the scientific literature for the first time. The short-term and thermal stabilities were also characterized. This demonstrated that neutral tetrazoles have good long-term compatibility with nitrated esters while some tetrazole salts and tetrazines did not.

The positive effects of nitrogen-rich materials on the erosivity of gun propellant formulations was also clearly demonstrated. This is one aspect which was markedly absent from the scientific literature with erosion characterization and modelling focusing on conventional and LOVA propellants. This part of the work presents a good foundation on which to base further research into nitrogen-rich materials and erosivity. Further research should focus on characterizing the exact ferrous compounds formed by the presence of nitrogen-rich materials and their depth profile in the steel. A combined approach with protective coatings and nitrogen-rich materials was not part of this work and is also recommended. The gains in barrel lifespan are expected to be very significant with a combined approach.

Finally, the recommendation to further the field in the aspects of modelling the burning rate and performance of complex propellants is to focus on the kinetics aspects of the combustion process. This kinetics will have to be determined experimentally and simulations regarding modern propellants are expected to be complex and computationally intensive. The current work is

expected to serve as a starting point to have experimental data on which future modelling work can be based on. In the meantime, the proposed set of heuristics can serve as a starting point for future nitrogen-rich propellant formulations.

An experimental aspect that came in as a potential source of error and that is not directly associated with nitrogen-rich materials is the heat transfer modelling in a closed vessel. The modelling used in the BRLCB and XLCB software is relatively simple. A more accurate modelling of heat transfer should provide better results from calculating the burning rate of the propellants. It is recommended that any improvements made to existing or new closed vessel software include better heat transfer modelling. Additionally, the burning rate software could be directly coupled with a thermochemical code to obtain better thermochemical parameters for each step taken by the burning rate software.

The environmental "friendliness" of nitrogen-rich materials is also largely an unknown at this point. Preliminary data mentioned in chapter 2 is promising. This is being investigated by DRDC-Valcartier using some of the materials synthesized for this work. Further research into that aspect of nitrogen-rich materials is recommended in addition to the work being currently performed.

REFERENCES

[1] P. E. Bruce Cranford, "Energetic materials; What are they?," in *2008 AIChE Annual Meeting, AIChE 100, November 16, 2008 - November 21, 2008*, Philadelphia, PA, United states, 2008.

[2] "Recommendations on the Transport of Dangerous Goods Manual of Tests and Criteria," United Nations, New York and Geneva2015.

[3] T. M. Klapotke and C. M. Sabate, "Bistetrazoles: nitrogen-rich, high-performing, insensitive energetic compounds," *Chemistry of Materials,* vol. 20, pp. 67-75, 2008.

[4] T. M. Klapötke and T. G. Witkowski, "Nitrogen-Rich Energetic 1,2,5-Oxadiazole-Tetrazole - Based Energetic Materials," *Propellants Explosives Pyrotechnics,* vol. 40, pp. 366-373, 2015.

[5] A. K. Sikder and N. Sikder, "A review of advanced high performance, insensitive and thermally stable energetic materials emerging for military and space applications," *Journal of Hazardous Materials,* vol. 112, pp. 1-15, 2004.

[6] J. P. Agrawal, *High Energy Materials*: Wiley-VCH, 2010.

[7] A. Hammerl, T. M. Klapötke, H. Nöth, M. Warchhold, G. Holl, M. Kaiser*, et al.*, "[N2H5]+2[N4C−NN−CN4]2-: A New High-Nitrogen High-Energetic Material," *Inorganic Chemistry,* vol. 40, pp. 3570-3575, 2001/07/01 2001.

[8] T. M. Klapötke, *Chemistry of High-Energy Materials*, 2 ed. Berlin: De Gruyer, 2012.

[9] T. M. Klapötke, P. C. Schmid, S. Schnell, and J. Stierstorfer, "3,6,7-Triamino-[1,2,4]triazolo[4,3-b][1,2,4]triazole: A Non-toxic, High-Performance Energetic Building Block with Excellent Stability," *Chemistry A European Journal,* 2015.

[10] H. Gao and J. n. M. Shreeve, "Azole-Based Energetic Salts," *Chemical Reviews,* vol. 111, pp. 7377-7436, 2011.

[11] J. Akhavan, *The Chemistry of Explosives*, 2 ed. Cambridge: RSC Publishing, 2011.

[12] P. He, J.-G. Zhang, K. Wang, X. Yin, and T.-L. Zhang, "Combination Multinitrogen with Good Oxygen Balance: Molecule and Synthesis Design of Polynitro-Substituted Tetrazolotriazine-Based Energetic Compounds," *Journal of Organic Chemistry,* vol. 80, pp. 5643-5651, 2015.

[13] M. B. Talawar, R. Sivabalan, T. Mukundan, H. Muthurajan, A. K. Sikder, B. R. Gandhe*, et al.*, "Environmentally compatible next generation green energetic materials (GEMs)," *Journal of Hazardous Materials,* vol. 161, pp. 589-607, 1/30/ 2009.

[14] P. Brousseau, "Revolutionary Insensitive, Green and Healthier Training Technology with Reduced Adverse Contamination Project (RIGHTTRAC Project)," in *Insensitive Munitions and Energetic Materials Symposium IMEMTS*, Tuscon, Az, USA, 2009.

[15] E. P. H. Best, K. N. Geter, H. E. Tatem, and B. K. Lane, "Effects, transfer, and fate of RDX from aged soil in plants and worms," *Chemosphere,* vol. 62, pp. 616-625, 1// 2006.

[16]   M. R. Walsh, M. E. Walsh, and A. D. Hewitt, "Energetic residues from field disposal of gun propellants," *Journal of Hazardous Materials,* vol. 173, pp. 115-122, 2010.

[17]   E. Delores and b. Delaney, "Unexploded Ordnance," Defense Science Board, Eashington DC, USA2003.

[18]   C. L. Madeira, S. A. Speet, C. A. Nieto, L. Abrell, J. Chorover, R. Sierra-Alvarez*, et al.*, "Sequential anaerobic-aerobic biodegradation of emerging insensitive munitions compound 3-nitro-1,2,4-triazol-5-one (NTO)," *Chemosphere,* vol. 167, pp. 478-484, 2017.

[19]   J. Lavoie, "Biodégradabilité et propriétés énergétiques d'élastomères azoturés ", Chemical Engineering Department, École Polytechnique de Montréal, Montréal, 2012.

[20]   *Internal Ballistics*. London: H. M. S. O., 1951.

[21]   P. K. Swain, H. Singh, and S. P. Tewari, "Energetic ionic salts based on nitrogen-rich heterocycles: A prospective study," *Journal of Molecular Liquids,* vol. 151, pp. 87-96, 2010.

[22]   R. P. Singh, R. D. Verma, D. T. Meshri, and J. n. M. Shreeve, "Energetic nitrogen-rich salts and ionic liquids," *Angewandte Chemie - International Edition,* vol. 45, pp. 3584-3601, 2006.

[23]   V. E. Zarko, "Searching for Ways to Create Energetic Materials Based on Polynitrogen Compounds (Review)," *Combustion, Explosion, and Shock Waves,* vol. 46, pp. 121-31, 2010.

[24]   D. Fischer, T. M. Klapötke, D. G. Piercey, and J. Stierstorfer, "Synthesis of 5-Aminotetrazole-1 N-oxide and Its Azo Derivative: A Key Step in the Development of New Energetic Materials," *Chemistry – A European Journal,* vol. 19, pp. 4602-4613, 2013.

[25]   D. Fischer, T. M. Klapotke, and J. Stierstorfer, "1,5-Di(nitramino)tetrazole: High Sensitivity and Superior Explosive Performance," *Angewandte Chemie - International Edition,* vol. 54, pp. 10299-10302, 2015.

[26]   N. Fischer, D. Izsak, T. M. Klapotke, S. Rappengluck, and J. Stierstorfer, "Nitrogen-rich 5,5-bistetrazolates and their potential use in propellant systems: A comprehensive study," *Chemistry - A European Journal,* vol. 18, pp. 4051-4062, 2012.

[27]   T. Fendt, N. Fischer, T. M. Klapötke, and J. r. Stierstorfer, "N-Rich Salts of 2-Methyl-5-nitraminotetrazole: Secondary Explosives with Low Sensitivities†," *Inorganic Chemistry,* vol. 50, pp. 1447-1458, 2011/02/21 2011.

[28]   J. Stierstorfer, T. M. Klapotke, A. Hammerl, and R. D. Chapman, "5-azido-1H-tetrazole: improved synthesis, crystal structure and sensitivity data," *Zeitschrift fur Anorganische und Allgemeine Chemie,* vol. 634, pp. 1051-7, 2008.

[29]   D. Fischer, T. M. Klapotke, and J. Stierstorfer, "Salts of tetrazolone - Synthesis and properties of insensitive energetic materials," *Propellants, Explosives, Pyrotechnics,* vol. 37, pp. 156-166, 2012.

[30]   S. Nimesh and H.-G. Ang, "1-(2H-Tetrazolyl)-1,2,4-triazole-5-amine(TzTA) - A thermally stable nitrogen rich energetic material: Synthesis, characterization and thermo-chemical analysis," *Propellants, Explosives, Pyrotechnics,* vol. 40, pp. 426-432, 2015.

[31]   N. Fischer, K. Karaghiosoff, T. M. Klapotke, and J. Stierstorfer, "New energetic materials featuring tetrazoles and nitramines - synthesis, characterization and properties," *Zeitschrift fur Anorganische und Allgemeine Chemie,* vol. 636, pp. 735-49, 2010.

[32]   T. M. Klapotke and F. X. Steemann, "Dinitromethyltetrazole and its salts - A comprehensive study," *Propellants, Explosives, Pyrotechnics,* vol. 35, pp. 114-129, 2010.

[33]   T. M. Klapotke and J. Stierstorfer, "Nitration products of 5-amino-1H-tetrazole and methyl-5-amino-1H-tetrazoles - Structures and properties of promising energetic materials," *Helvetica Chimica Acta,* vol. 90, pp. 2132-2150, 2007.

[34]   S. Lobbecke, A. Pfeil, H. H. Krause, J. Sauer, and U. Holland, "Thermoanalytical Screening of Nitrogen-Rich Substances," *Propellants, Explosives, Pyrotechnics,* vol. 24, pp. 168-175, 1999.

[35]   G. Xiong, Z. Liu, Q. Wu, W. Zhu, and H. Xiao, "Theoretical study of energetic carbon-oxidized triazole and tetrazole derivatives," *Canadian Journal of Chemistry,* vol. 93, pp. 368-374, 2014.

[36]   H. Xiao, Z. Chen, and X. Gong, "Theoretical study on tetrazole and its derivatives (I)," *Chinese Science Bulletin,* vol. 43, pp. 480-480, 1998.

[37]   D. E. Chavez, M. A. Hiskey, and D. Naud, "High-nitrogen Fuels for Low-Smoke Pyrotechnics," *Journal of Pyrotechnics,* vol. 10, pp. 17-36, 1999.

[38]   T. M. Klapötke and J. Stierstorfer, "HIGH-NITROGEN COMPOUNDS FOR USE IN LOW EROSIVITY GUN PROPELLANTS," Ludwig-Maximilian University, Munich2008.

[39]   T. M. Klapötke, P. C. Schmid, S. Schnell, and J. Stierstorfer, "Thermal stabilization of energetic materials by the aromatic nitrogen-rich 4,4,5,5-tetraamino-3,3-bi-1,2,4-triazolium cation," *Journal of Materials Chemistry A,* vol. 3, pp. 2658-2668, 2015.

[40]   M. A. Hiskey, N. Goldman, and J. R. Stine, "High-nitrogen materials derived from azotetrazolate," *Journal of Energetic Materials,* vol. 16, pp. 119-127, 1998.

[41]   J. Neutz, O. Grosshardt, S. Schaufele, H. Schuppler, and W. Schweikert, "Synthesis, characterization and thermal behaviour of guanidinium-5-aminotetrazolate (GA) - A new nitrogen-rich compound," *Propellants, Explosives, Pyrotechnics,* vol. 28, pp. 181-188, 2003.

[42]   N. Fischer, D. Izsak, T. M. Klapotke, and J. Stierstorfer, "The chemistry of 5-(tetrazol-1-yl)-2H-tetrazole: An extensive study of structural and energetic properties," *Chemistry - A European Journal,* vol. 19, pp. 8948-8957, 2013.

[43]   C. Radack, J. Salan, and L. Shelly, "Bis Triaminoguanidinium Azotetrazolate (TAGzT) Scale Up And Production," Naval Surface Warfare Center, Indian Head Division2006.

[44]   A. Hammerl, M. A. Hiskey, G. Holl, T. M. Klapotke, K. Polborn, J. Stierstorfer*, et al.*, "Azidoformamidinium and guanidinium 5,5-azotetrazolate salts," *Chemistry of Materials,* vol. 17, pp. 3784-3793, 2005.

[45]   T. M. Klapotke, H. A. Laub, and J. Stierstorfer, "Synthesis and characterization of a new class of energetic compounds - Ammonium nitriminotetrazolates," *Propellants, Explosives, Pyrotechnics,* vol. 33, pp. 421-430, 2008.

[46]   T. M. Klapotke and C. M. Sabate, "Nitrogen-rich tetrazolium azotetrazolate salts: a new family of insensitive energetic materials," *Chemistry of Materials,* vol. 20, pp. 1750-63, 2008.

[47]   J. Geith, T. M. Klapotke, J. Weigand, and G. Holl, "Calculation of the Detonation Velocities and Detonation Pressures of Dinitrobiuret (DNB) and Diaminotetrazolium Nitrate (HDAT-NO3))," *Propellants, Explosives, Pyrotechnics,* vol. 29, pp. 3-8, 2004.

[48]   M. Von Denffer, T. M. Klapotke, G. Kramer, G. Spie, J. M. Welch, and G. Heeb, "Improved synthesis and X-ray structure of 5-aminotetrazolium nitrate," *Propellants, Explosives, Pyrotechnics,* vol. 30, pp. 191-195, 2005.

[49]   T. M. Klapotke, D. G. Piercey, and J. Stierstorfer, "Amination of energetic anions: high-performing energetic materials," *Dalton Transactions,* vol. 41, pp. 9451-9459, 2012.

[50]   T. M. Klapotke and J. Stierstorfer, "The CN7- Anion," *Journal of the American Chemical Society,* vol. 131, pp. 1122-1134, 2009.

[51]   A. Brand, T. W. Hawkins, G. Drake, I. Ismail, L. Hudgens, and G. Warmoth, "Energetic Ionic Liquids as TNT Replacement," Air Force Research Laboratory (AFMC)2006.

[52]   G. Drake, T. Hawkins, A. Brand, L. Hall, M. McKay, A. Vij, *et al.*, "Energetic, low-melting salts of simple heterocycles," *Propellants, Explosives, Pyrotechnics,* vol. 28, pp. 174-180, 2003.

[53]   T. M. Klapotke, A. Preimesser, S. Schedlbauer, and J. Stierstorfer, "Highly Energetic Salts of 3,6-Bishydrazino-1,2,4,5-tetrazine," *Central European Journal of Energetic Materials,* vol. 10, pp. 151-170, 2013.

[54]   H. Wei, H. Gao, and J. n. M. Shreeve, "N-Oxide 1,2,4,5-Tetrazine-Based High-Performance Energetic Materials," *Chemistry - A European Journal,* vol. 20, pp. 16943-16952, 2014.

[55]   D. E. Chavez, B. C. Tappan, M. A. Hiskey, S. F. Son, H. Harry, D. Montoya, *et al.*, "New high-nitrogen materials based on nitroguanyl-tetrazines: Explosive properties, thermal decomposition and combustion studies," *Propellants, Explosives, Pyrotechnics,* vol. 30, pp. 412-417, 2005.

[56]   D. E. Chavez and B. C. Tappan, "Synthesis and combustion characteristics of novel high-nitrogen materials," *International Journal of Energetic Materials and Chemical Propulsion,* vol. 12, pp. 173-82, / 2013.

[57]   D. E. Chavez and M. A. Hiskey, "Synthesis of the Bi-Heterocyclic Parent Ring System 1,2,4-Triazolo[3,4-b][1,2,4,5]Tetrazine and Some 3,6-Disubstituted Derivatives," *Journal of Heterocyclic Chemistry,* vol. 35, pp. 1329-1332, 1998.

[58]   D. E. Chavez, M. A. Hiskey, and D. L. Naud, "Tetrazine explosives," *Propellants, Explosives, Pyrotechnics,* vol. 29, pp. 209-215, 2004.

[59]   N. Fischer, D. Fischer, T. M. Klapotke, D. G. Piercey, and J. Stierstorfer, "Pushing the limits of energetic materials - the synthesis and characterization of dihydroxylammonium 5,5'-bistetrazole-1,1'-diolate," *Journal of Materials Chemistry,* vol. 22, pp. 20418-22, 2012.

[60] A. A. Dippold and T. M. Klapotke, "Nitrogen-rich bis-1,2,4-triazoles - A comparative study of structural and energetic properties," *Chemistry - A European Journal,* vol. 18, pp. 16742-16753, 2012.

[61] H. Muthurajan, R. Sivabalan, M. B. Talawar, M. Anniyappan, and S. Venugopalan, "Prediction of heat of formation and related parameters of high energy materials," *Journal of Hazardous Materials,* vol. 133, pp. 30-45, 5/20/ 2006.

[62] D. Fischer, J. L. Gottfried, T. M. Klapotke, K. Karaghiosoff, J. Stierstorfer, and T. G. Witkowski, "Synthesis and Investigation of Advanced Energetic Materials Based on Bispyrazolylmethanes," *Angewandte Chemie - International Edition,* vol. 55, pp. 16132-16135, 2016.

[63] S. F. Son, H. L. Berghout, C. A. Bolme, D. E. Chavez, D. Naud, and M. A. Hiskey, "Burn rate measurements of HMX, TATB, DHT, DAAF, and BTATz," in *28th International Symposium on Combustion, July 30, 2000 - August 4, 2000*, Edinburgh, United kingdom, 2000, pp. 919-924.

[64] T. M. Klapotke, P. Mayer, J. Stierstorfer, and J. J. Weigand, "Bistetrazolylamines-synthesis and characterization," *Journal of Materials Chemistry,* vol. 18, pp. 5248-58, 2008.

[65] J. Kerth and S. Lobbecke, "Synthesis and characterization of 3,3-azobis(6-amino-1,2,4,5-tetrazine) DAAT - A new promising nitrogen-rich compound," *Propellants, Explosives, Pyrotechnics,* vol. 27, pp. 111-118, 2002.

[66] C. B. Jones, R. Haiges, T. Schroer, and K. O. Christe, "Oxygen-Balanced Energetic Ionic Liquid," *Angewandte Chemie,* vol. 118, pp. 5103-5106, 2006.

[67] D. E. Chavez and D. A. Parrish, "Synthesis and characterization of 1-nitroguanyl-3-nitro-5-amino-1,2,4- triazole," *Propellants, Explosives, Pyrotechnics,* vol. 37, pp. 536-539, 2012.

[68] J. Quinchon, J. Tranchant, and M. Nicolas, *Les poudres pour armes*. Paris: Lavoisier, 1986.

[69] L. E. Fried, M. W. Howard, and C. P. Souers, "Cheetah 2.0 User's Manual," ed. Lawrence Livermore National Laboratory: Energetic Materials Center, 1998.

[70] D. E. Carlucci and S. S. Jacobson, *Ballistics Theory and Design of Guns and Ammunition*, Second ed. Boca Raton: CRC Press, 2013.

[71] N. Kubota, *Propellants and Explosives Thermochemical Aspects of Combustion*: Wiley-VCH, 2007.

[72] A. N. Ali, S. F. Son, M. A. Hiskey, and D. L. Naud, "Novel High Nitrogen Propellant Use in Solid Fuel Micropropulsion," *Journal of Propulsion and Power,* vol. 20, pp. 120-126, 2004.

[73] B. C. Tappan, A. N. Ali, S. F. Son, and T. B. Brill, "Decomposition and ignition of the high-nitrogen compound triaminoguanidinium azotetrazolate (TAGzT)," *Propellants, Explosives, Pyrotechnics,* vol. 31, pp. 163-168, 2006.

[74] B. E. Homan and A. A. Juhasz, "XLCB: A New Closed-Bomb Data Acquisition and Reduction Program," U.S. Army Research Laboratory, MD, Aberdeen Proving Ground2001.

[75]   W. F. Oberle, "Dynamic vivacity and Its Application to Conventional and Electrothermal-Chemical (ETC) Closed Chamber Results," U.S. Army Research Laboratory, Aberdeen Proving Ground, MD2001.

[76]   C. F. Petre, F. Paquet, C. Nicole, and S. Brochu, "Optimization of the Mechanical and Combustion Properties of a New Green and Insensitive Gun Propellant Using Design of Experiments," *International Journal of Energetic Materials and Chemical Propulsion,* vol. 10, pp. 437-453, 2011.

[77]   R. E. Carter and R. C. Warren, "Extrusion Stresses, Die Swell, and Viscous Heating Effects in Double-Base Propellants," *Journal of Rheology,* vol. 31, pp. 151-173, 1987.

[78]   B. Lawton, "Thermal and Chemical Effects of Gun Barrel Wear," presented at the 21st International Symposium on Ballistics, Orlando, Unites-States, 1984.

[79]   B. Lawton, "Thermo-chemical erosion in gun barrels," *Wear,* vol. 251, pp. 827-838, 2001.

[80]   I. A. Johnston, "Understanding and Predicting Gun Barrel Erosion," Weapons Systems Division - Defence Science and Technology Organisation 2005.

[81]   S. Sopok, C. Rickard, and S. Dunn, "Thermal-chemical-mechanical gun bore erosion of an advanced artillery system part one: theories and mechanisms," *Wear,* vol. 258, pp. 659-70, 2005.

[82]   P. J. Cote and C. Rickard, "Gas–metal reaction products in the erosion of chromium-plated gun bores," *Wear,* vol. 241, pp. 17-25, 6// 2000.

[83]   J. Kimura, "Hydrogen Gas Erosion of High-Energy LOVA Propellants," presented at the 16th International Synposium on Ballistics, San Francisco, CA, 1996.

[84]   P. J. Conroy, C. S. Leveritt, J. K. Hirvonen, and J. D. Demaree, "The Role of Nitrogen in Gun Tube Wear and Erosion," U.S. Army Research Laboratory, Aberdeen Proving Ground, MD ARL-TR-3795, 2006.

[85]   S. Jaramaz, D. Mickovic, and P. Elek, "Determination of gun propellants erosivity: Experimental and theoretical studies," *Experimental Thermal and Fluid Science,* vol. 34, pp. 760-765, 2010.

[86]   J. Kimura, "Thermal and Chemical Effects of Combustion Gases on Gun Erosion," in *ICT Combustion and Detonation Abstracts*, Karlsruhe, Allemagne, 1997.

[87]   A. C. Hordijk and O. Leurs, "Gun barrel Erosion-comparison of conventional and LOVA gun propellants," *Transactions of the ASME. Journal of Pressure Vessel Technology,* vol. 128, pp. 246-50, 2006.

[88]   W. T. Ebihara and D. Rorabaugh, T., *Mechanisms of Gun-Tube Erosion and Wear in Progress in Astronautics and Aeronautics* vol. 109. Washington DC, United States: AIAA, 1988.

[89]   S. Sopok, C. Rickard, and S. Dunn, "Thermal-chemical-mechanical gun bore erosion of an advanced artillery system part two: modeling and predictions," *Wear,* vol. 258, pp. 671-83, 2005.

[90]   P. J. Conroy, P. Weinacht, and M. J. Nusca, "Gun Tube Coatings in Distress," U.S. Army Research Laboratory, Aberdeen Proving Ground, MD ARL-TR-2393, 2001.

[91]   P. J. Conroy, "Vented Fixture Modeling," U.S Army Research Laboratory, Aberdeen Proving Ground, MD ARL-TR-2952, 2003.

[92]   R. S. Damse and A. K. Sikder, "Suitability of nitrogen rich compounds for gun propellant formulations," *Journal of Hazardous Materials,* vol. 166, pp. 967-971, 2009.

[93]   R. S. Damse, N. H. Naik, M. Ghosh, and A. K. Sikder, "Thermoanalytical screening of nitrogen-rich compounds for ballistic requirements of gun propellant," *Journal of Propulsion and Power,* vol. 25, pp. 249-256, 2009.

[94]   B. C. Tappan, S. F. Son, A. N. Ali, D. E. Chavez, and M. A. Hiskey, "Decomposition and Performance of New High Nitrogen Propellants and Explosives," presented at the 6th International Symposium on Special Topics in Chemical Propulsion: Advancements in Energetic Materials and Chemical Propulsion, Santiago, Chile, 2005.

[95]   V. P. Sinditskii, V. Y. Egorshev, G. F. Rudakov, A. V. Burxhava, S. A. Filatov, and L. D. Sang, "Thermal behavior and combustion mechanism of high nitrogen energetic materials DHT and BTATz," *Thermochimica Acta,* vol. 535, pp. 48-57, 2012.

[96]   B. C. Tappan and D. E. Chavez, "Combustion Properties of Amino-Substituted Guanidinium   4,4',5,5'-Tetranitro-2,2'biimidazolate(N4BIM)   Salts," *Propellants, Explosives, Pyrotechnics,* vol. 40, pp. 13-15, 2015.

[97]   J.-H. Yi, F.-Q. Zhao, B.-Z. Wang, Q. Liu, C. Zhou, R.-Z. Hu*, et al.*, "Thermal behaviors, nonisothermal decomposition reaction kinetics, thermal safety and burning rates of BTATz-CMDB propellant," *Journal of Hazardous Materials,* vol. 181, pp. 432-439, 2010.

[98]   J.-H. Yi, F.-Q. Zhao, Y.-H. Ren, B.-Z. Wang, C. Zhou, X.-N. Ren*, et al.*, "BTATz-CMDB propellants: High-pressure thermal properties and their correlation with burning rates," *Journal of Thermal Analysis and Calorimetry,* vol. 104, pp. 1029-1036, 2011.

[99]   J.-H. Yi, J.-G. Zhang, B.-Z. Wang, T. An, Y. Wang, and H.-X. Gao, "BTATz-HNIW-CMDB Propellants Decomposition reaction kinetics and thermal safety," *Journal of Thermal Analysis and Calorimetry,* vol. 115, pp. 1227-1234, 2014.

[100]   B. A. Mason, J. M. Lloyd, S. F. Son, and B. C. Tappan, "Burning rate studies of bis-triaminoguanidinium azotetrazolate (TAGzT) and hexahydro-1,3, 5-trinitro-1, 3, 5-triazine (RDX) mixtures," *International Journal of Energetic Materials and Chemical Propulsion,* vol. 8, pp. 31-8, 2009.

[101]   N. Kumbhakarna, S. T. Thynell, A. Chowdhury, and P. Lin, "Analysis of RDX-TAGzT pseudo-propellant combustion with detailed chemical kinetics," *Combustion Theory and Modelling,* vol. 15, pp. 933-956, 2011.

[102]   J. C. St-Charles, "Résumé de résultats de projet UPIR Étude de synthèse de matériaux énergétiques azotés: synthèse de 5,5'-hydrazinebistétrazole,", 2013, unpublished.

[103]   J. C. Gálvez-Ruiz, G. Holl, K. Karaghiosoff, T. M. Klapötke, K. Löhnwitz, P. Mayer*, et al.*, "Derivatives of 1,5-Diamino-1H-tetrazole: A New Family of Energetic Heterocyclic-Based Salts," *Inorganic Chemistry,* vol. 44, pp. 4237-4253, 2005/06/01 2005.

[104]   M. B. Talawar, R. Sivabalan, N. Senthilkumar, G. Prabhu, and S. N. Asthana, "Synthesis, characterization and thermal studies on furazan- and tetrazine-based high energy materials," *Journal of Hazardous Materials,* vol. 113, pp. 11-25, 2004.

[105] D. E. Chavez and M. A. Hiskey, "High-Nitrogen Pyrotechnic Compositions," *Journal of Pyrotechnics,* pp. 11-14, 1998.

[106] M. D. Codburn, G. A. Buntain, B. W. Harris, M. A. Hiskey, K.-Y. Lee, and D. G. Ott, "An Improved Synthesis of 3,6-Diamino-1,2,4,5-tetrazine. II. From Triaminoguanidine and 2,4-Pentanedione.," *Journal of Heterocyclic Chemistry,* vol. 28, pp. 2049-2050, 1991.

[107] U. S. Department of Defense, "MIL-STD-286C," ed, 1991.

[108] W. F. Oberle and D. E. Kooker, "BRLCB: A Closed-Chamber Data Analysis Program Part I - Theory and User's Manual," U.S. Army Research Laboratory, Aberdeen Proving Ground, MD1993.

[109] K. W. Klingaman and J. K. Domen, "The Role of Vivacity in Closed Vessel Analysis," in *JANNAF Propellant Development and Characterization Subcommittee Meeting*, Patrick AFB, Fl, 1994.

[110] R. E. Kaczmarek, M. S. Firebaugh, B. M. Rice, T. M. Klapötke, J. M. Short, R. D. Lynch*, et al.*, *Topics in Energetics Research and Development*: ESPC Press, 2013.

[111] J. Lavoie, C.-F. Petre, P.-Y. Paradis, and C. Dubois, "Burning Rates and Thermal Behavior of Bistetrazole Containing Gun Propellants," *Propellants, Explosives, Pyrotechnics,* vol. 42, pp. 149-157, 2017.

[112] D. E. Chavez and B. C. Tappan, "Synthesis And Characteristics Of Novel High-Nitrogen Material," *International Journal of Energetic Materials and Chemical Propulsion,* vol. 12, pp. 173-182, 2013.

[113] D. E. Chavez, B. C. Tappan, B. A. Mason, and D. Parrish, "Synthesis and energetic properties of bis-(triaminoguanidinium) 3,3-dinitro-5,5-azo-1,2,4-triazolate (TAGDNAT): A new high-nitrogen material," *Propellants, Explosives, Pyrotechnics,* vol. 34, pp. 475-479, 2009.

[114] N. Kubota, "The Mechanism of Super-Rate Burning of Catalyzed Double Base Propellants," Princeton University, Princeton, NJ1973.

[115] J. H. Flynn and L. A. Wall, "General Treatment of the Thermogravimetry of Polymers," *Journal of Research of the National Bureau of Standards,* vol. 70A, pp. 487-523, 1966.

[116] ASTM, "Standard Test Method for Arrhenius Kinetic Constants for Thermally Unstable Materials Using Differential Scanning Calorimetry and the Flynn/Wall/Ozawa Method. Standard E698-11," ed. Conshohocken, PA: ASTM International, 2011.

[117] N. Fischer, T. M. Klapotke, S. Scheutzow, and J. Stierstorfer, "Hydrazinium 5-Aminotetrazolate: an Insensitive Energetic Material Containing 83.72% Nitrogen " *Central European Journal of Energetic Materials,* vol. 5, pp. 3-18, 2008.

[118] R. R. Nickel, "Fast-Burning Nitrocellulose Compositions," US Patent 6,645,325 B1, 2003.

[119] NATO Standardization Bureau, "Chemical compatibility of ammunition components with explosives (non-nuclear applications)," vol. STANAG 4147, ed, 2001.

[120] P. Lessard and F. Beaupré, "Effect of Porosity on the Burn Rate of a Gas-Generating Composition," *Propellants, Explosives, Pyrotechnics,* vol. 28, pp. 132-137, 2003.

[121] P. J. Conroy, J. S. Montgomery, L.-S. Lussier, F. Beaupré, and B. Jones, "TTCP WPN/TP4 KTA 4-26 Gun Tube Wear and Erosion Final Report," U.S. Army Research LAboratory, Aberdeen Proving Ground, MD ARL-TR-2935, 2003.

[122] R. L. Simpson, P. F. Pagoria, A. R. Mitchell, and C. L. Coon, "Synthesis, properties and performance of the high explosive ANTA," *Propellants, Explosives, Pyrotechnics,* vol. 19, pp. 174-179, 1994.

[123] D. Naud, M. A. Hiskey, and H. H. Herbert, "Synthesis and Explosive Properties of 5,5′-Dinitro-3,3′-azo-1 H -1,2,4-triazole (DNAT)," *Journal of Energetic Materials,* vol. 21, pp. 57-62, 2003.

[124] Y. Zhang, D. A. Parrish, and J. N. M. Shreeve, "Derivatives of 5-nitro-1,2,3-2H-triazole-high performance energetic materials," *Journal of Materials Chemistry A,* vol. 1, pp. 585-593, 2013.

[125] A. A. Dippold and T. M. Klapotke, "Synthesis and characterization of 5-(1,2,4-Triazol-3-yl)tetrazoles with various energetic functionalities," *Chemistry - An Asian Journal,* vol. 8, pp. 1463-1471, 2013.

[126] T. Musil, R. Matya, A. Lycka, and A. Ruzicka, "Characterization of 4,6-diazido-N-nitro-1,3,5-triazine-2-amine," *Propellants, Explosives, Pyrotechnics,* vol. 37, pp. 275-281, 2012.

[127] G.-H. Tao, Y. Guo, Y.-H. Joo, B. Twamley, and J. M. Shreeve, "Energetic nitrogen-rich salts and ionic liquids: 5-aminotetrazole (AT) as a weak acid," *Journal of Materials Chemistry,* vol. 18, pp. 5524-5530, 2008.

APPENDIX A – PROPERTIES OF NITROGEN-RICH EMS

EM	ρ [g·cm^{-3}]	N* [%]	Ω^* [%]	IS [J]	FS [N]	$\Delta_f H^o$ [kJ·g^{-1}]	V_{det} [m·s^{-1}]
Common explosives							
TNT [59]	1.71	18.5	-74.0	15	353	0.24	6.9
RDX [3, 8, 60]	1.80	37.8	-21.6	7.5	120	0.32	8885
HMX [8, 63]	1.91	37.8	-21.6	7.5	120	0.25	9216
CL-20 [3]	2.02	38.4	-11.0	2.5	50	0.83	9632
Neutral nitrogen-rich EMs							
DHT [37, 63]	1.61	78.8	-78.8	16	-	3.77	-
BT [37]	-	81.1	-57.9	4	-	-	-
BTA [38]	1.86	82.3	-57.5	30	>360	4.13	9120
DAAF [63]	1.75	52.8	-52.8	-	-	2.09	-
BTATz [58, 63]	1.74	79.0	-64.5	7	>360	3.55	-
DAAT [58, 65]	1.76	76.0	-72.7	5	324	4.70	7400
5-AT [38]	1.71	82.3	-65.8	>40	>100	2.44	-
Tetrazolone [29]	1.70	65.1	-37.2	>40	360	0.06	7401
HBT [3, 38]	1.84	83.3	-57.1	>30	>108	2.46	8523
4,5-dihydro-1-methyl-5-(nitrimino)-1H-tetrazole [33]	1.76	58.3	-44.1	12.5	160	1.80	8433
1-(2-nitro-2-azapropyl)-5-aminotetrazole [31]	1.63	56.6	-69.3	>100	120	2.21	8467
1-(2-nitro-2-azapropyl)-tetrazolone [31]	1.61	53.1	-70.8	15	128	1.80	8085
1-methyl-4-(2-nitro-2-azapropyl)-aminotetrazole [31]	1.53	52.4	-89.8	40	120	0.67	7542
2-methyl-5-(2-nitro-2azapropyl)-nitriminotetrazole [31]	1.59	48.3	-55.1	8	96	1.43	7902
ANTA [122]	1.73	54.2	-43.4	43	168	0.47	7710
DNAT [123]	1.88	61.9	-63.7	12	250	1.83	7950
ANTA-NQ [67]	1.79	51.8	-29.6	46	>360	0.64	8300

* Values were calculated from the atomic formula when not available in the literature.

EM	ρ [g·cm^{-3}]	N [%]	Ω [%]	IS [J]	FS [N]	$\Delta_f H^o$ [kJ·g^{-1}]	V_{det} [m·s^{-1}]
4-amino-2-methyl-5-nitro-1,2,3-2H-triazole [124]	1.58	48.9	-72.7	>40	-	0.87	7497
2-methyl-4-nitramino-5-nitro-1,2,3-2H-triazole [124]	1.74	44.6	-32.0	25	-	1.04	8350
2-methyl-4.5-dinitro-1,2,3-2H-triazole [124]	1.70	40.5	-32.4	35	-	1.01	8126
2-amino-4,5-dinitro-1,2,3-2H-triazole [124]	1.83	48.3	-9.2	24	-	1.58	8843
1-amino-4,5-dinitro-1,2,3-2H-triazole [124]	1.83	48.3	-9.2	30	-	1.31	8725
DNBT [60]	1.90	49.4	-35.4	10	360	1.58	8413
DNMBT [60]	1.95	40.7	-27.9	20	360	0.87	8499
ATT [125]	1.61	73.7	-44.6	>40	>360	3.36	7193
NTT [125]	1.73	61.5	-43.9	25	288	2.85	8020
DANT [126]	1.85	78.6	-62.8	1.68	40.7	4.06	-
Ionic nitrogen-rich EMs							
GA [41, 127]	1.54	77.8	-75.1	>50	>360	1.54	8055
HDAT-NO$_3$ [47]	1.72	60.1	-14.7	6	-	1.56	8774
HAT-NO$_3$ [48]	1.85	25.7	-10.8	10	324	0.59	8898
Triaminoguanidinium 5-dinitromethyl-1H-tétrazolate [32]	1.74	60.4	-40.3	10	144	1.72	8820
Uronium 5-dinitromethyl-1H-tetrazolate [32]	1.84	47.9	-27.3	40	144	0.50	8509
Ammonium 1-methyl-5-nitriminotetrazolate [45]	1.64	60.9	-54.6	<24	>360	-0.11	7884
Ammonium 2-methyl-nitriminotetrazolate [45]	1.65	60.9	-54.6	10	>360	0.69	7984
Guanidinium 5-oxotetrazolate [29]	1.61	67.7	-71.6	>40	>360	0.00	7257
Aminoguanidinium 5-oxotetrazolate [29]	1.59	70.0	-69.9	>40	>360	0.72	7586
Diaminoguanidinium 5-oxotetrazolate [29]	1.65	72.0	-68.5	>40	>360	1.28	8161
Triaminoguanidinium 5-oxotetrazolate [29]	1.63	73.7	-67.3	15	240	1.79	8308
Ammonium 5-oxotetrazolate [29]	1.62	67.9	-54.3	>40	>360	0.16	7749
Hydrazinium 5-oxotetrazolate [29]	1.59	71.2	-54.2	>40	>252	1.46	8284
Hydroxylammonium*NH$_3$O 5-oxotetrazolate [29]	1.63	55.3	-31.5	>40	>360	1.10	9034
G2MNAT [27]	1.63	62.1	-66.9	30	192	1.11	8059
DAG2MNAT [27]	1.57	66.1	-65.2	10	160	2.05	8184

EM	ρ [g·cm⁻³]	N [%]	Ω [%]	IS [J]	FS [N]	$\Delta_f H^o$ [kJ·g⁻¹]	V_{det} [m·s⁻¹]
Uro2MNAT [27]	1.59	54.9	-54.9	10	288	0.59	7800
AAT [40]	1.53	84.0	-63.9	21.4 cm[14]	44	2.21	7600
TAGZT [40, 44]	1.52	82.3	-72.7	4	84	2.87	9050[15]
GZT [40, 44]	1.54	78.8	-78.8	32	>360	1.44	7100
AGZT [44]	1.54	80.2	-76.4	15	>360	1.39	6418
DAGZT [44]	1.60	81.4	-74.4	4	>360	2.06	7045
BHaTz [7]	1.52	85.2	-52.8	>25	low	3.73	6330
Diammonium 5,5'-bistetrazolate [26]	1.59	81.4	-74.3	35	>360	1.75	7417
Dihydrazinium 5,5'-bistetrazolate [26]	1.53	83.1	-71.2	40	360	3.44	8265
Dihydroxylammonium 5,5'-bistetrazolate [26]	1.74	68.6	-47.0	10	240	2.22	8854
Bis(guanidinium) 5,5'-bistetrazolate [26]	1.59	76.5	-87.4	40	>360	1.57	7199
Bis(triaminoguanidinium) 5,5'-bistetrazolate [26]	1.54	80.9	-78.5	15	285	3.42	8181
Bis(diaminouronium) 5,5'-bistetrazolate hydrate [26]	1.74	70.4	-65.3	35	360	1.96	8562
Ammonium 5-5'-bis(1-méthyltétrazolyl)triazene [38]	1.60	74.3	-92.0	-	-	-	8484
G₂ZT [3]	1.71	78.2	-77.1	>30	>360	1.33	7683
(DMAT)₂ZT [46]	1.43	71.4	-97.8	>30	>360	3.80	7803
(MeDAT)₂ZT [46]	1.43	78.1	-77.1	>30	>360	4.10	7977

---

[14] Weight used to measure IS not mentioned

[15] Hammerl *et al*. reported V_{det}= 7654 m/s [44]

APPENDIX B – SUPPORTING INFORMATION: BURNING RATES AND THERMAL BEHAVIOR OF BISTETRAZOLE CONTAINING PROPELLANTS
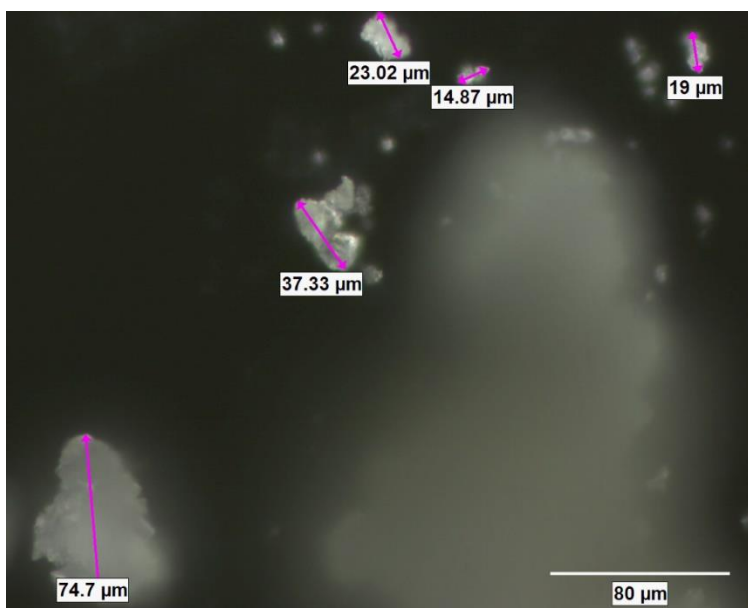
BTA crystals at 200x magnification
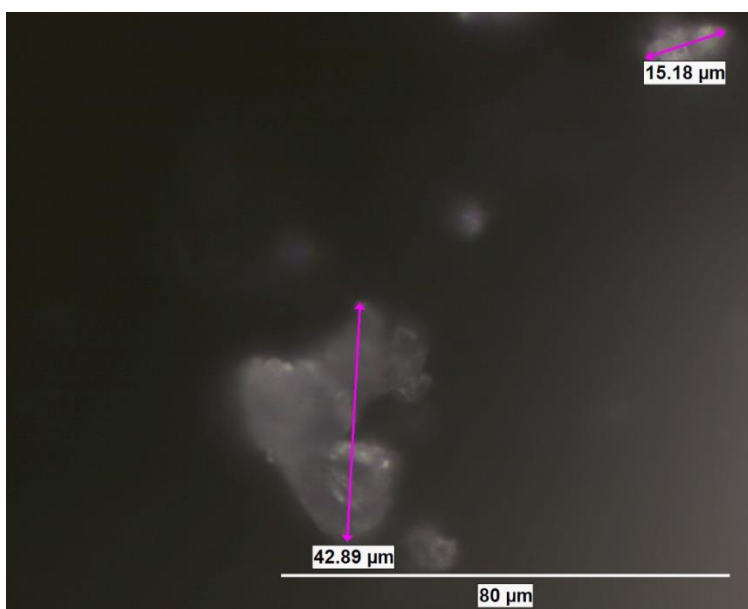
BTA agglomerate at 500x magnification
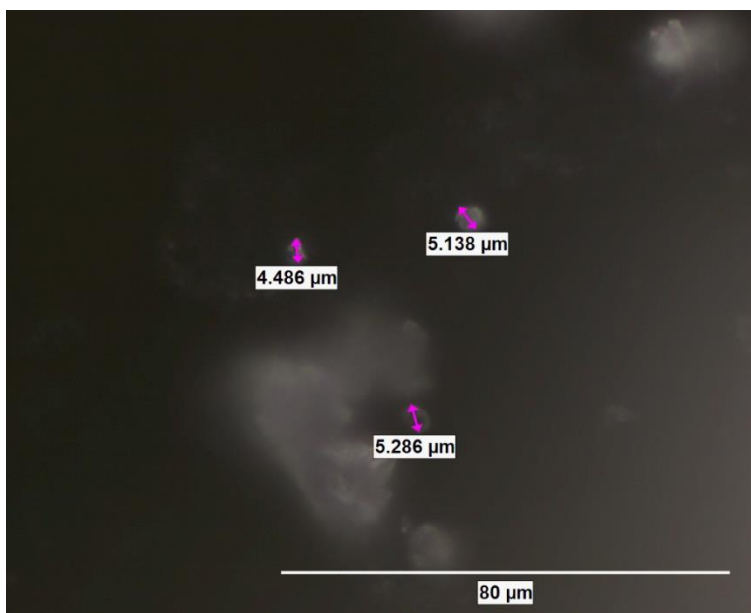
Small BTA crystals at 500x magnification
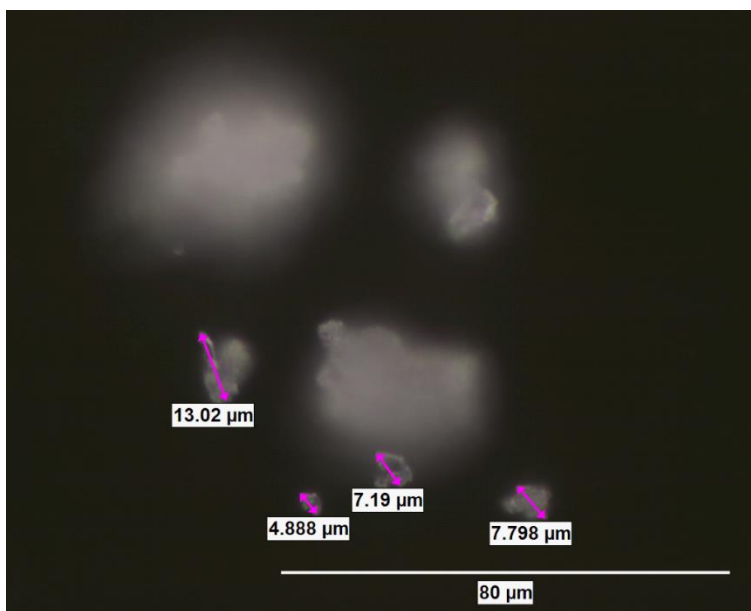
BTA crystals at 500x magnification

The tendency of BTA to form agglomerates made it difficult to get a good field of view of the agglomerates.
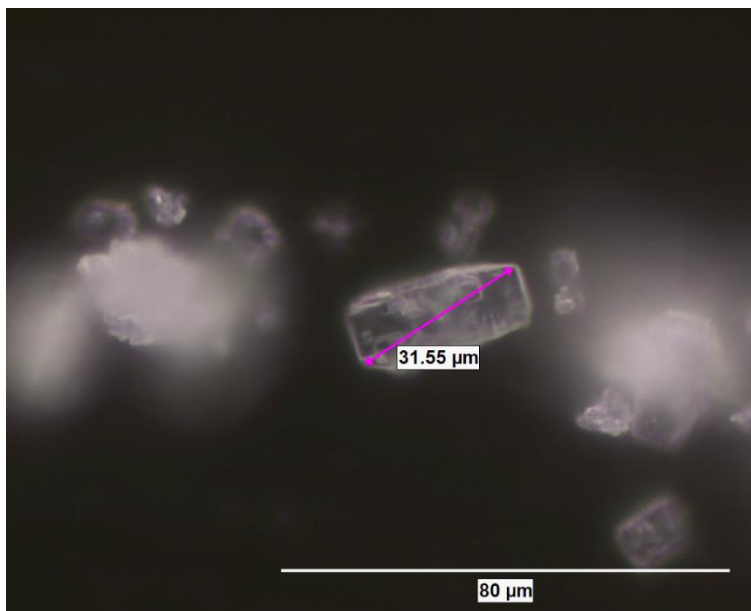
Large HBT crystal at 500x magnification
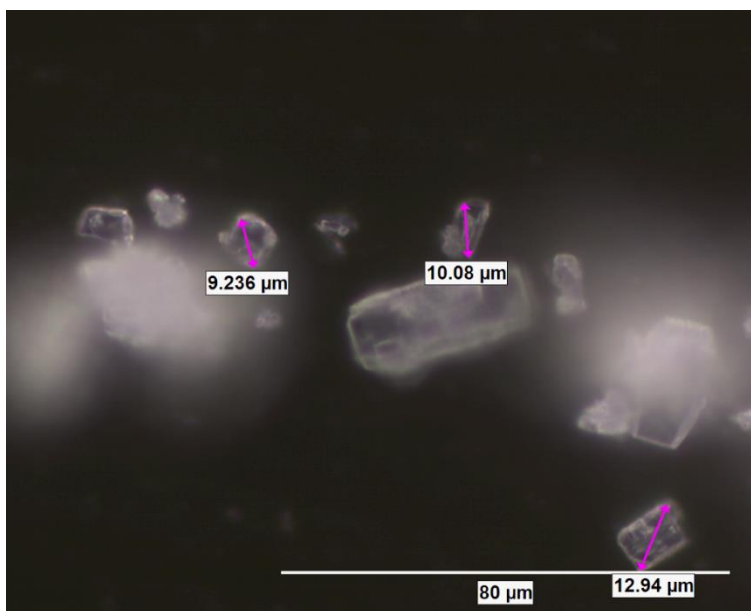
Small HBT crystals at 500x magnification
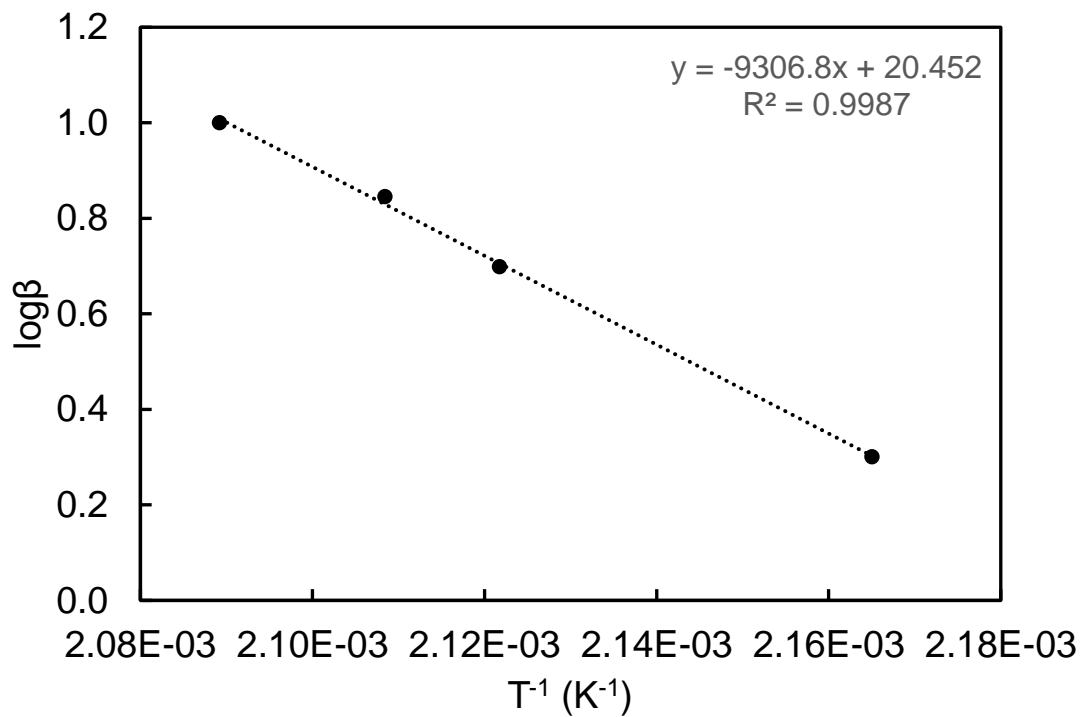
Arrhenius plot of the reference propellant
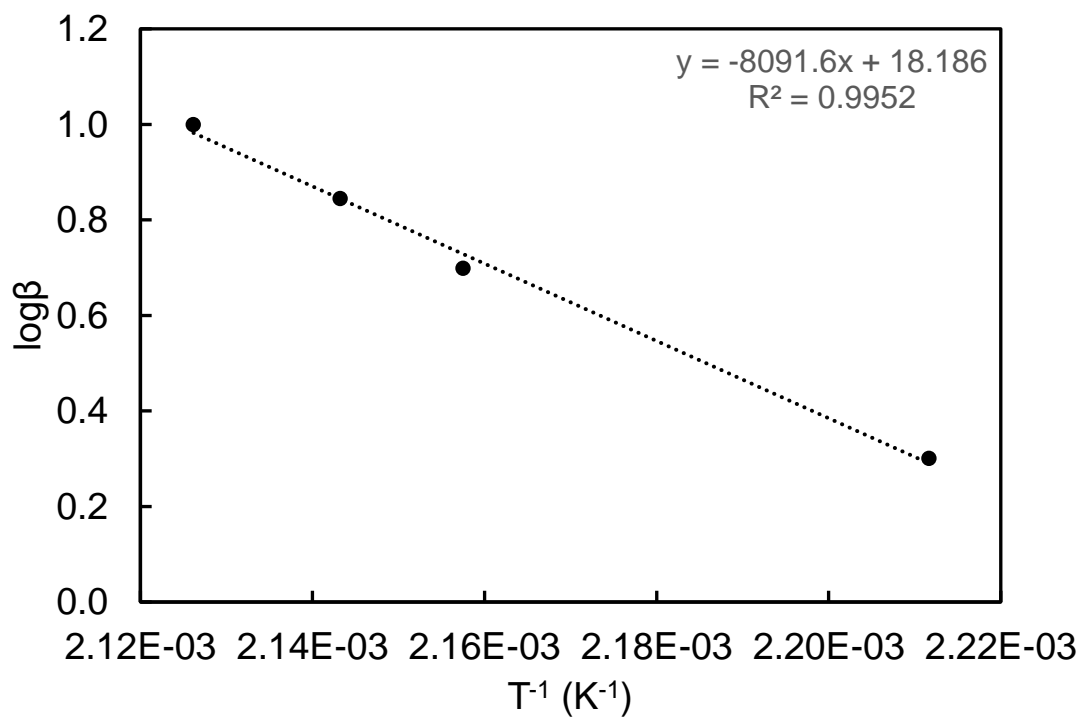
Arrhenius plot of the propellant containing 5% BTA
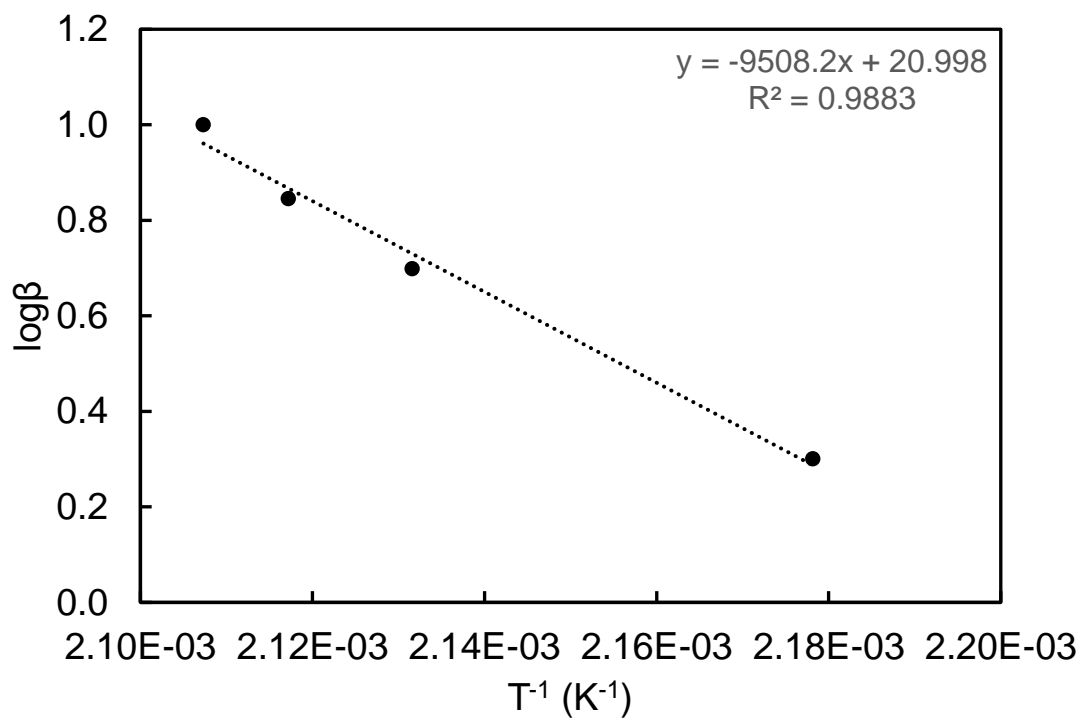
Arrhenius plot of the propellant containing 5% HBT
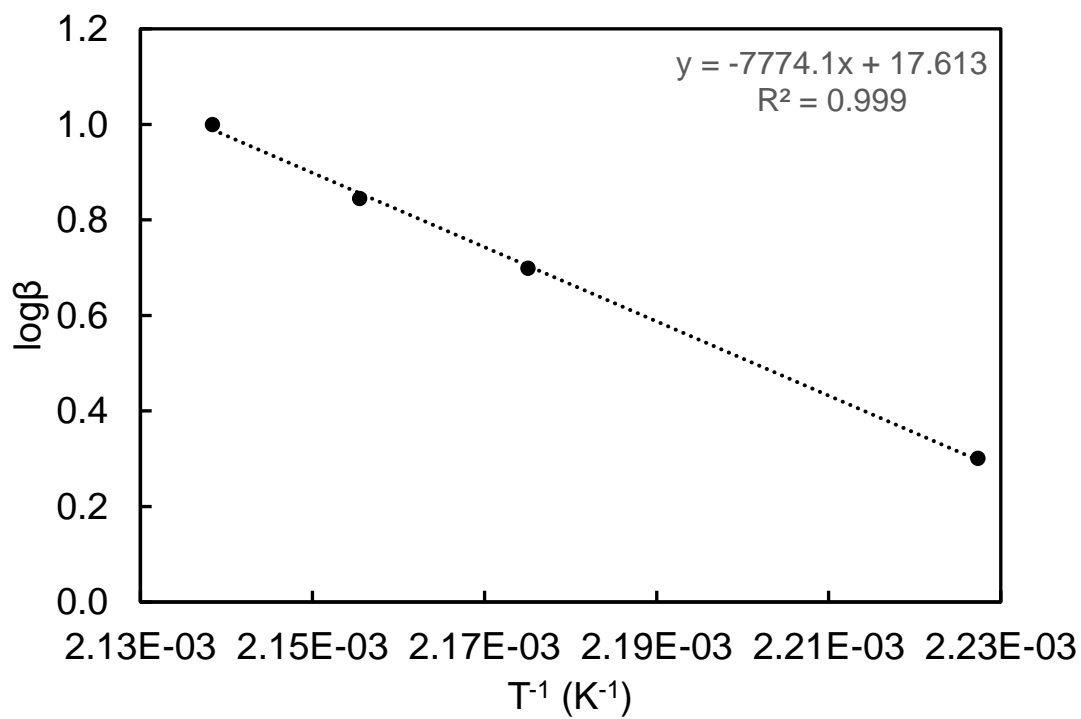
Arrhenius plot of the propellant containing 15% BTA
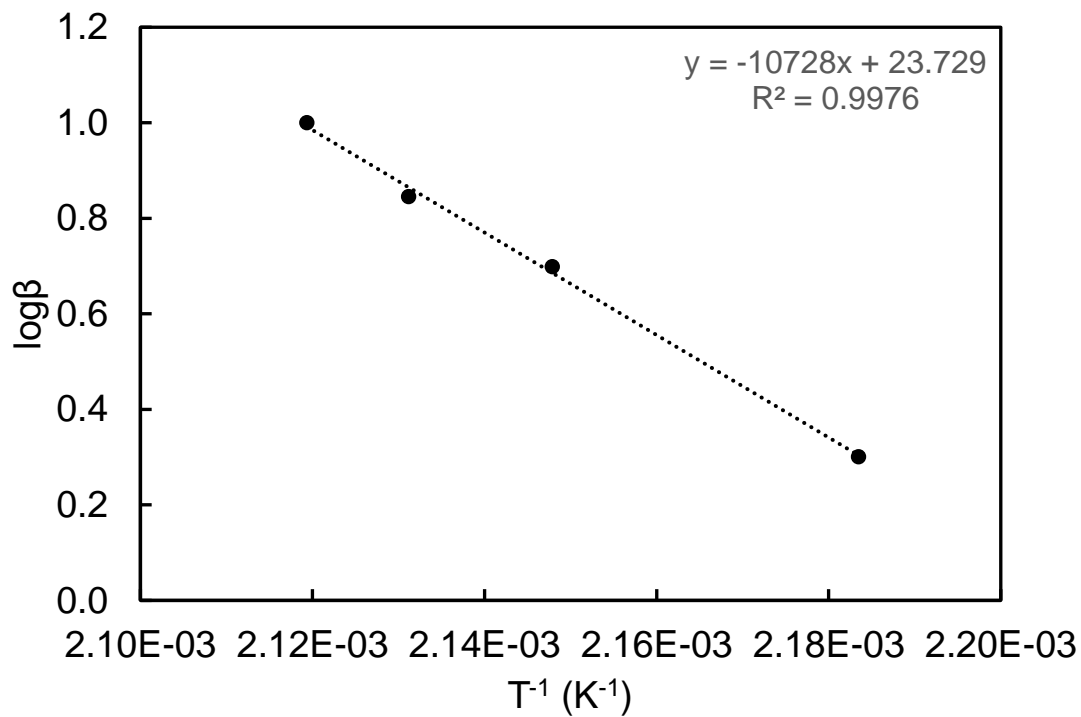
Arrhenius plot of the propellant containing 15% HBT
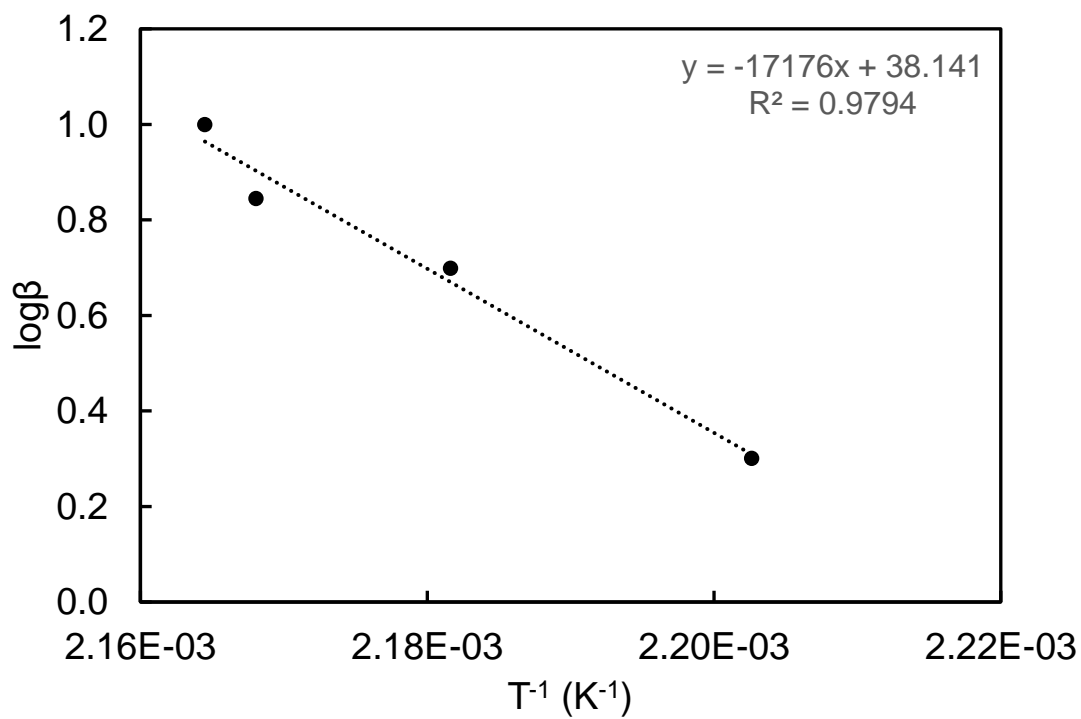
Arrhenius plot of the propellant containing 25% BTA
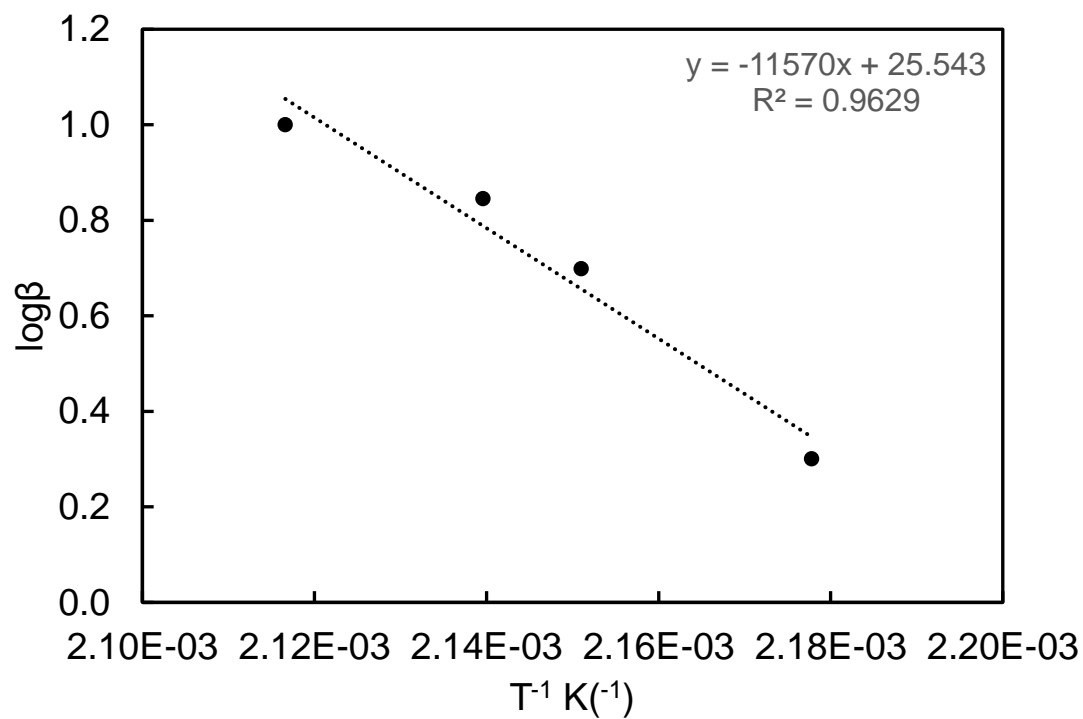
Arrhenius plot of the propellant containing 25% HBT
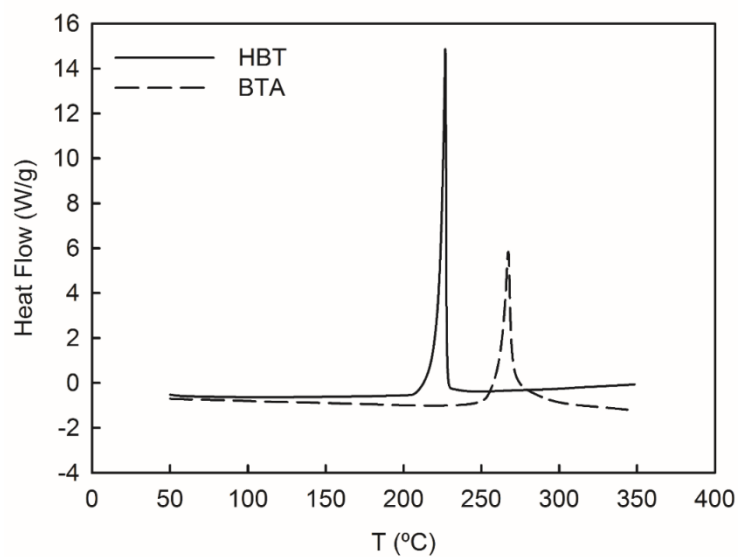
DSC of the pure nitrogen rich materials

APPENDIX C – SUPPORTING INFORMATION: STABILITY AND PERFORMANCE OF GUN PROPELLANTS INCORPORATING 3,6-DIHYDRAZINO-S-TETRAZINE AND 5-AMINOTETRAZOLIUM NITRATE

Dynamic vivacity curves

All dynamic vivacity curves presented in this section are representative of a cylindrical (cord) geometry. This indicates that the combustion of the propellant follows the assumption that the combustion occurs in the direction normal to the propellant grain surface. Additionally, a quick sensitivity analysis on the number of grains revealed that this underestimation had very little effect on the calculated burning parameters. An error on the surface area of around 7%-10% for the DHT propellants resulted in minimal differences compared to the error of 4% or less mentioned in the article.
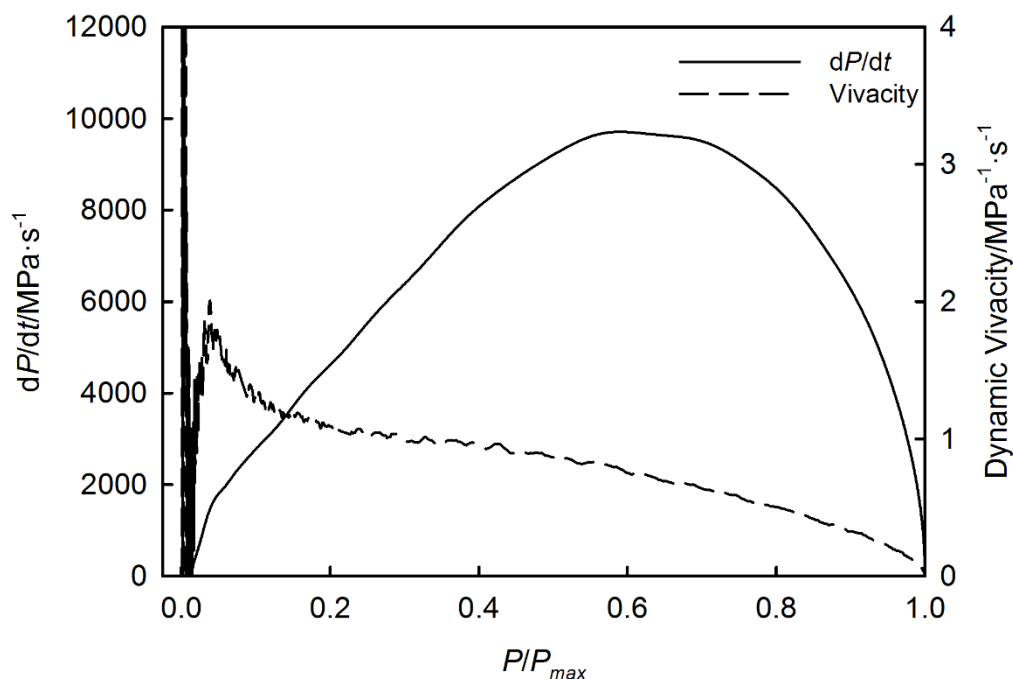
Figure C1: Typical vivacity curve of the reference propellant
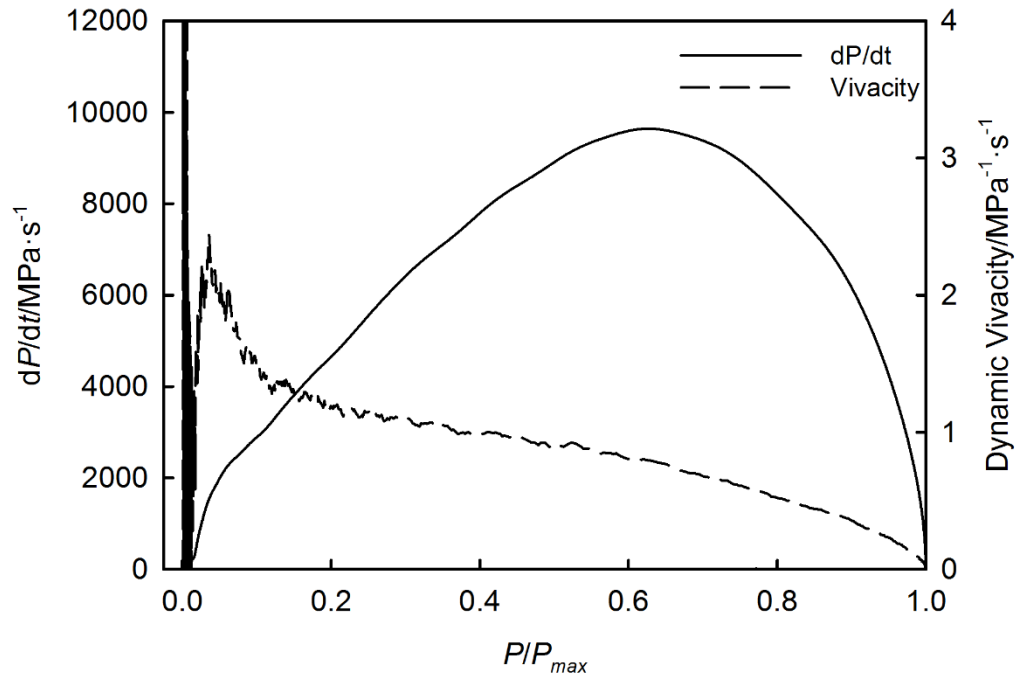
Figure C2: Typical vivacity curve of the 5% DHT propellant
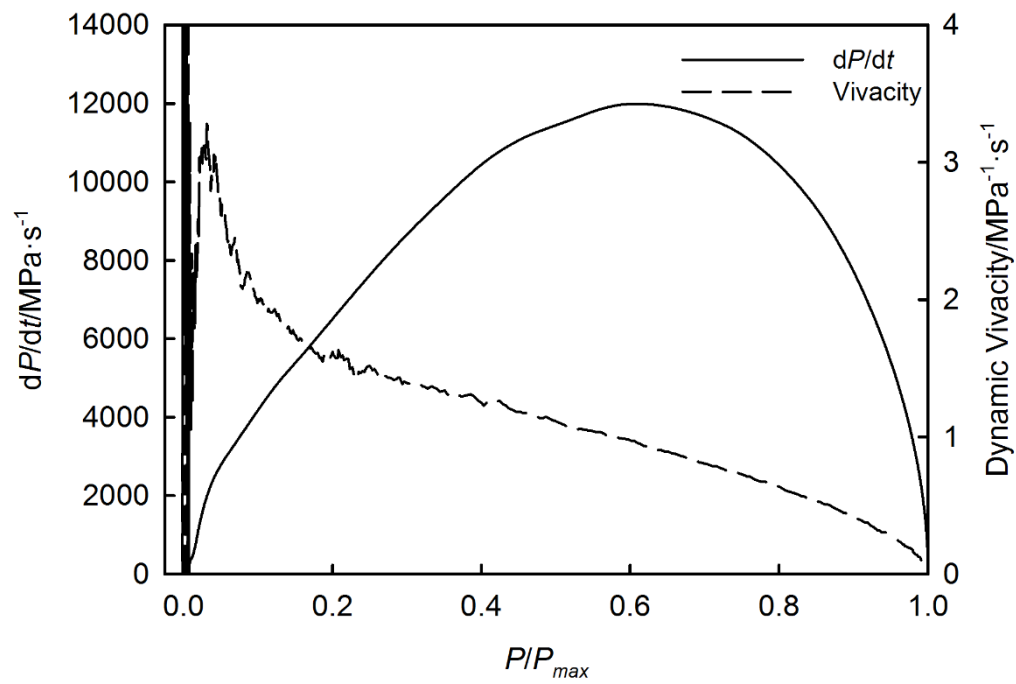
Figure C3: Typical vivacity curve of the 15% DHT propellant

143
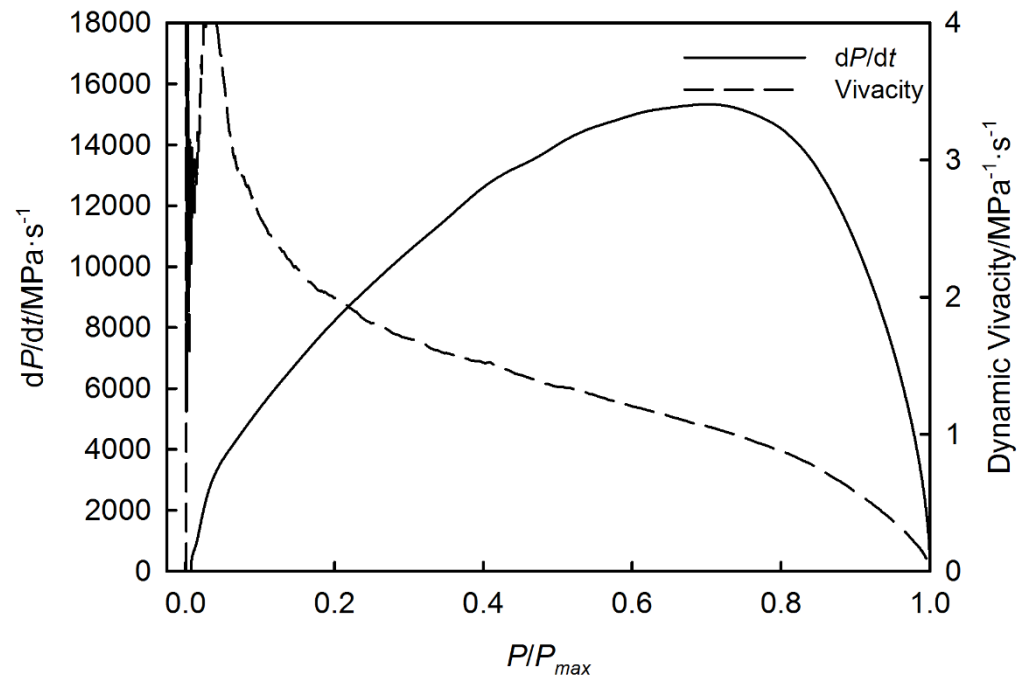
Figure C4: Typical vivacity curve of the 25% DHT propellant
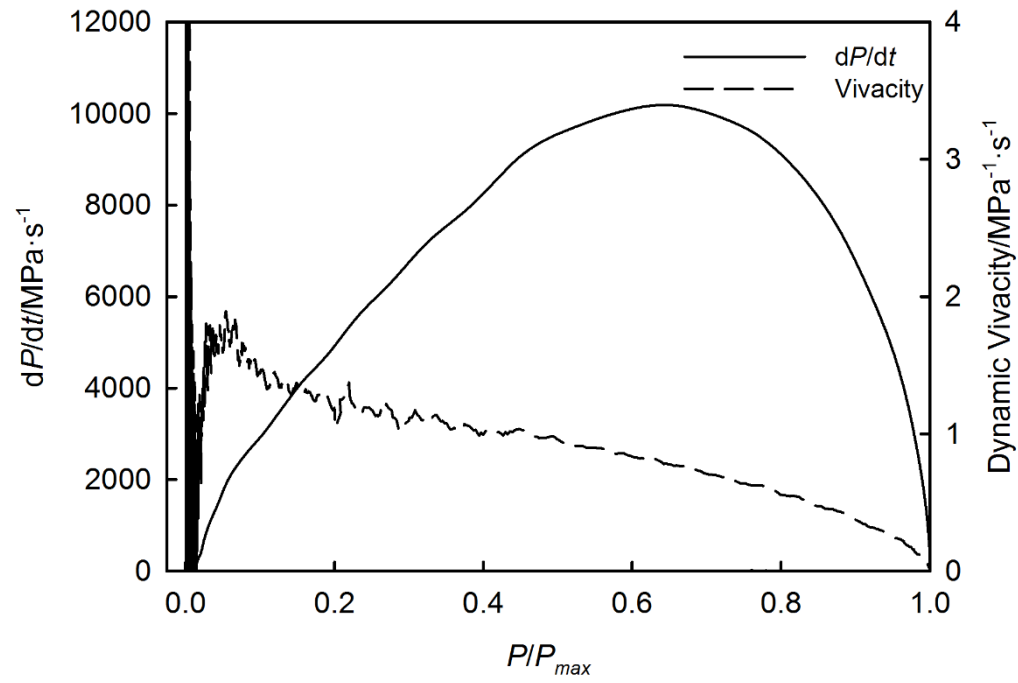
Figure C5: Typical vivacity curve of the 5% HAT-NO$_3$ propellant
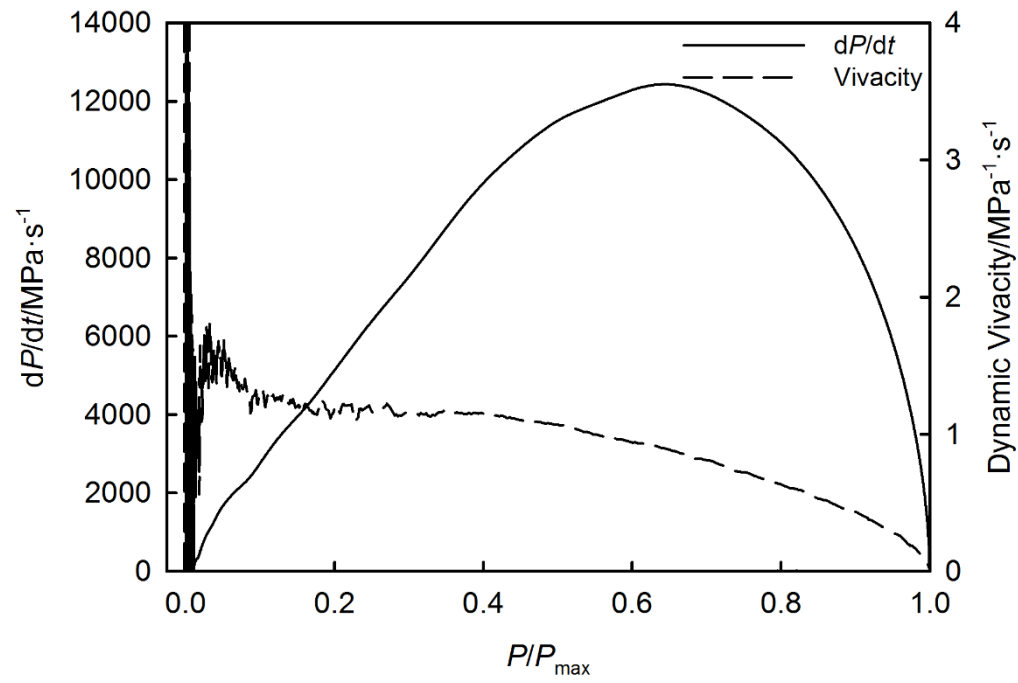
Figure C6: Typical vivacity curve of the 15% HAT-NO$_3$ propellant
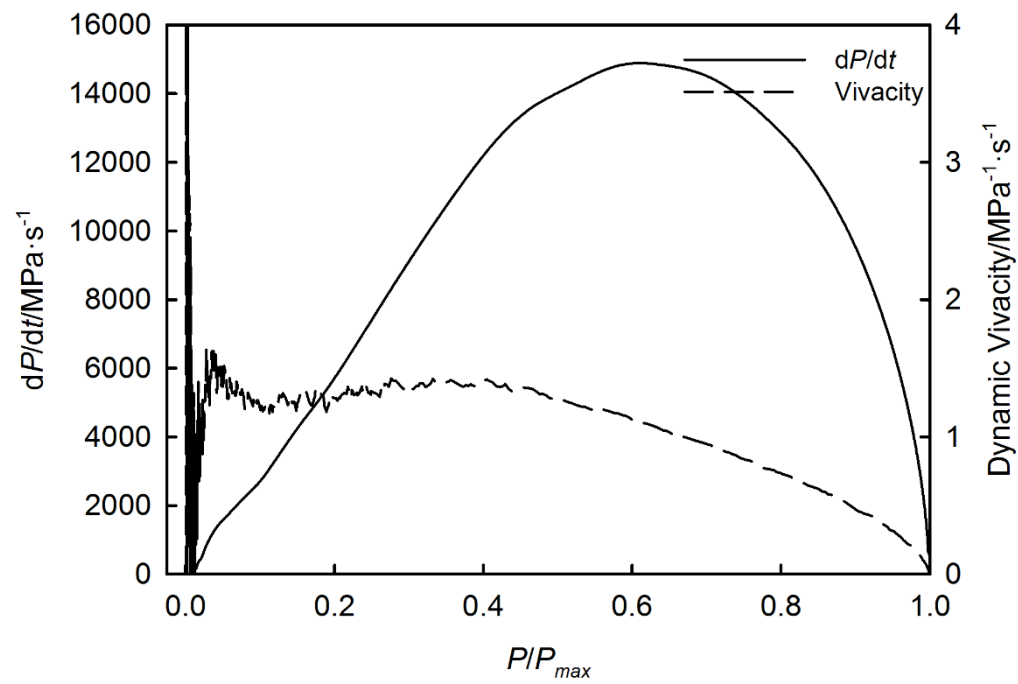
Figure C7: Typical vivacity curve of the 25% HAT-NO$_3$ propellant

DSC data

Table C1: Thermal Decomposition of Nitrogen-Rich Materials and Propellants

Propellant	Onset [°C]	Peak 1 [°C]	Peak 2 [°C]	E_{a1} [kJ·mol^{-1}]	ln[Z_1[min])	E_{a2} [kJ·mol^{-1}]	ln(Z_2[min])
Reference	170	188	N/A	170±9	42.7±5.0	N/A	N/A
DHT	138	143	N/A	128±13	35.5±3.8	N/A	N/A
5% DHT	137	144	183	128±8	35.3±2.3	136±17	34.0±4.3
15% DHT	139	143	182	164±9	46.0±2.5	195±8	50.0±2.0
25% DHT	139	143	181	171±26	48.0±7.4	157±13	40.1±3.3
HAT-NO$_3$	170	174	N/A	219±7	57.6±1.7	N/A	N/A
5% HAT-NO$_3$	132	143	188	114±6	31.4±1.6	156±11	39.0±2.8
15% HAT-NO$_3$	140	149	186	145±16	39.9±4.5	149±7	37.3±1.9
25% HAT-NO$_3$	144	149	187	174±9	48.2±2.5	149±15	37.2±3.9

Arrhenius plots

All errors on the regressions fell within 15% or below which is expected for this type of thermal analysis data with most of the calculated activation energies having lower error. Interestingly, the error on the activation energy of HAT-NO$_3$ is among the lowest considering that the number of data points used was lower. This was a result of the highly energetic nature of the material as evidenced by the signal in the DSC at 5 K·min^{-1} reaching near 50 mW. This limited the heating rates and sample mass that could be used to avoid rupturing the pans or attaining energy release beyond what the DSC instrument could track accurately. The fit was considered quite good however and no additional experiments were deemed necessary.
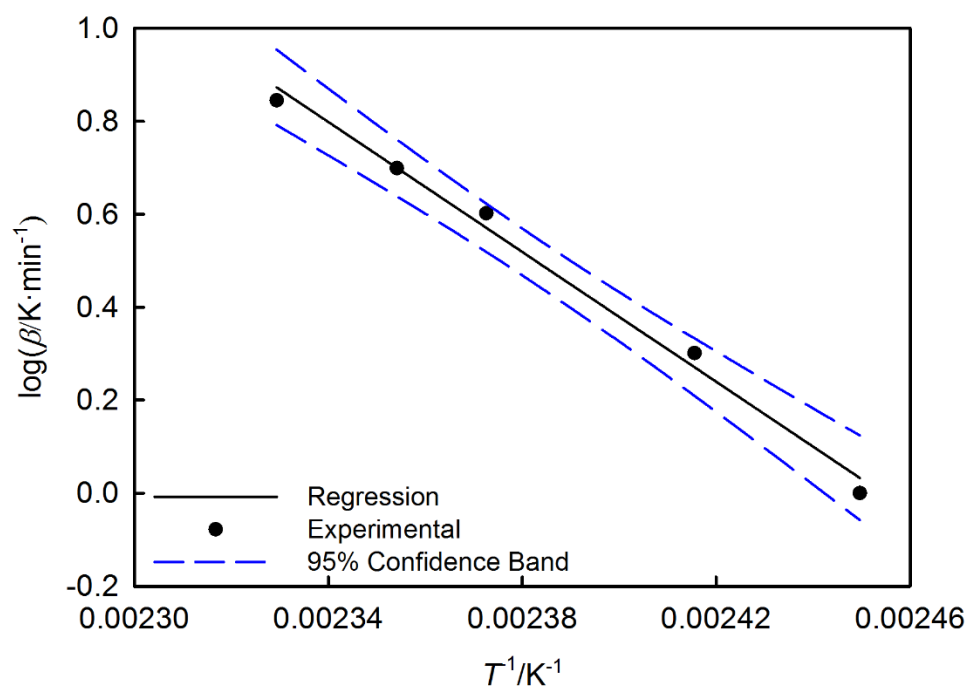
Figure C8: Arrhenius plot, DHT
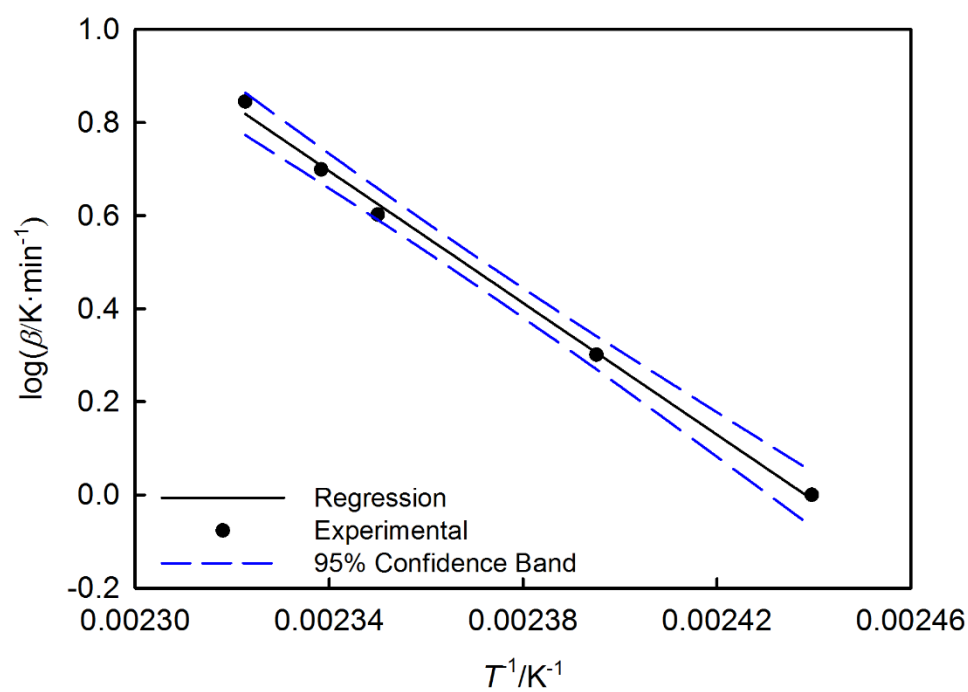
Figure C9: Arrhenius plot, first decomposition 5% DHT
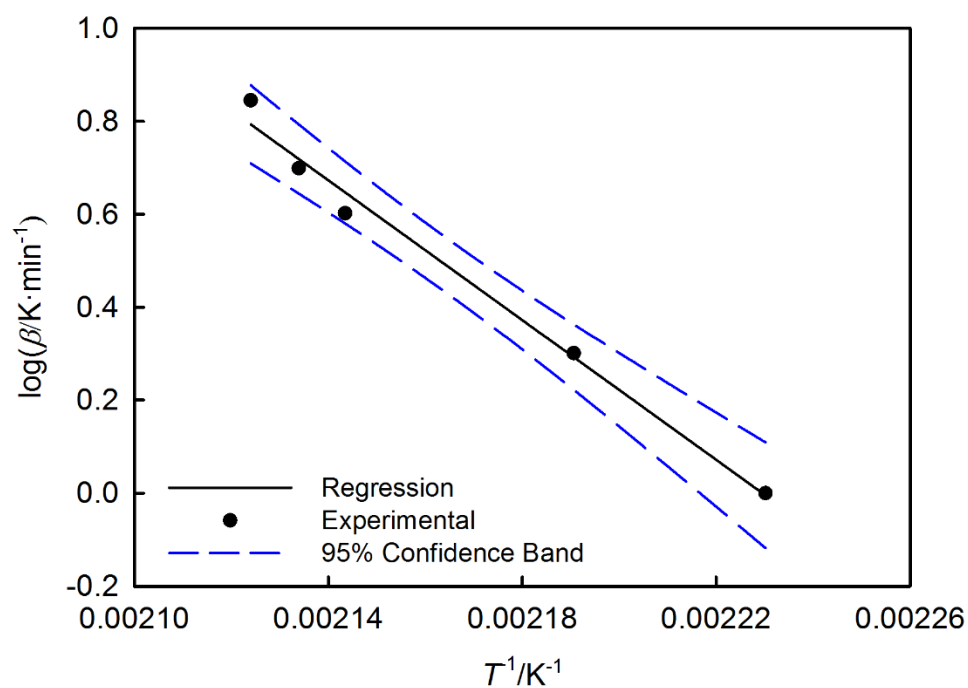
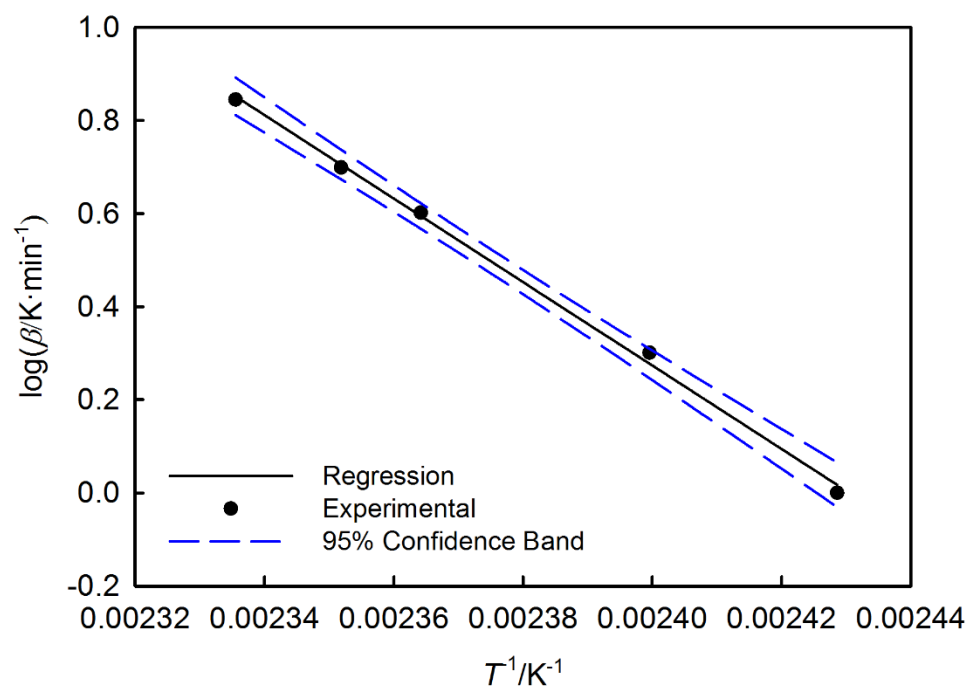Figure C10: Arrhenius plot, second decomposition 5% DHT

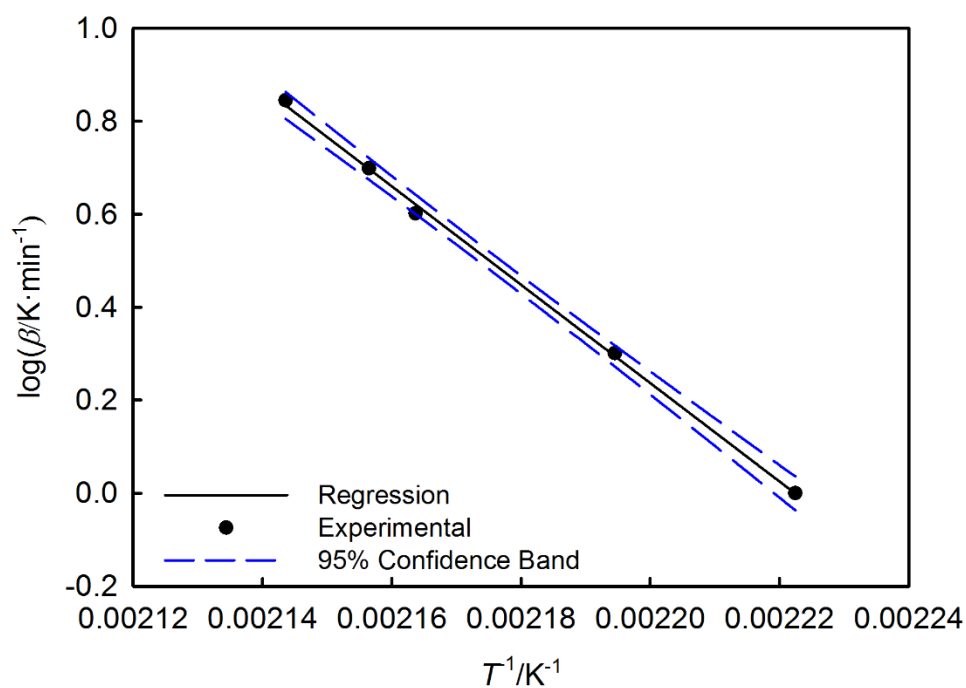Figure C11: Arrhenius plot, first decomposition 15% DHT

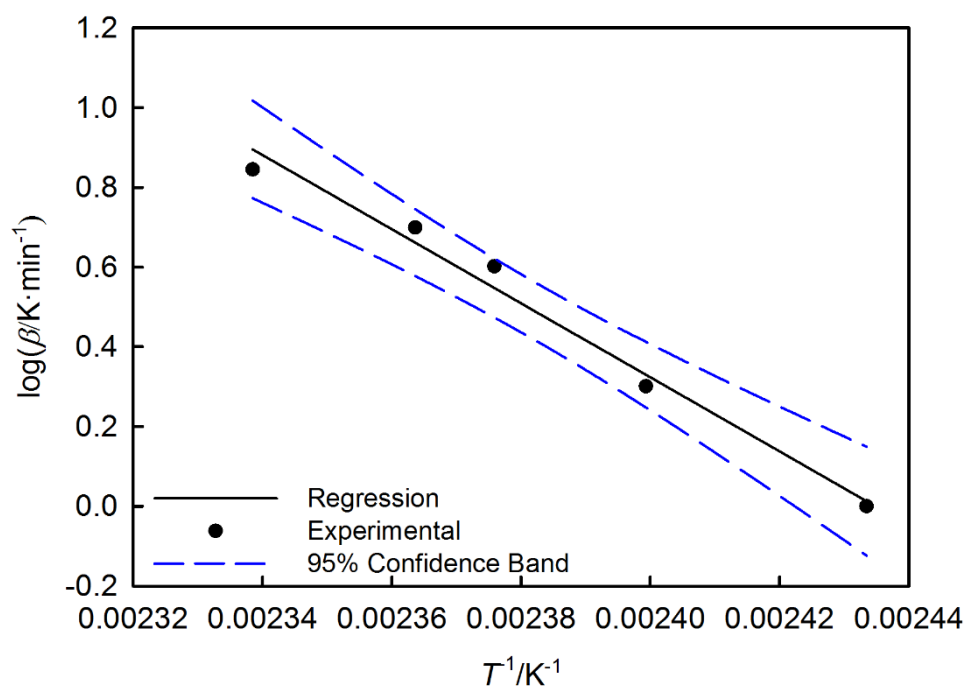Figure C12: Arrhenius plot, second decomposition 15% DHT

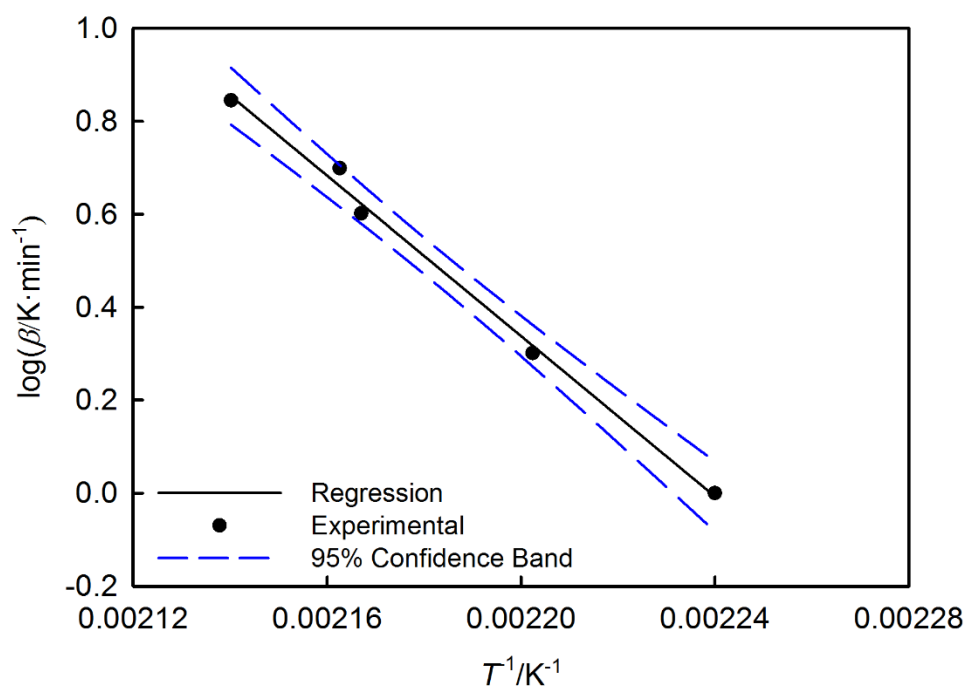Figure C13: Arrhenius plot, first decomposition 25% DHT

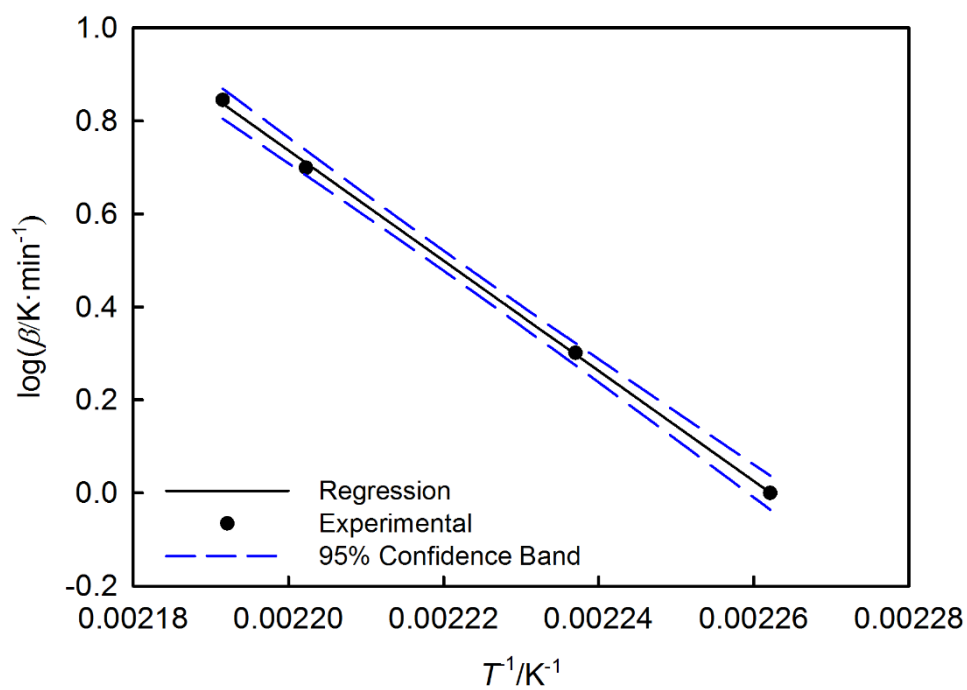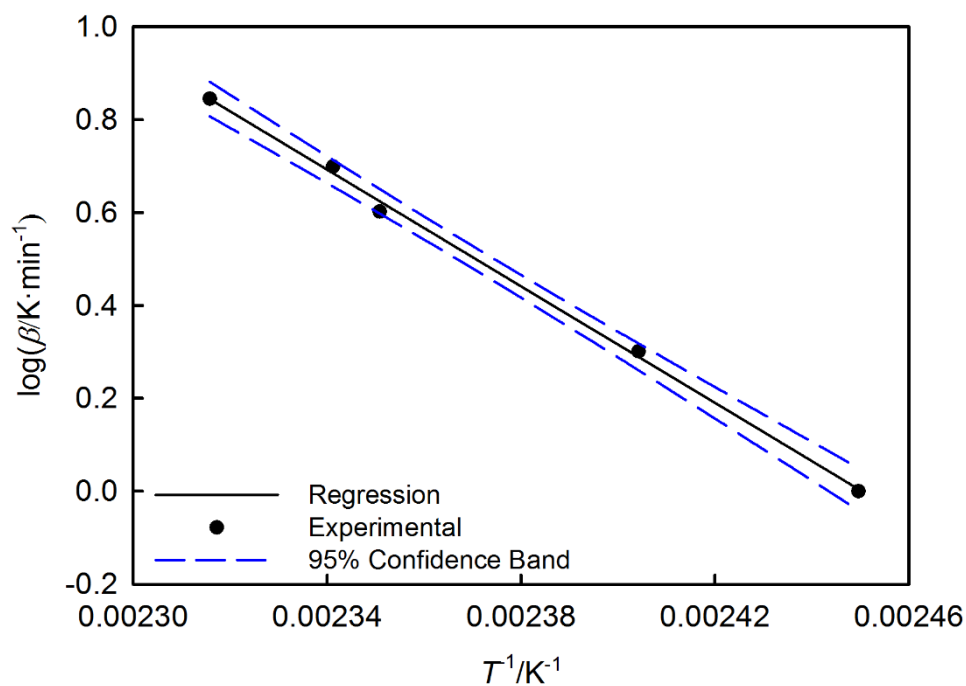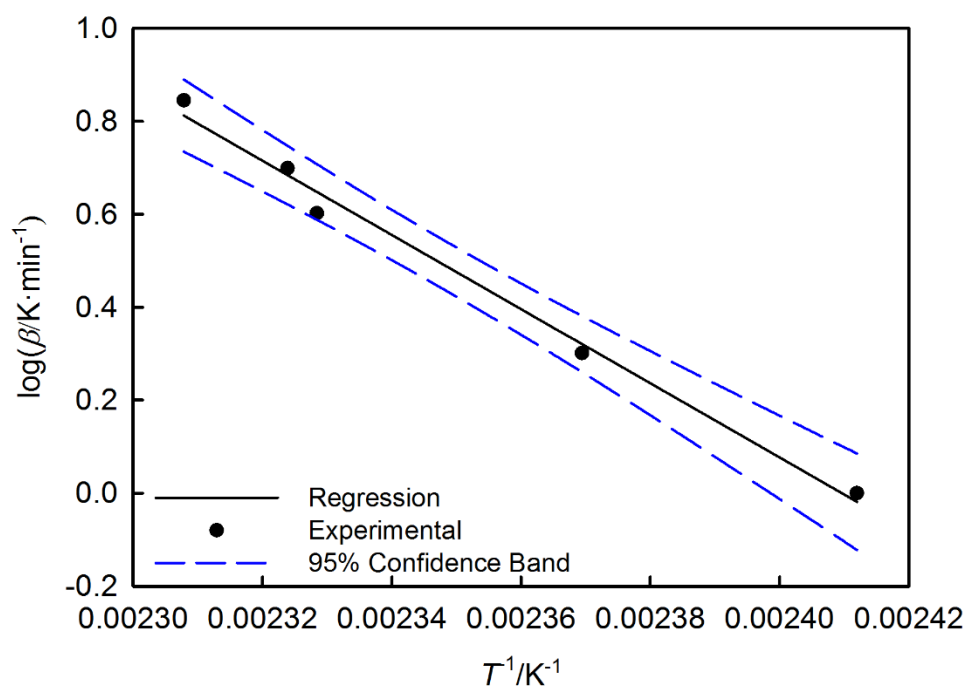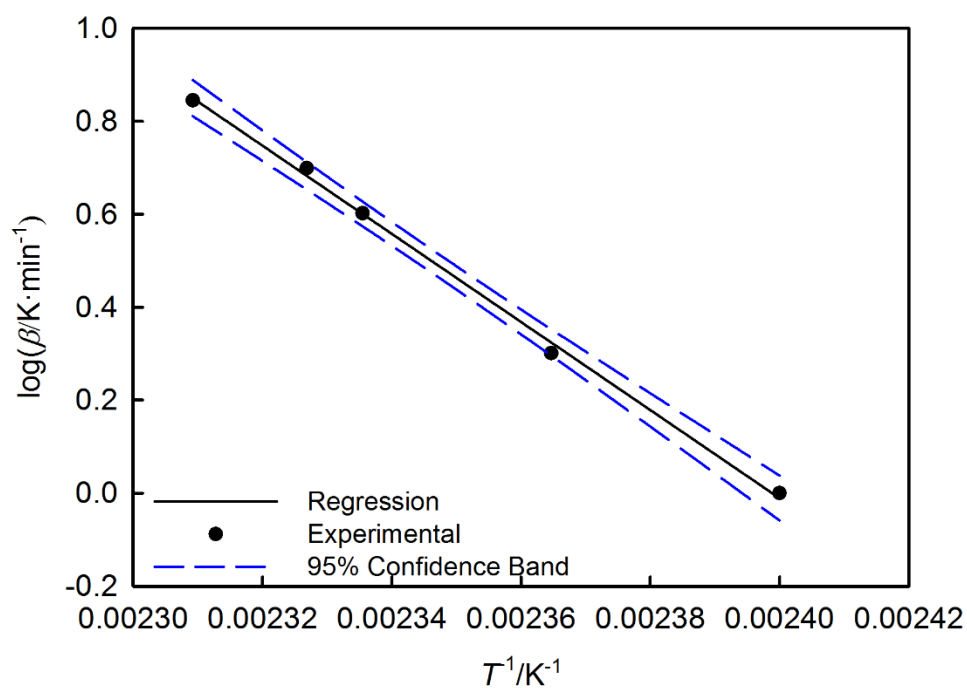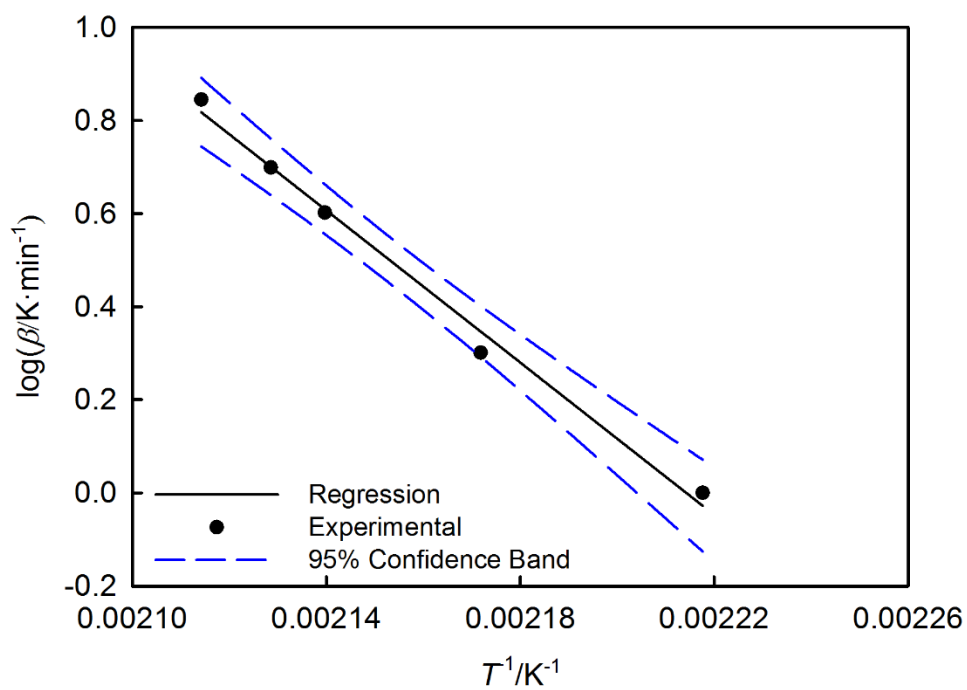Figure C14: Arrhenius plot, second decomposition 25% DHT

Figure C15: Arrhenius plot, HAT-NO$_3$

Figure C16: Arrhenius plot, first decomposition 5% HAT-NO$_3$
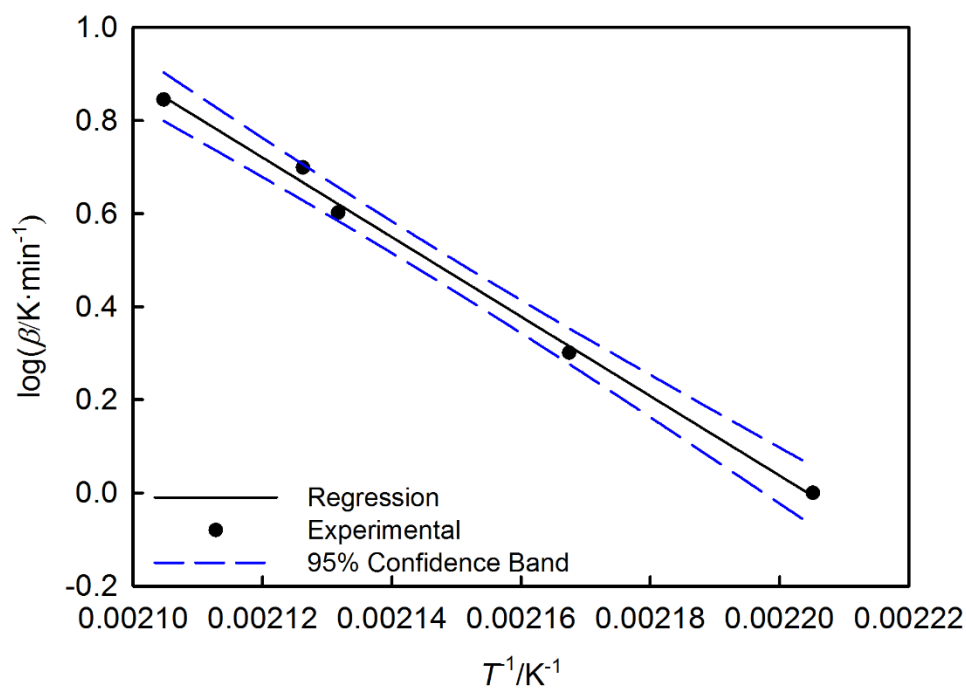
Figure C17: Arrhenius plot, second decomposition 5% HAT-NO$_3$

Figure C18: Arrhenius plot, first decomposition 15% HAT-NO$_3$
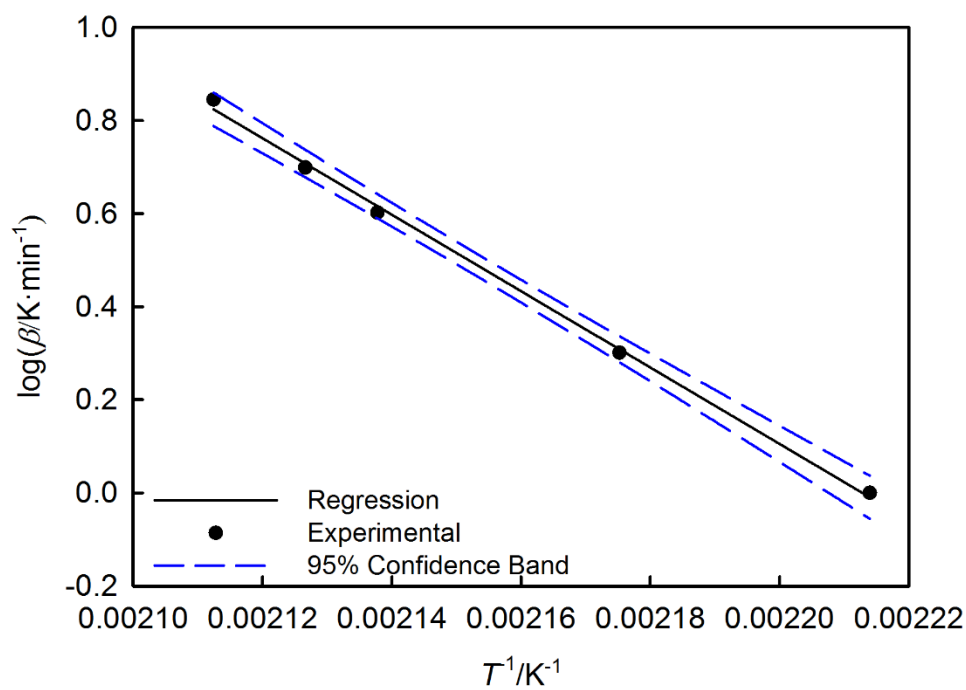
Figure C19: Arrhenius plot, second decomposition 15% HAT-NO$_3$

Figure C20: Arrhenius plot, first decomposition 25% HAT-NO$_3$

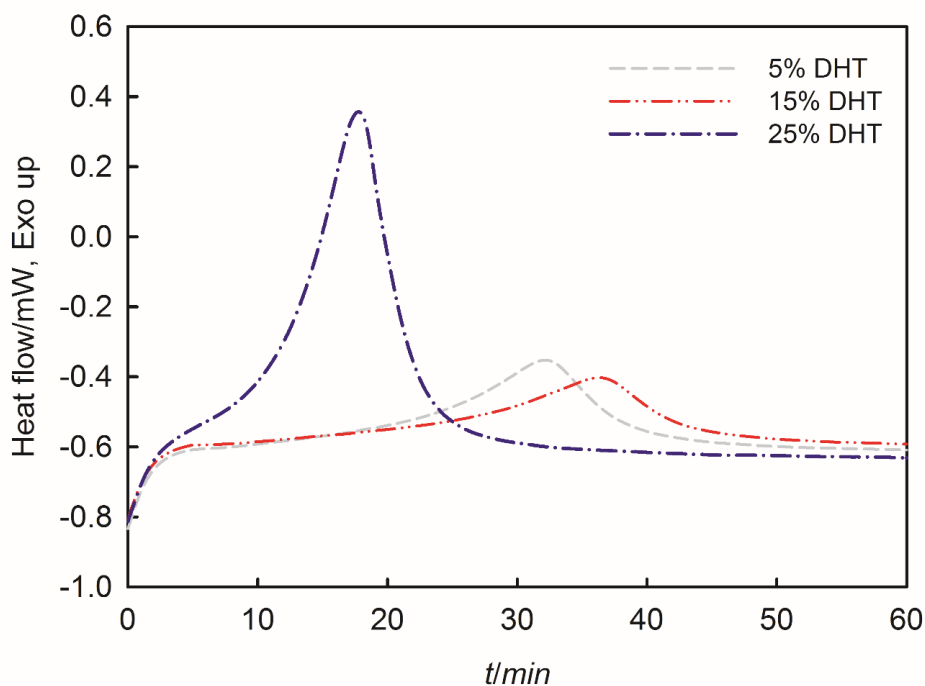Figure C21: Arrhenius plot, second decomposition 25% HAT-NO$_3$

Figure C22: Isothermal decomposition of DHT propellants at 121°C

The autocatalytic nature of the propellants can be seen by the shape of the peaks. The reaction accelerates slowly and then attains a maximum to finish in a similar fashion than the beginning of the reaction. Nth order reactions have a sharp rise in reaction rate and by extension heat generated followed by a slower decrease of the heat generated. The less stable nature of the propellant containing 25% DHT can also be seen as the reaction starts much more rapidly. The difference in decomposition time for the 5% DHT and 15% DHT can be attributed to slight differences in sample weight which resulted faster a higher amount of heat generated for the 5% DHT propellant. This was also evidenced by the fact that after 120 minutes, the propellant containing 5% DHT did not decompose when maintained isothermally at 118°C while the propellant containing 25% DHT readily decomposed within less than an hour at that temperature.